

Molecular Beam Epitaxy of InAs Quantum Dot and Quantum Dot Molecule Heterostructures

submitted to the Department of Physics
at the University of Paderborn

In partial fulfillment of requirements

for the degree

-Dr. rer. nat.-

Dissertation

by

Akshay Kumar Verma

from India,

Paderborn, January 2022

Doctoral committee

Prof. Dr. Dirk Reuter

Prof. Dr. Cedrik Meier

Prof. Dr. Stefan Schumacher

Dr. Thomas Riedl

To my family.....

This page has been intentionally left blank

Abstract

Strain-driven self-assembled InAs quantum dots (QDs) on GaAs(100) substrates fabricated via the Stranski-Krastanov (S-K) growth mode is evidently the most widely studied QD system. QD densities in the order of ≤ 1 QD per μm^2 are required for different applications. However, preparing such low densities is challenging due to the extreme dependence on the Indium (In) amount.

In this work, self-assembled InAs QDs and quantum dot molecules (QDMs) are grown on GaAs(100) substrate by the molecular beam epitaxy (MBE). In the first part, low-density InAs QDs are fabricated using two In-deposition schemes: the In-gradient approach and the homogenous In-deposition approach with subsequent annealing to attain densities in the order of 1×10^7 - 10^8 QDs cm^{-2} . In the In-gradient approach, the substrate rotation is stopped during In-deposition, either for the full deposition (full-gradient) or for half of the deposition time (half-gradient).

A comparison of the two In-deposition schemes has been done to better comprehend low areal density coverage. For the full-gradient, the low-density region stretches only over a small area along the gradient, which corresponds in the best case to less than 10 % of a full 3" wafer, whereas for a half-gradient, it increases to 15 %. In comparison, for the homogenous deposition approach, we were able to achieve for more than 70% of a 3" wafer a QD density between 1×10^7 and 1×10^8 QDs cm^{-2} . However, this process is less reproducible due to the high sensitivity to the substrate temperature and the In amount.

In the second part various QD growth parameters, such as QD growth temperature, growth interruption, and In-flux, are studied to observe the QD size modification leading to emission wavelength variation.

In the last part of this work, QDM heterostructures for electron and hole storage were fabricated. The low-density QDMs were grown utilizing the homogenous In deposition approach. The various parameters such as QD density, emission energy tuning, and tunnel coupling were optimized to achieve high-quality QDM samples for quantum storage applications.

Kurzfassung

Verspannungsgetriebene selbstorganisierte InAs-QDs auf GaAs(100), die über den Stranski-Krastonov-Wachstumsmodus hergestellt wurden, sind wohl das am häufigsten untersuchte QD-System. Für verschiedene Anwendungen werden QD-Dichten in der Größenordnung von ≤ 1 pro QD μm^2 benötigt. Allerdings ist die Herstellung solch geringer Dichten aufgrund der extrem starken Abhängigkeit von der In-Menge recht anspruchsvoll.

In dieser Arbeit werden selbstorganisierte InAs-Quantenpunkte (QDs) und Quantenpunktmoleküle (QDMs) durch Molekularstrahlepitaxie auf GaAs(100)-Substrat aufgewachsen. Im ersten Teil werden InAs-QDs mit niedriger Dichte unter Verwendung von zwei In-Deposition-Verfahren hergestellt: Der In-Gradient-Ansatz und der homogene In-Deposition-Ansatz mit anschließendem Tempern, um Dichten in der Größenordnung von 1×10^7 - 10^8 QDs cm^{-2} zu erreichen. Beim In-Gradienten-Ansatz wird die Substratrotation während der In-Abscheidung gestoppt, entweder für die vollständige Abscheidung (Vollgradient) oder für die Hälfte der Abscheidungszeit (Halbgradient).

Ein Vergleich der beiden In-Deposition-Schemata wurde durchgeführt, um ein besseres Verständnis der Region geringer Flächendichte zu erlangen. Beim Full-Gradienten erstreckt sich der Niedrig-Dichte-Bereich nur über einen kleinen Bereich entlang des Gradienten, was im besten Fall weniger als 10 % eines vollen 3"-Wafers entspricht, während er bei einem Halb-Gradienten auf 15 % ansteigt. Im Vergleich dazu konnten wir für den homogenen Abscheidungsansatz für mehr als 70 % eines 3"-Wafers eine QD-Dichte zwischen 1×10^7 und 1×10^8 QDs cm^{-2} erreichen. Dieser Prozess ist jedoch aufgrund der hohen Empfindlichkeit gegenüber der Substrattemperatur und der In-Menge weniger reproduzierbar.

Die verschiedenen QD-Wachstumsparameter wie QD-Wachstumstemperatur, Wachstumsunterbrechung und In-flux werden untersucht, um die QD-Größenmodifikation zu beobachten, die zu einer Variation der Emissionswellenlänge führt.

Im letzten Teil dieser Arbeit wurden QDM-Heterostrukturen zur Elektronen- und Lochspeicherung hergestellt. Die QDMs mit niedriger Dichte wurden unter Verwendung des homogenen In-Abscheidungsansatzes hergestellt.

Die verschiedenen Parameter wie QD-Dichte, Emissionsenergieabstimmung und Tunnelkopplung wurden optimiert, um qualitativ hochwertige QDM-Proben für Quantenspeicheranwendungen zu erhalten.

This page has been intentionally left blank

Contents

Table of Contents

| | |
|------------------------------------------|----------|
| Table of Contents..... | ix |
| List of Figures..... | xiii |
| Abbreviation and Acronyms..... | xvii |
| 1 Introduction..... | 1 |
| 1.1 Motivation..... | 1 |
| 1.2 Dissertation Outline | 3 |
| 2 Fundamentals | 5 |
| 2.1 Semiconductors | 5 |
| 2.1.1 III-V Semiconductors..... | 7 |
| 2.2 Epitaxy | 10 |
| 2.2.1 Epitaxial growth modes..... | 12 |
| 2.3 Low-dimensional nanostructures | 15 |
| 2.3.1 Semiconductor Quantum Dots | 17 |

| | | |
|----------|--------------------------------------------------------|-----------|
| 2.3.2 | Molecular Beam Epitaxy..... | 19 |
| 2.4 | Self-assembled quantum dots..... | 21 |
| 2.4.1 | Low-density InAs quantum dots | 22 |
| 2.5 | Quantum Dot Molecules | 25 |
| 2.6 | Optical states in QDs and QDMs | 27 |
| 3 | Experimental techniques..... | 29 |
| 3.1 | Molecular beam epitaxy system and growth process | 29 |
| 3.1.1 | Substrate Temperature Control..... | 33 |
| 3.1.2 | RHEED and surface reconstructions..... | 36 |
| 3.1.3 | Calculation of growth rate..... | 39 |
| 3.2 | Atomic force microscopy | 42 |
| 3.3 | Photoluminescence spectroscopy | 44 |
| 3.4 | PI imaging and electrical measurements | 46 |
| 4 | Results and discussion..... | 49 |
| 4.1 | Quantum Dot Growth..... | 49 |
| 4.1.1 | Homogenous Deposition Approach | 51 |
| 4.1.2 | In-gradient Approach | 54 |
| 4.2 | QD morphology and height distribution | 56 |
| 4.3 | Low-density characterization | 59 |
| 4.3.1 | Homogenous In deposition | 61 |
| 4.3.2 | In-gradient Approach | 64 |

| | |
|-------------------------------------------------------|------------|
| Shallower In-gradient..... | 68 |
| 4.4 Comparison of two In deposition approaches | 69 |
| 4.5 QD Size modification/ Emission energy tuning..... | 69 |
| 4.5.1 Low growth rate QDs | 70 |
| 4.5.2 QD growth at different temperature | 72 |
| 4.5.3 Different growth interruption time | 74 |
| 4.5.4 Comparison of these parameters | 75 |
| 4.5.5 In-flushed technique | 76 |
| 4.6 Quantum dot Molecules | 79 |
| 4.6.1 Electron/ Hole storage for quantum memory | 80 |
| 4.7 Heterostructure design | 81 |
| 4.7.1 Enhancing extraction efficiency..... | 82 |
| 4.8 Characterization | 87 |
| 4.8.1 Low-density optimization | 87 |
| 4.8.2 Emission energy tuning | 89 |
| 4.8.3 Electrical characterization | 91 |
| 5 Summary and Outlook | 96 |
| 6 APPENDIX A | 108 |
| 7 APPENDIX B | 109 |
| Growth reports | 109 |

| | |
|------------------------------------------------|-----|
| Publication | 157 |
| Submissions to international conferences | 157 |
| Curriculum Vitae | 158 |
| Acknowledgments | 159 |

List of Figures

| | |
|---------------------------------------------------------------------------------------------------------------------------------------------------------------------------------------------------------------|----|
| Figure 2.1: The Band structure of GaAs with bandgap E_g , obtained using the 40-band k·p model [21]. | 6 |
| Figure 2.2: Room-temperature bandgap, E_g , vs. lattice constant. Lines connecting binary compounds represent alloy composition with either a direct bandgap (black) or indirect bandgap (red) [24]. | 7 |
| Figure 2.3: Crystal structure of GaAs [25]. | 8 |
| Figure 2.4: Band alignment for different types of heterojunctions. | 9 |
| Figure 2.5: Illustration of the various kinetic processes that occur during epitaxial growth. | 11 |
| Figure 2.6: The sketch of nuclei formation on a substrate results in a wetting angle with the equilibrium of surface energies. | 12 |
| Figure 2.7: Nucleation-based growth modes: Vollmer-Weber (V-W), Frank-van der Merve (F-M), and Stransky-Krastanov (S-K). | 13 |
| Figure 2.8: The DOS and quantum confinement for the bulk, two-dimensional (2D), one dimensional (1D), and zero-dimensional (0D) semiconductor nanostructures. | 15 |
| Figure 2.9: Schematic illustration of the lens-shaped QD's with different heights representing potential width. | 18 |
| Figure 2.10: Schematic illustration of an MBE growth chamber for group III arsenide materials. | 20 |
| Figure 2.11: A schematic representation of elastic strain relaxation in InAs QD on GaAs. | 22 |
| Figure 2.12: Graph showing InAs QDs density variation with increase InAs coverage [64]. | 23 |
| Figure 2.13: a) The effusion cell and substrate position in the MBE growth chamber [76]. b) Schematic of In thickness profile with and without substrate rotation. | 24 |
| Figure 2.14: TEM image of an InAs/GaAs QDM. Adapted from [78]. | 26 |
| Figure 3.1: The schematic representation of the III-V MBE system employed in this thesis (MBE Komponenten). | 30 |

| | |
|------------------------------------------------------------------------------------------------------------------------------------------------------------------------------------------------------------|----|
| Figure 3.2: The configuration of different cells attached to the MBE (MBE Komponenten). | 31 |
| Figure 3.3: The schematic of BandiT configuration. | 34 |
| Figure 3.4: The different temperature measurements while ramping the substrate temperature. | 35 |
| Figure 3.5: The schematic of the RHEED diagram showing the incidence angle with respect to substrate and detector. | 36 |
| Figure 3.6: Schematic of different kinds of epitaxial surfaces and the corresponding pattern as observed in RHEED [88]. | 37 |
| Figure 3.7: Surface phase diagram for the epitaxial growth of GaAs from Ga and As ₄ beams on GaAs (100) substrate. | 38 |
| Figure 3.8: Pyrometric oscillations from BandiT pyrometry for AlAs and GaAs. | 40 |
| Figure 3.9: AFM image atomically smooth GaAs deposited after deoxidation with RMS roughness of 0.3 nm, b) The linescan along the image. | 41 |
| Figure 3.10: Schematic sketch of an AFM setup. | 42 |
| Figure 3.11: a) AFM image of GaAs surface with RMS roughness of 0.2 nm. | 43 |
| Figure 3.12: Schematic sketch of the photoluminescence setup. | 44 |
| Figure 3.13: shows a room temperature of the PL spectrum of a QD ensemble with different energy states. | 45 |
| Figure 3.14: a) Wafer mapping of QD sample represented in the false-color plot. b) Shows the photoluminescence image of the same sample. | 47 |
| Figure 4.1: The layer sequence for the InAs QDs heterostructure. | 50 |
| Figure 4.2: AFM images of InAs grown on GaAs(100) at 480°C substrate temperature: a) close to $T\theta$, atomic steps can be observed and b) InAs QDs formed with deposition above $T\theta$ | 51 |
| Figure 4.3: Temperature profile for InAs QD samples grown by Homogenous deposition approach (Series A with three samples) and In- gradient approach (Series D). | 52 |
| Figure 4.4: InAs QDs grown by homogenous deposition approach showing density variation with change in In amount. | 53 |
| Figure 4.5: Schematic sketch of MBE growth chamber with In cell geometry (MBE Komponenten). The In-gradient on full and quarter 3" GaAs(100) substrate due to substrate rotation stop. | 54 |

| | |
|-------------------------------------------------------------------------------------------------------------------------------------------------------------------------------------------------------------------------------------------------------------------------------------------------------------------------------------------------------------------------------|----|
| Figure 4.6: AFM images of InAs QDs grown by the In-gradient approach. Sketch of 1/4 3" wafer with marked positions (a-e) where AFM measurements have been performed. | 55 |
| Figure 4.7: a) AFM image of InAs QD, b) The linescan show the QD height and diameter. | 56 |
| Figure 4.8: AFM images for InAs QD grown by the Homogenous deposition approach; a) low density and b) high density with height distribution for the respective densities. ... | 57 |
| Figure 4.9: In-gradient approach (c-d) low and high density, respectively. | 58 |
| Figure 4.10: (a) AFM image showing surface QDs. b) low-temperature PL spectrum of low-density QDs (corresponds to $I=0.7$), (c) PL map in a false-color representation of the area including the point, from which the PL spectrum in (b) was taken; (d) PL image of buried InAs QDs from the yellow region in (c) (density ~ 0.2 QDs μm^{-2}). | 60 |
| Figure 4.11: PL spectra of InAs QDs grown by homogenous deposition approach at 300 K and 77 K. | 61 |
| Figure 4.12: PL spectra of 2.8 nm flushed InAs QDs at 16 K, grown with Homogenous deposition approach. | 62 |
| Figure 4.13: a) PL-wafer mapping for InAs QDs grown by homogenous deposition approach over 3" GaAs (100) wafer. b) QD density for surface QDs. | 63 |
| Figure 4.14: PL spectra of InAs QDs grown by In-gradient at 300 K. Inset shows the points where measurements were done. | 64 |
| Figure 4.15: PL spectra of 2.8 nm flushed InAs QDs at 16 K grown with In-gradient approach. | 65 |
| Figure 4.16: The graph shows the density vs. position plot for the full-gradient and half-gradient deposition approach calculated from AFM images for the surface QDs. | 66 |
| Figure 4.17: Graph showing ratio I , the WL intensity normalized to total intensity (peak WL+ QD), vs. position on the wafer. The ratio above 0.7 corresponds to a density $< 10^8 \text{ cm}^{-2}$ | 67 |
| Figure 4.18: The PL spectra of Shallower QD samples with respect to position on the wafer. | 68 |
| Figure 4.19: AFM images of InAs QDs grown with growth rate of 0.017 ML s^{-1} and 0.008 ML s^{-1} | 70 |
| Figure 4.20: PL spectra at 300 K for InAs QDs grown with different In LGRs. | 71 |
| Figure 4.21: InAs QDs grown at 470°C and 505°C | 72 |
| Figure 4.22: PL spectra for InAs QDs grown at QD growth temperature at 300 K. | 73 |

| | |
|-----------------------------------------------------------------------------------------------------------------------------------------------------------------------------------------------------------------------------------------------|----|
| Figure 4.23: PL spectra for InAs QD grown with different growth interruption times at 300 K. | 75 |
| Figure 4.24: The comparison of different QD parameters with respect to the emission wavelength of GS..... | 76 |
| Figure 4.25: Schematic diagram of the modification in confinement potential of InAs QDs due to the In-flush technique in both directions [001] and [110]. | 77 |
| Figure 4.26: The schematic of the In-flush technique. | 78 |
| Figure 4.27: PL spectra of InAs QD ensemble grown without flushing (as-grown) and with flushing at 16 K. | 78 |
| Figure 4.28: PL spectra of 2.8 nm flushed QDs along the In-gradient at 16 K..... | 79 |
| Figure 4.29: (a) Shows the growth structure. (b) The energy band profiles to Schottky diode structures to implement electron and hole storage. The AlGaAs layer (green color) for hole structures is placed above the QDM layers. | 82 |
| Figure 4.30: pin diode structure grown with AlAs/GaAs DBR. b) The reflectivity measurements at room temperature for the corresponding cavity structure. | 83 |
| Figure 4.31: SEM image of cavity sample showing 16 and 10 pairs of AlAs/GaAs DBR layers for the bottom and top respectively. | 84 |
| Figure 4.32: The PL spectra of InAs QDs observed in the pin cavity structure at low temperatures..... | 84 |
| Figure 4.33: Basic layer sequences of hole storage QDM heterostructure; a) pi-Schottky diode structure and b) pin diode structure..... | 86 |
| Figure 4.34: AFM image of the QDM sample surface with RMS roughness of 0.5 nm. | 87 |
| Figure 4.35: PL map in a false-color representation of QDM samples calculated from the PL spectrum with the corresponding PL image of buried InAs QDM in the right. | 88 |
| Figure 4.36: PL spectra of flushed QDMs for the low-density region at 10 K..... | 90 |
| Figure 4.37: PL spectra of an ensemble of QDMs (black) and μ PL for single QDM (red) at 10 K..... | 91 |
| Figure 4.38: μ PL image of contacted InAs QDM sample at 0 V illuminated with 850 nm laser..... | 92 |
| Figure 4.39: Electric field-dependent PL measurements for a hole storage QDM sample having barrier thickness of 10 nm (top). A magnified image of the marked part shows the anticrossing peaks (bottom). | 93 |

Abbreviation and Acronyms

| | |
|--------|---------------------------------------------|
| 0D | Zero-dimensional |
| 1D | One-dimensional |
| 2D | Two-dimensional |
| 3D | Three-dimension |
| AFM | Atomic force microscopy |
| Al | Aluminum |
| As | Arsenic |
| BEP | Beam equivalent pressue |
| DOS | Density of states |
| eV | Electron volt |
| FWHM | Full-width half maxima |
| GS | Ground-state emission |
| HS | Heating station |
| In | Indium |
| InAs | Indium Arsenide |
| AlGaAs | Aluminium Gallium Arsenide |
| LGR | Low-growth rate |
| MBE | Molecular Beam Epitaxy |
| ML | Monolayer |
| QD | Quantum dot |
| QDM | Quantum dot molecule |
| RHEED | Reflection high energy electron diffraction |
| UHV | Ultra-high vacuum |

| | |
|------------|--------------------|
| Tc | Thermocouple |
| T θ | Critical thickness |
| WL | Wetting layer |

This page has been intentionally left blank

CHAPTER 1

1 Introduction

The first recognition of nanoscale semiconductor structures was observed in 1932 [1]. The development of quantum wells with two-dimensional confinement marked the beginning of the QDs' history in the early 1970s [2]. In the next several years, significant advancements in epitaxial techniques such as liquid-phase epitaxy (LPE), metal-organic chemical vapor deposition (MOCVD), and molecular beam epitaxy (MBE), spurred revolution into semiconductor nanostructures [3]. By the early 1990s, researchers had observed three-dimensional confinement in QDs [4]. The emergence of self-assembled QDs provided researchers with a simple fabrication approach. In 1995, the demonstration of self-organized quantum dots in the InAs/GaAs material system led to significant advances in the field [5]. Subsequently, significant effort has been put into understanding the self-assembly of these three-dimensional islands.

1.1 Motivation

Semiconductor QDs have been intensively explored and have been promising candidates for the realization of different optoelectronic devices such as light-emitting diodes (LEDs), lasers, and photodetectors [6]. In the last several years, extensive research has been carried on integrating semiconductor QDs into different quantum technologies such as quantum information processing [7]. Quantum information processing, which encompasses quantum computing and quantum communication, has sparked considerable interest in basic and applied research, which offers the

possibility of physically observable secure data storage and transmission. QDs have demonstrated their ability to generate photons with such a high degree of indistinguishability, making them an appealing candidate for implementing complex quantum operations. Different theoretical and experimental schemes have been proposed for the realization of quantum information processing systems using semiconductor QDs [8]. These semiconductor QDs have been realized to generate on-demand single photons or entangled photon pairs [9,10]. The simplest scenario is a QDM formed by the coupling of two QDs. It can be considered the fundamental building block for the development of quantum computation devices [11].

Semiconductor QDs have prime importance due to their atomic like properties. Alike in atoms, the energy levels are discrete and quantized in QDs due to the confinement of charge carriers [12]. QDs typically have dimensions ranging from nanometers to a few microns. Semiconductor QDs have the advantage of being incorporated during epitaxial growth in complex structures and can be integrated into existing electronics and photonics. This has already made QDs one of the brightest and most efficient non-classic light sources. Several QD fabrication techniques have been established over time. Among those, QDs fabricated by self-assembly have been widely investigated because of their remarkable optical quality.

InAs/GaAs (100) heteroepitaxial system is the most established material system, having undergone several experiments and the most refined understanding of the optimal growth conditions [13]. In MBE, the self-assembly of three-dimensional islands called QDs occurs due to the lattice mismatch of deposited materials. After the InAs layer reaches a critical thickness, three-dimensional islands are formed due to accumulated strain energy due to growth transition, known as Stranski-Krastanov (S-K) transition [14]. The QD characteristics are dependent on various growth factors as the InAs growth rate, the growth temperature, InAs coverage, and the III/V flux ratio [15,16]. For single dot spectroscopy, the QD density should be in the order of 1 QD per μm^2 to be spatially resolvable and with sufficiently high extraction efficiencies. Despite this advancement, precise control of the size, density, and spatial position of QDs is required to exploit their use in such applications fully. The performance of different devices is dependent on dot density, dot size, and distribution uniformity.

In this work, self-assembled InAs/GaAs QDs and QDMs are grown on GaAs (100) by MBE. This dissertation realizes low InAs QD densities in the order of 10^8 QDs cm^{-2} utilizing two approaches: the homogeneous In-deposition approach and the In-gradient approach. Further, the In-gradient approach was extended to achieve a much shallower In-gradient (half-gradient). Following this, a comparison of the two approaches was made to better understand the two. The various QD growth parameters, such as In-flux rate, QD growth temperature, and growth interruption time, were explored for emission energy tuning. The second objective was to grow low-density QDMs heterostructures for electron/hole storage applications.

1.2 Dissertation Outline

The findings are organized and presented in five chapters in the following way:

- **Chapter 2** describes the fundamental concepts of III-V semiconductors, in particular, arsenide-based semiconductors. The following section introduces the basic principle of epitaxial growth in MBE. Then is outlined the properties and characteristics of the low-dimensional nanostructure, QDs in general. Furthermore, the fabrication of InAs quantum dots and vertically stacked QDMs using MBE is described.
- **Chapter 3** elaborates on the experimental techniques used to fabricate and characterize the nanostructures. The first section provides a comprehensive description of the MBE system. The second part discusses the ex-situ characterization techniques to investigate the samples' morphological and optical properties.
- **Chapter 4** describes and discusses the experimental findings. A detailed investigation of InAs QDs fabrication and their optimization to achieve low areal density is presented. Then, the effect of different QD growth factors on the size, shape, and density of QDs was examined. Further, we describe the precisely tailored growth of vertically stacked quantum dot molecules heterostructures.
- **Chapter 5** summarizes the results presented in chapter 4 and presents future prospects for the stated results in this dissertation.

This page has been intentionally left blank

CHAPTER 2

2 Fundamentals

This chapter describes the theoretical description of the work presented in this dissertation. Section 2.1 gives an overview of semiconductors and their properties. Following that, the basic concepts related to the III-V material system are discussed, particularly in arsenide-based semiconductors. *Section 2.2* describes the principle underlying the epitaxy in the MBE. The following part discusses the physical properties of low-dimensional nanostructures. Furthermore, the fabrication of self-assembled InAs QDs using two different In-deposition schemes is discussed. Section 2.3 introduces QDMs and their optical states.

2.1 Semiconductors

The significant advances of semiconductor research and development commenced in the late 19th century, beginning with the discovery of the temperature dependence of the conductivity of AgS by *Michael Faraday* [17] in 1833 to the fabrication of the first silicon transistor in 1947 [18]. The first use of the term 'semiconductor' was coined by *J. Königsberger* and *J. Weiss* in 1911 [19]. The discovery of a transistor by the scientist's *John Bardeen*, *Walter Houser Brattain*, and *William Bradford Shockley* in 1947 sparked a revolution in electronics and semiconductor devices [20]. The invention of the transistor and integrated circuit resulted in the development of modern computers, telecommunications, and other different technologies that radically changed the structure of the world.

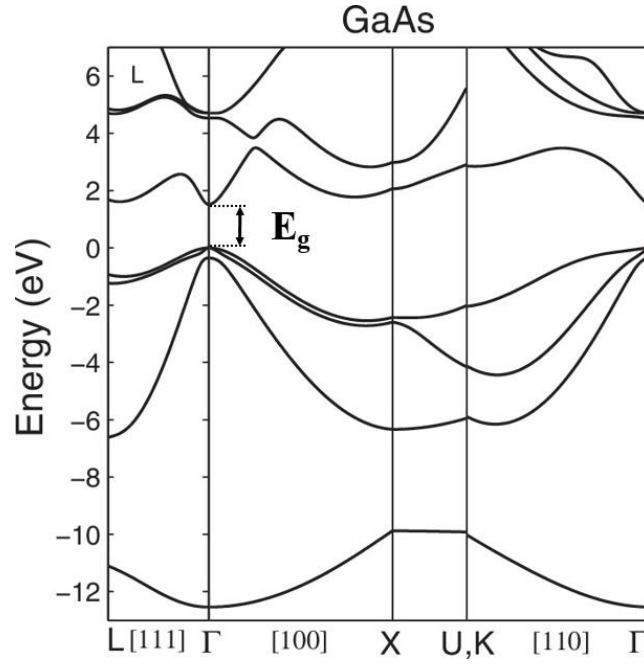


Figure 2.1: The Band structure of GaAs with bandgap E_g , obtained using the 40-band k·p model [21].

Semiconductors are a class of materials with conductivities intermediate to those of conductors and insulators, with a filled valence band (VB) and a nearly empty conduction band (CB) separated by a bandgap. The bandgap of semiconductors is an important characteristic; it is a range of forbidden energies within the material's electronic structure. Semiconductors generally have bandgaps generally less than 4 eV, whereas insulators typically have larger bandgaps, frequently exceeding 5 eV [22]. Their resistance, for example, may vary with temperature. At low temperatures, they conduct nearly no electricity. However, as the temperature increases, they conduct electricity through them efficiently. This variability of electrical properties by changing the concentration of dopants, optical excitation, and temperature change makes the semiconductor materials ideal for electronic and optoelectronic devices. The electrical and optoelectronic properties of a semiconductor can be explained using the dispersion relation's CB minima and VB maxima. For example, the maxima and minima coincide in the Γ point at $k = 0$. for GaAs, as shown in Figure 2.1, making this semiconductor a direct-bandgap material. Direct band semiconductors are especially useful in optics because they are capable of direct interactions with photons.

In semiconductors, the variation of bandgap with temperature (T) is described by the empirical Varshni formula [23] given as;

$$E_g(T) = E_g(T_0) - \frac{\alpha T^2}{T + \beta} \quad (2.1)$$

where the parameters, $E_g(T_0)$, α , and β are fitted to experimental data.

2.1.1 III-V Semiconductors

III–V semiconductors play a significant role in a number of different optical and electronic devices because of their superior electronic characteristics, such as high electron mobility, the direct bandgap of materials, and low binding energy. For example, devices made of these materials are used in various optoelectronic devices such as LEDs, Lasers, and telecommunications devices. A combination of elements from the periodic table groups III namely

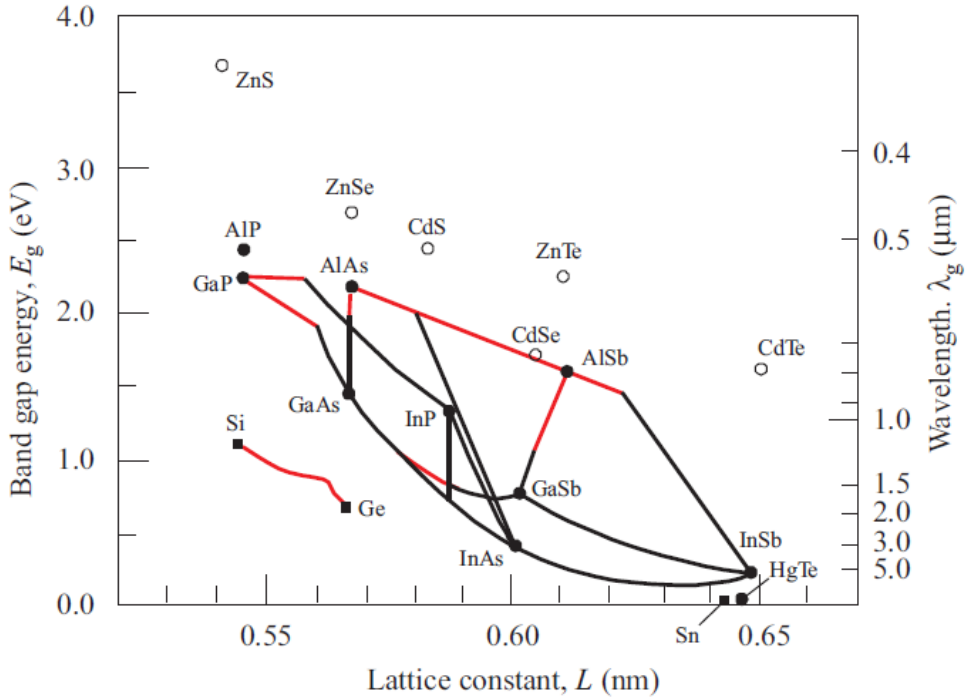


Figure 2.2: Room-temperature bandgap, E_g , vs. lattice constant. Lines connecting binary compounds represent alloy composition with either a direct bandgap (black) or indirect bandgap (red) [24].

Al, Ga, and In and group V elements namely N, P, As, and Sb, create these III-V compound semiconductor alloys. Si is the most common semiconductor material and has been extensively researched and used in commercial electronic devices. Besides Si, GaAs is another essential compound semiconductor widely studied for photonic applications, notably because of its direct bandgap. Moreover, they have succeeded in optoelectronics due to their quality interfaces with compounds with variable bandgap energies, such as AlGaAs and GaAs, and InGaAsP-InP. These high-quality interfaces with minimal impurities enable efficient carrier transport over numerous interfaces and low non-radiative recombination rates.

The most widely used III-V semiconductors are represented in Figure 2.2, which shows bandgap energy vs lattice constant diagram. The III-V compound semiconductor crystallized either in Zinc blende (GaAs, InP) or Wurtzite (GaN) structures. In both the structures, the primitive unit cells consist of two atoms at $(0,0,0)$ and $a(1/4,1/4,1/4)$, where a is the lattice constant. The zinc blende crystal structure is a cubic point lattice with a face-centered cubic point lattice and a two-atomic basis. The Zinc blende structure of GaAs is illustrated in Figure 2.3.

In semiconductors, energy bands can be efficiently explained using the effective mass approximation in the perspective of a multiband k.p approach that requires a minimal number of experimentally established parameters. Dispersions of valence band are classified into bands for heavy holes, light holes, split-off holes (zinc blende), and crystal holes (wurtzite). The valence-

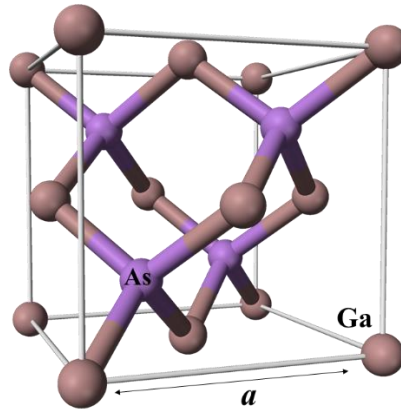


Figure 2.3: Crystal structure of GaAs [25].

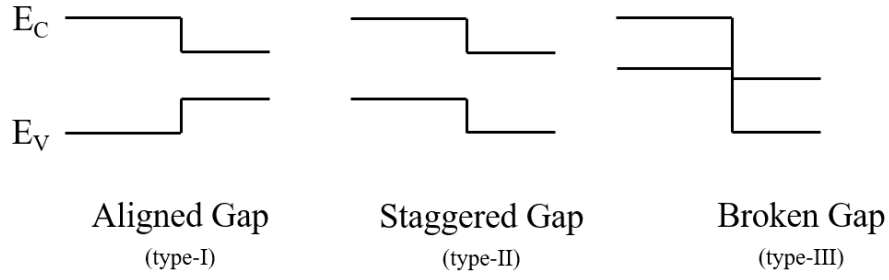


Figure 2.4: Band alignment for different types of heterojunctions.

band structure of a typical zincblende semiconductor (GaAs) is displayed in Figure. 2.1 as it approaches the Brillouin zone's center (point at $k = 0$).

III-V semiconductor heterojunctions are classified into type I, II, and III according to the nature of the band alignment at the interface, with aligned, staggered, and broken bands, respectively (Figure 2.4). An aligned bandgap is marked by the discontinuities in the CB and VB, for example, the case of the GaAs/Ga_xAl_{1-x}As heterojunction. In a staggered band alignment, the CB of one compound is located above the neighboring compound's energy level but still have some overlapping, as is the case with the GaSb/GaAs heterojunction. The broken bandgap configuration arises when the CB level is lower than the VB from the other semiconductor layer, as in the InAs/GaSb material system. A major benefit of III-V materials is that they have a wide range of band structures having different bandgaps and band alignments. This allows for the fabrication of complicated heterostructures by bandgap engineering. Bandgap engineering is a term that describes the ability to precisely control the chemical composition of III-V alloys during the epitaxial process, resulting in a range of electronic properties. Random alloying is done in III-V semiconductors for different applications to engineer properties like lattice parameters and

Table 2.1: The fundamental characteristics of GaAs, AlAs, and InAs at absolute zero temperature [26].

| Property | GaAs | AlAs | InAs |
|---------------------------|-------|-------|-------|
| Direct bandgap E_g (eV) | 1.519 | 3.099 | 0.417 |
| Lattice constant (Å) | 5.643 | 5.661 | 6.050 |

bandgap. This is stated according to Vegard's law [27]; lattice constant of a ternary alloy A_xB_{1-x} can be linearly interpolated from the primary materials A and B, given by the following relationship:

$$a_{AB} = xa_A + (1 - x)a_B \quad (2.2)$$

with lattice constant a_A and a_B respectively. The bandgap E_g of a ternary alloy semiconductor is generally approximated by a quadratic dependence with a primarily positive bowing parameter b [28] is given by

$$E_{g,AB} = xE_A + (1 - x)E_B - b_{AB}x(1 - x) \quad (2.3)$$

where E_A , E_B , and $E_{g,AB}$ are the respective properties of material A, B, and the alloy A_xB_{1-x} , and x is the mole fraction of one ingredient in a material and b_{AB} is the bowing parameter. The bowing parameter value for $\text{Al}_x\text{Ga}_{1-x}\text{As}$ and $\text{In}_x\text{Ga}_{1-x}\text{As}$ at Γ -point are given as $b_{\text{Al}_x\text{Ga}_{1-x}\text{As}} = -0.127 + 1.310x$ and $b_{\text{In}_x\text{Ga}_{1-x}\text{As}} = 0.477$ [26].

2.2 Epitaxy

Epitaxy is the assembly of atoms on a crystalline substrate. Epitaxial growth is the formation of a crystalline film suitably orientated onto a substrate by deposition of new material. It is most commonly used to describe the growth of monocrystalline films [29]. The work of Louis Royer in 1920 marked the beginning of the scientific study of epitaxial growth. Royer coined the term epitaxy, derived from the Greek words 'epi', meaning upon, and 'taxis,' meaning order [24]. Significant advancements in epitaxial growth techniques have resulted in the ability to create different materials with atomic-level precision. Several epitaxial techniques have been widely used for the epitaxial growth of III-V compound semiconductors and other materials such as Liquid Phase Epitaxy (LPE) [30], Vapor Phase Epitaxy (VPE) [31], MBE [32], and Atomic Layer Deposition (ALD) [33]. In this work, MBE is used for the epitaxial growth of nanostructures, as described in section 2.4.

In thin films epitaxy, growth takes place either through the deposition of a film of the same material on the same material substrate, known as homoepitaxy (e.g., GaAs on GaAs substrate, doped Si on Si substrate), or through the deposition of a film of a different material on a different substrate, known as heteroepitaxy (GaAs on Si, InAs on GaAs). In

heteroepitaxy, the layer and the substrate are strained due to bond length and thermal expansion differences. In this instance, the strain in the film is determined by the lattice mismatch (f), given as:

$$f = \frac{d_{\text{substrate}} - d_{\text{film}}}{d_{\text{film}}} \quad (2.4)$$

where d is the lattice constant of the bulk material. This lattice mismatch between heterosystems is accommodated either elastically by increasing the lattice strain or plastically by generating misfit dislocations.

Epitaxial growth tends to occur in two stages. The first step involves surface processes such as atoms chemisorption, movement, and forming of bonds from impinging atoms. The subsequent step includes the thermodynamic interaction and rearrangement of atoms at the surface. As soon as atoms have been absorbed on the surface, they tend to move to thermodynamically stable places and forms bond at those lattice sites, form defects where contaminants are present, aggregate with related species, or move across the surface and desorb [24]. Figure 2.5 depicts a schematic representation of the different kinetic processes that take place during epitaxial growth. An Arrhenius correlation with an activation energy E can typically characterize these

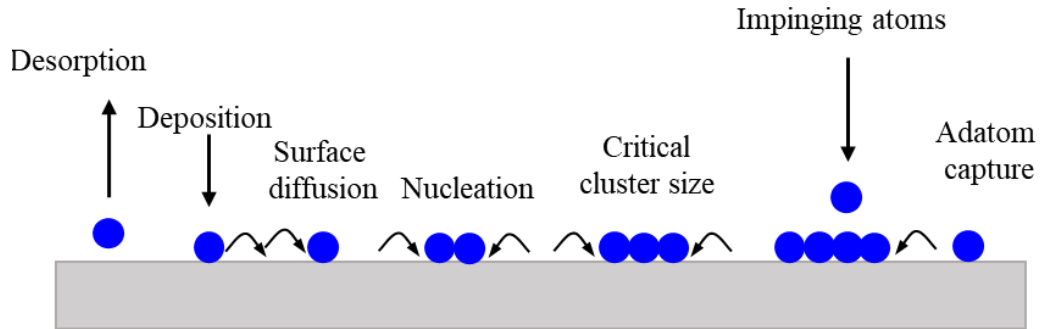


Figure 2.5: Illustration of the various kinetic processes that occur during epitaxial growth.

thermally induced processes, such as diffusion, evaporation, and desorption given by the equation:

$$P = P_0 \exp\left(-\frac{\Delta E}{RT}\right) \quad (2.5)$$

where P and P_0 are the probability of the process and probability constant, ΔE is the activation energy, and T is the temperature. In the particular case of adatom diffusion on a surface with the diffusion coefficient D , described as $D = D_0 \exp\left(-\frac{E_a - E_d}{k_B T}\right)$ where E_a is the surface activation energy, and E_d is the diffusion barrier and ν are the vibrational frequency ($\nu = \frac{2k_B T}{h}$), where h is plank constant. The epitaxial growth system described above is simplified and does not account for surface reconstructions, interdiffusion processes, dislocations, or chemical reactions between the substrate and deposited material.

2.2.1 Epitaxial growth modes

Epitaxial growth is generally carried out at high temperatures well above room temperature, for example, typically around 600 °C, which allows for adequate adatom mobility on the crystalline surface [24]. It is possible to model the growth process using a structural model combined with the kinetic processes that an impinging atom goes through before getting absorbed into the lattice sites [24]. The early growth phase requires nucleation that is clusters of particles creating solid nuclei After a stable nucleus is formed the crystal grows in accordance with growth parameters that are required by the

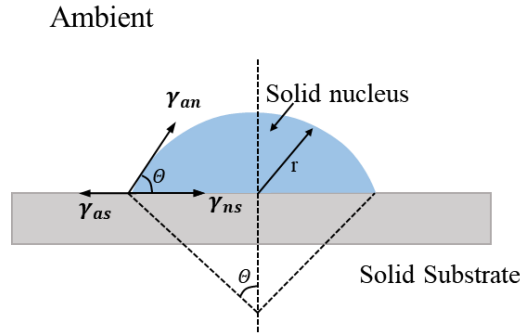


Figure 2.6: The sketch of nuclei formation on a substrate results in a wetting angle with the equilibrium of surface energies.

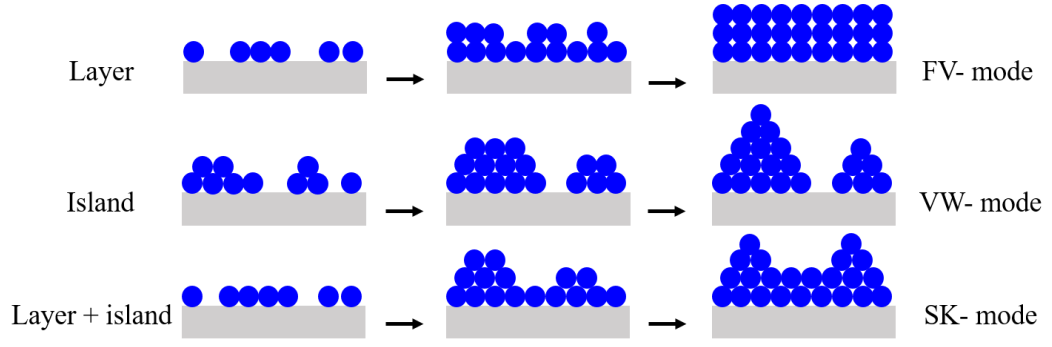


Figure 2.7: Nucleation-based growth modes: Vollmer-Weber (V-W), Frank-van der Merve (F-M), and Stranski-Krastanov (S-K).

phase transition. In heterogeneous nucleation, the crystalline substrate provides favorable sites for nuclei formation. The overall change in Gibbs energy (nucleus formation) is defined as the sum of volume, surface, and stress.

$$\Delta G_N = \Delta G_V + \Delta G_S + \Delta G_E \quad (2.6)$$

ΔG_V is the Gibbs energy proportional to the volume of the nucleus, surface energy, and ambient, respectively. The interface energies for three-dimensional nucleation between the substrate, nucleus, and ambient are calculated assuming a spherical nucleus with radius r (Figure 2.6). Young's relation for absolute tension in equilibrium is

$$\gamma_{as} = \gamma_{ns} + \gamma_{an} \cos \theta \quad (2.7)$$

where γ_{as} is ambient-substrate surface, γ_{ns} is nucleus-substrate tension and γ_{an} is the ambient-nucleus surface tension. The wetting angle varies with the degree of wetting and determines the geometry of the nucleus. The wetting angle varies depending on the nucleus and substrate affinity and defines the nucleus shape. The volume of a sphere is $\frac{4}{3}\pi r^3 \times f$, where f is a geometric factor

$$f = (2 - 3\cos\theta + \cos^3\theta)/4 \quad (2.8)$$

The critical free energy of the nucleation ΔG_N heterogeneous nucleation [24] with no strain is given by

$$\Delta G_N^* = \frac{16\pi}{3} \frac{\gamma_{an}^3 v^2}{(\Delta g)^2} \times f \quad (2.9)$$

Epitaxy is always aimed at depositing a smooth growth surface, i.e., the wetting angle in Young's relation is equal to zero or is specified as $\gamma_{as} = \gamma_{ns} + \gamma_{an}$. The dislocations or the strain induced by the lattice mismatch results in three different types of growth [34], as illustrated in *fig. 3.5*. These are described as follows [24]:

- Layered growth or Frank–van der Merwe (F-M) growth occurs when the layer is completely wetted on the substrate surface i.e. $\gamma_{as} \geq \gamma_{ns} + \gamma_{an}$, implying that layer atoms tend to prefer the substrate to each other. After that, growth occurs in a layer by layer growth. The crystalline orientation of the first layer significantly influences the growth of crystalline thin films. This type of growth is usually preferred in epitaxy because it results in planar growth.
- Island growth or Volmer–Weber (V-W) growth mode occurs when $\gamma_{ns} \geq \gamma_{as} + \gamma_{an}$ i.e., the layer atoms are attracted to one another more strongly than they are to the substrate. Hence, doesn't wet the substrate, minimizing surface energy. The atoms form a small island on the substrate's surface, before growing or dissolving into single atoms. This results in layer growth in three dimensions.
- The Stranski–Krastanov (S-K) Growth mode is a mixture of layered and island growth. This growth model generally starts from layered growth. The initial monolayers deposited here adhere to the Frank-Van der Merve growth criteria. When the critical thickness coverage is exceeded, the growth transitions to the Volmer-Weber case. This may be caused by strain accumulation in the epitaxial layer. As a result, three-dimensional islands form beneath a two-dimensional wetting layer. SK growth has gained importance as a method for growing defect-free quantum dots.

2.3 Low-dimensional nanostructures

In a bulk semiconductor material, conduction electrons and holes can move in any of the three spatial directions. When the charge carrier is confined in one or more directions within these nanostructures, it reduces effective dimensionality, referred to as low dimensional nanostructures. Low-dimensional structures exhibit distinctive properties primarily due to variations in the electronic density of states (DOS) generated by charge carrier confinement. The DOS and quantum confinement for low-dimensional nanostructures is illustrated in Figure 2.8. Confinement refers to the spatial confinement of electron-hole

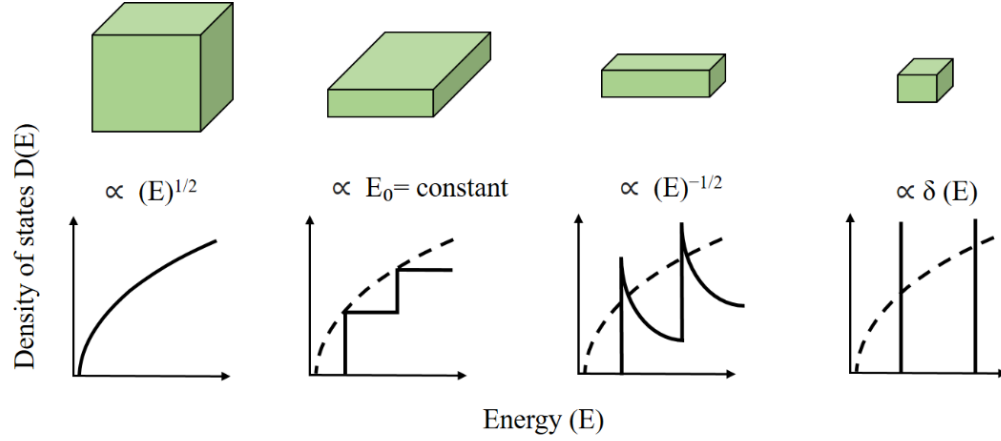


Figure 2.8: The DOS and quantum confinement for the bulk, two-dimensional (2D), one dimensional (1D), and zero-dimensional (0D) semiconductor nanostructures.

pairs (excitons) within a material in one or more dimensions. When atoms are combined in a bulk material, the number of energy states significantly increases, forming nearly continuous bands of states. When the particle's diameter approaches that of de Broglie wavelength (λ_b) of electrons in the conduction band, electron-hole pairs become spatially confined [35]. As the particle size decreases, the energy states inside it shifts upwards, increasing the energy difference between the different energy states. In general, the energy states can be determined for a free particle in a semiconductor by solving the Schrödinger equation via the effective mass approximation

$$\left[-\frac{\hbar^2}{2m^*}\nabla^2 + V(r)\right]\Psi(r) = E\Psi(r) \quad (2.10)$$

where Ψ is the carrier-envelope wavefunction, m^* is the carrier's effective masses, V is the electron's potential energy, and E is the energy in x , y , and z spatial directions. The Schrödinger equation may be solved in the conventional model of infinitely deep, rectangular potential wells with dimensions L_x , L_y , and L_z by separation of variable methods, yielding confinement energies for various semiconductor systems.

Bulk materials have free motion in all three directions, [36] with energy (E) given by

$$E = \frac{\hbar^2}{2m^*}(k_x^2 + k_y^2 + k_z^2) \quad (2.11)$$

where $k_{x,y,z}$ are the wave vectors in each direction. Consequently, the energy spectrum is continuous, and the corresponding density of states (DOS) is the same as for the bulk system, $D(E) \propto E^{1/2}$. In a 2D system, however, the movement of electrons in the z -direction is quantized, resulting in discrete electric subbands for each electron while the motion is still free in xy -plane

$$E = \frac{\hbar^2}{2m^*}(k_x^2 + k_y^2) + E_z^i \quad (2.12)$$

$i=1,2,3\dots$ and the 3D-DOS exhibits step-function-like behavior in this case near the quantization energies. Further lateral confinement of the electron motion results in a one-dimensional system.

$$E = \frac{\hbar^2}{2m^*}k_y^2 + E_x^i + E_z^j \quad (2.13)$$

$j=1,2,3\dots$ where the DOS is highly peaked, and the 2D-DOS is modified at all relevant energies. Finally, when the electron motion is constrained in all directions, the result is a zero-dimensional system

$$E = \frac{\hbar^2}{2m^*}E_x^i + E_y^k + E_z^j \quad (2.14)$$

$k=1,2,3,\dots$ with a discrete energy spectrum, and the DOS is a series of δ -function peaks. In QDs, all available states exist only at discrete energies.

2.3.1 Semiconductor Quantum Dots

The bulk dimension of materials can be reduced to generate different nanostructures with varying degrees of carrier confinement, as discussed in section 2.3. QDs are nanostructures with such small dimensions that their electronic states resemble those of an atom or molecule rather than that of its crystal [36]. They are also called "artificial atoms" due to the charge carrier confinement resulting in quantized electron and hole states similar to those seen in an atom. The energies and wave functions of quantum states depend on the dots' size, shape, composition, and density, and they can be modified to precisely control their electronic and optical properties. Recent advances in QD research have been driven by the ability of a semiconductor to prepare atom-like structures and the possibility of incorporating QDs into existing optoelectronic technologies [35,37]. Their applications include semiconductor lasers [38–40], storage devices [41,42], infrared detectors [43,44], and quantum computation [45]. Different approaches for the fabrication of semiconductor QDs have been explored over the years, including chemical synthesis, pre-growth lithographic patterning [46], ion-beam synthesis [47], and self-assembled epitaxial growth [13].

In order to achieve carrier confinement, a narrower bandgap material is embedded within a higher bandgap material, resulting in the spatial confinement of both electrons and holes in all three directions of the material. Quantum confinement comes into play when the size of the solid becomes of the order of the de Broglie wavelength of electrons. This thickness should be less than the de-Broglie wavelength

$$\lambda_b = \frac{h}{p} = \sqrt{2m^*E} \quad (2.15)$$

where $p = m_n v$ denotes the momentum, m^* is the effective mass, and v is the electron velocity. In semiconductors, λ is of the order of 1-100 nm due to their small effective masses comparable to the size of the dot.

2.3.1.1 Energy states in a Quantum Dot

The energy states of a QD are highly dependent on the geometry of the QD and the potential barrier, both of which are affected by growth parameters. Several experimental and theoretical studies have been done over the years. Many models, including the multiband k.p model [48] and empirical pseudopotential theory [49], have been used to determine the electronic structure of a QD with varying degrees of precision

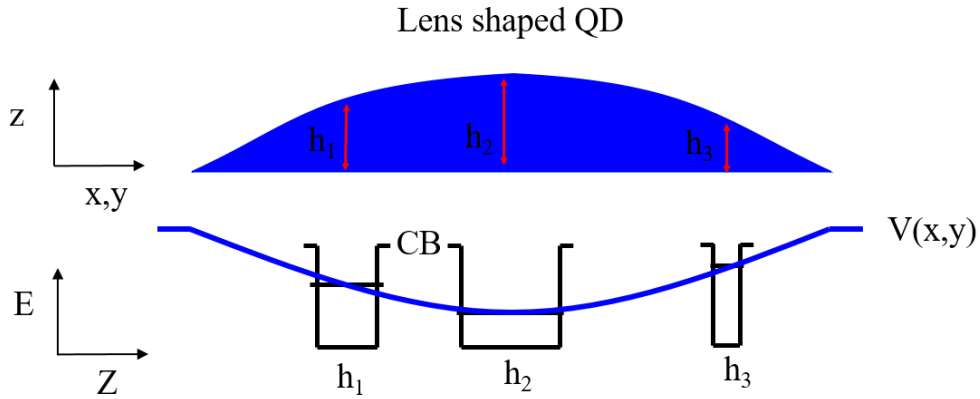


Figure 2.9: Schematic illustration of the lens-shaped QD's with different heights representing potential width.

by solving the Schrodinger equation (*eq. 2.10*). These models largely depend on dot structural properties. However, it is possible to develop a model system that provides qualitative insight into QD physics by assuming simple geometries.

Electronic structure in semiconductor QDs can be described using a simple theoretical model of the harmonic oscillator. It is possible to describe the energy spectrum of a particle confined to a QD by considering the dot as a disk or a lens shape [50]. Generally, a lens-shaped geometry is assumed for self-assembled quantum dots where the dimension of the growth direction is smaller than the lateral dimensions, as shown in Figure 2.9. The lens-shaped QDs produce spectra that resemble a spectrum of a pair of harmonic oscillators with similar spacing and degeneracy.

When applied to the Hamiltonian, the harmonic oscillator potential (analogous to the classical Hook potential) yields the following discrete Eigen energies

$$E_n(\delta) = \hbar\omega_0(2n + |l| + 1) \quad (2.16)$$

where $n \in N, l = [0 \pm (n - 1)]$. The principal n represents the energy levels evenly spaced by an amount $\hbar\omega_0$ and l , the azimuthal number, denotes the orbitals s ($l = 0$), p ($l = 1$), $d...$ According to the Pauli principle, each shell can only be inhabited by a pair of electrons with opposite spin. Different electrical and optical characteristics of QDs have already been studied and explained by several academics based on these harmonic potential models.

2.3.2 Molecular Beam Epitaxy

MBE is an epitaxial growth technique in which one or more atomic or molecule beams interact on the crystalline substrate in an ultra-high-vacuum (UHV) environment. It allows precise control over epitaxial deposition of material with extreme purity, structures with tailored compositions, and different doping concentrations by physical vapor deposition or vacuum evaporation in UHV conditions [51]. The MBE technique is an ultrahigh vacuum deposition technique for epitaxial growth pioneered by J. R Arthur [52] and A. Y. Cho [53] at Bell Laboratories in the late 1960s. MBE, in particular, has resulted in the fabrication of novel devices.

The foundation of MBE enhanced the fundamental understanding of the atomic level of epitaxial film growth. It is broadly used in the field of electronics and optoelectronics in various research labs and industrial production. UHV environments are characterized by extremely low background impurity gases partial pressure ($< 10^{-12}$ Torr), which results in extremely low impurity levels in the resulting grown structures. Because of its atomic precision, MBE can produce epitaxial layers as thin as a few monolayers. MBE grows at a rate of approximately $1\mu\text{m/h}$ or monolayer/sec (ML/s). This allows for finer control over interface thickness across layers with varying content and doping concentration. For III-V compound semiconductors and alloys, the commonly employed elements are Al, Ga, In, P, As, and Sb, with Si or C as extrinsic doping. The chemical structure of an element governs its reactivity and certain characteristics of its growth kinetics. These materials are usually contained in effusion cells in pyrolytic crucibles. This can be then evaporated or sublimated to form molecular beams. Typically, the material flux generated by the effusion cells is

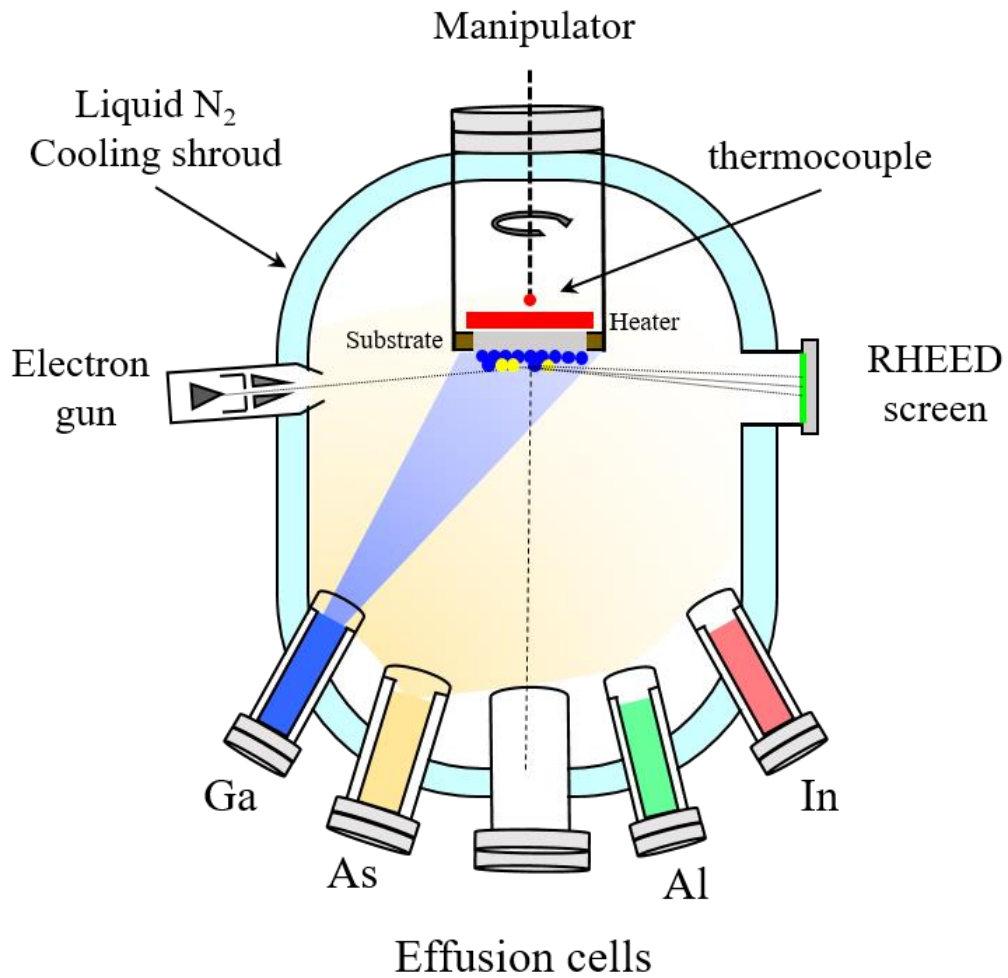


Figure 2.10: Schematic illustration of an MBE growth chamber for group III arsenide materials.

determined by the temperature of the source, and these effusion cells are linked with a mechanical shutter that allows the beams to be started or stopped in a fraction of the time. This allows for precise alloy compositions and doping concentrations by controlling individual fluxes of constituent materials. An ion gauge is typically used to measure and calibrate the fluxes using beam-equivalent pressure (BEP) in effusion cells that are maintained at a constant temperature. The MBE chamber is covered by a cooling shroud, which is generally filled with liquid nitrogen. This ensures that any particle striking the chamber walls is condensed and cannot interact with the growth surface again. The UHV environment allows molecules or atoms of source materials to flow from source to heated substrate without interfering with

one other. Additionally, the UHV environment enables the adoption of various in situ monitoring techniques, including reflection high-energy electron diffraction (RHEED), and mass spectrometry, during growth. When paired with other different techniques such as pyrometry, and band edge thermometry, MBE becomes a very effective instrument for studying fundamental science and fabricating high-quality materials and devices. Figure 2.10 shows the schematic of a solid source MBE growth chamber.

In general, flux distribution from each source follows a cosine $[a(\cos^2 \theta)/r^2]$ distribution from the source's opening, here r is the distance between source and the substrate and θ represents the angle between the source opening to the normal. Substrate rotation is used to achieve uniform flux distribution over the substrate as the film is grown. Unlike other epitaxial growth techniques like liquid phase epitaxy, which occur near thermodynamic equilibrium, MBE epitaxial growth is governed by the kinetics of surface processes that occur during the reaction of impinging atoms with the substrate crystal's outermost atomic layers [54].

2.4 Self-assembled quantum dots

The term 'self-assembly' corresponds to the spontaneous nature of the formation of the nanostructures. The self-assembled quantum dots (SAQDs) have gained substantial attention during the last few decades in scientific research and technological domains such as single-photon emitters [9], lasers [55,56], light-emitting diodes [57], photodetectors [58], optical amplifiers [59], and quantum information processing systems [60]. SAQDs form due to lattice-mismatch between the deposited material and substrate during MBE deposition. Many different material systems have been observed to exhibit island formation in strained heteroepitaxy such as InAs/GaAs, InAs/InP, InP/GaAs, CdSe/ZnSe, and GaN/AlGaN [61]. as Goldstein et al.[5] first reported the occurrence of self-assembled QDs in the InAs/GaAs material system in 1995 [5]. InAs had a lattice mismatch of 7.2 % with GaAs [62,63]. These dislocation-free InAs SAQDs are most often fabricated by S-K growth [64,65] as described below:

2.4.1 S-K growth of InAs on GaAs(001)

InAs growth on GaAs(001) begins with the nucleation of 2D islands that coalesce into coherently strained layers (S-K growth mode, section 2.2). Due

to the low surface free energy of some InAs layer material, they do not disperse and continue to stay as a 2D layer. This layer wets the material's surface underneath and is called the wetting layer (WL). Figure 2.11 shows the elastic strain relaxation for the formation of QD. When deposited InAs material exceeds a critical thickness, 3D coherent islands are formed due to the relaxation of built-up strain [66]. The transition to 3D island growth occurs in less than 0.1 monolayers. The typical critical layer thickness for InAs/GaAs QDs is around 1.5 -3 monolayers (MLs), and the specific point at which this occurs is dependent on the growth conditions.

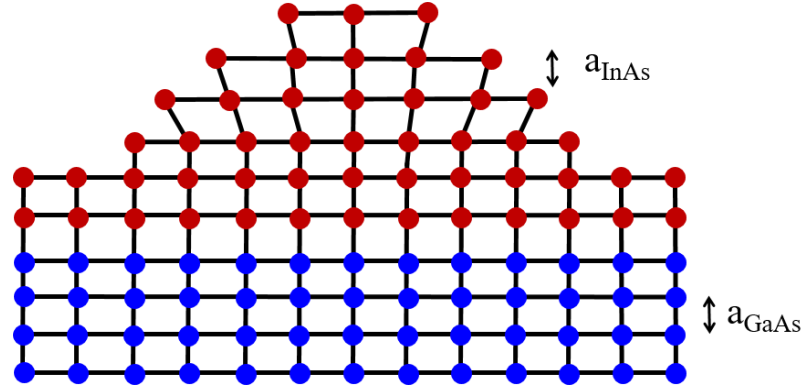


Figure 2.11: A schematic representation of elastic strain relaxation in InAs QD on GaAs.

2.4.1 Low-density InAs quantum dots

A recent focus has been on the research of single QDs for different applications such as single-photon light sources [9,67], pillar microcavities [68] due to the atomic-like spectra of individual QDs [69]. For single dot spectroscopy, the QD density should be in the order of 1 QD per μm^2 to be spatially resolvable. It's usually determined by the laser spot size used in spectroscopy or the aperture size used in masking techniques. In conventional SAQDs in S-K mode, the QD density increases quickly from no QDs to 10^{10} QD cm^{-2} at the critical point during the transition from 2D to 3D growth mode, as shown in Figure 2.12 [64]. InAs QDs on GaAs substrate with densities in the order of 10^9 – 10^{11} QD cm^{-2} can easily be obtained by varying optimum growth conditions. However, fabricating such low-density QDs (~ 1 QDs per μm^2) is exceptionally challenging due to this highly narrow coverage range, owing to extreme sensitivity to 0.01 ML of InAs

deposition [64]. Furthermore, this is due to the geometry of the MBE chamber, as shown in Figure 2.10. Uniform thickness can be achieved by rotating the substrate at constant rotation. The impinging molecular beams are oriented at a certain angle towards the substrate; therefore, the variation in QD density is proportional to the position of the indium cell. Although the As flux changes across the wafer, its influence appears to be negligible.

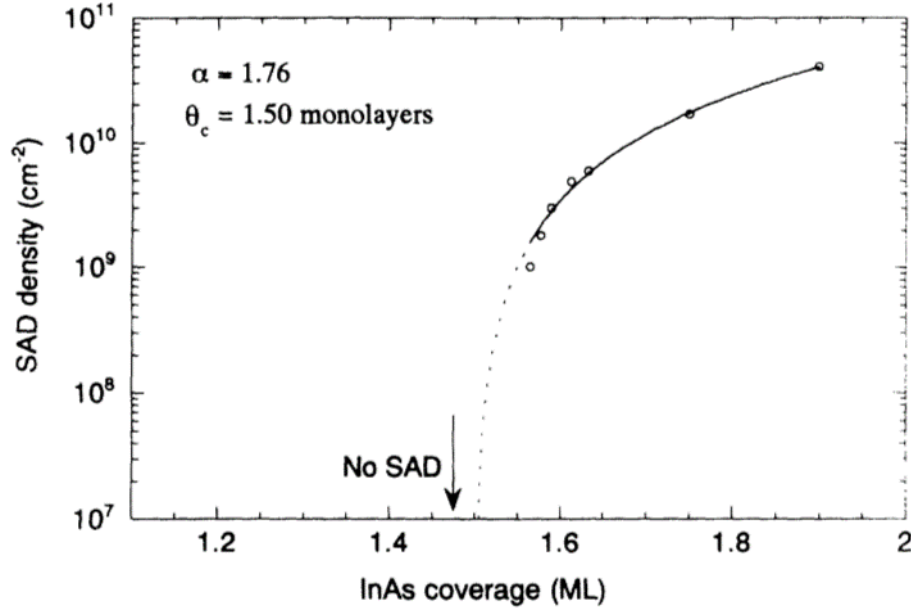


Figure 2.12: Graph showing InAs QDs density variation with increase InAs coverage [64].

Controlling the density, size, and distribution of these SAQDs is extremely difficult during the self-assembly process, even when temperature T , flux F , and coverage C are constrained. Such as if the growth temperature is low, deposited atoms do not have enough thermal energy to diffuse. This restricts the applicability of these devices and also restricts investigations of their underlying physics. To obtain such low-density QDs, many research groups have used techniques such as In-gradient [64,70,71], temperature gradient approach [72], annealing approach [73], and the growth on pre-patterned substrates [74]. In this work, the low-density InAs QDs are grown using two different deposition techniques, the homogenous In deposition and the In-gradient approach, as described in the following subsection.

2.4.1.1 Homogenous In-Deposition Approach

The homogenous deposition approach is also known as the annealing approach. In this approach, a subcritical InAs deposition, with subsequent annealing, leads to the formation of QDs. InAs is deposited with continuous substrate rotation close to the critical deposition thickness, which results in homogenous InAs deposition across the wafer, as illustrated in Figure 2.13.b. This subcritical InAs deposition with subsequent annealing results in a finite QD density. *Song et al.* have demonstrated that post-growth annealing of a WL with a thickness less than the T_c can result in the desired low-density QD ensemble in a controlled manner [73,75]. Annealing at slightly higher temperatures result in the formation of QDs and mitigate the QDs' inhomogeneous broadening by the Ostwald Ripening process [75,76]. A significantly low In growth rate and QD growth temperature are employed, which can be drastically reduced reduce the density by enhancing the migration of InAs. In this approach, densities in the order of 0.1-1 QDs per μm^2 can be achieved after careful calibration of substrate temperature and In-amount in QD.

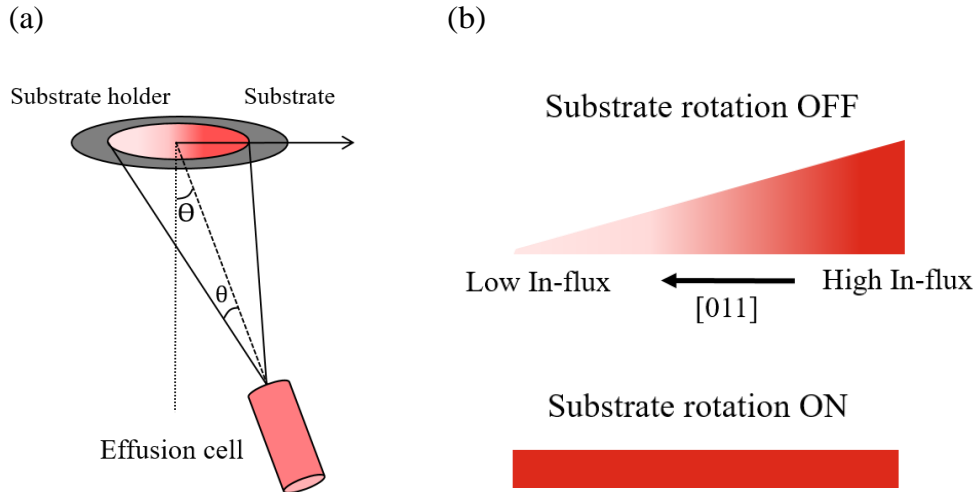


Figure 2.13: a) The effusion cell and substrate position in the MBE growth chamber [77]. b) Schematic of In thickness profile with and without substrate rotation.

2.4.1.2 In-gradient Approach

The In-gradient approach is the most widely used method to obtain low-density QDs. The angle of the effusion cell source to the substrate results in the uniform thickness gradient across the substrates as illustrated in Figure 2.13.a [13]. When the substrate rotation is turned off, the In-flux increases across a substrate direction. This results in flux distribution of over 10% from one side to other in a quarter of a 3" wafer (Fig. 2.13). In this approach, substrate rotation is stopped during the InAs deposition, producing an In gradient across the wafer with high QD density on one side of the wafer and no QDs on the other side. The dot density varies from no QDs at the low In-flux region to 10^{10} cm^{-2} on the high In-flux region. The beam flux distribution along the direction of the substrate gives a repeatable and continuous deposition of the deposited material (coverage). However, the desired low QD density is found in a small transition region between these two regions. It delivers quite reproducible low QD densities but only on a relatively small fraction of the wafer [9, 11].

In the In-gradient approach, the substrate rotation can be stopped during In deposition either for the full deposition (*full-gradient*) or for half of the deposition (*half-gradient*) or parts of deposition.

2.5 Quantum Dot Molecules

QDMs are vertically stacked pairs of self-assembled QDs. Coherent tunneling between two individual QDs results in the formation of quantum dot molecules. QDMs are analogous to hydrogen molecules and are made up of “artificial atoms” (individual QDs) paired together to form delocalized orbitals. However, unlike conventional molecules, the energy confinement and coupling between the two QDs can be modified individually. QDMs were first discovered to understand how two separate QDs interact with one another. Figure 2.14 shows the transmission electron micrograph (TEM) image of InAs QDMs with a barrier thickness of 6 nm [78].

Advances in the fabrication techniques and understanding of single QDs have brought coupled QDMs to the forefront of scientific research. Depending on the desired device application, the QDs can be organized in either vertical or lateral alignment in QDMs [11]. The most widely studied

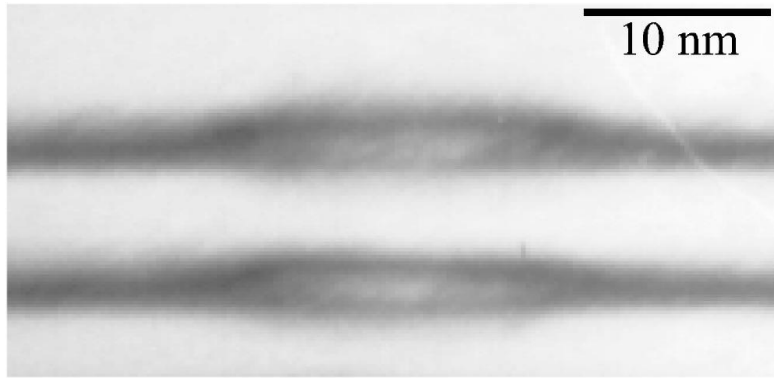


Figure 2.14: TEM image of an InAs/GaAs QDM. Adapted from [78].

are the vertically stacked QDMs, formed via strain-driven self-assembly process with two QD layers sandwiched by an intermediary epitaxial layer of different material that acts as a potential tunneling barrier. QDs in the second layer tend to nucleate directly above the dots in the first layer due to the strain caused by the first QD layer in the thin spacer layer (few nanometers), which drives the adatom migration in the second layer [47,79–81]. Different research groups have systematically investigated the probability of arrangement as a function of the distance between the QD positions and the shape and size of the QDs in the bottom layer [82].

The study vertical self-assembled InAs QDMs has been the focus of extensive research and opened the possibility of different novel and advanced device applications [79,80]. Initial research focused on high QD densities and the ordering process itself and found that InAs arrange self-assembled InAs vertically one above the other if the distance between the QD layers does not exceed approximately 20 nm [83]. The relative size and density of the QDs can be engineered by controlling the InAs deposition of each layer. The QDMs can be embedded in field-controllable heterostructure to precisely control the tunneling of charge carriers, electrons, and holes. The energy states of the two QD layers can then be varied relatively by applying an electric field. Thus, the electronic coupling, the state of charge of the molecule, and the transition energy can be determined [82].

In this work, low-density QDM heterostructures for quantum storage applications are grown, as described in detail in section 4.6.

2.6 Optical states in QDs and QDMs

Optical excitation of a single QD results in the generation of an electron-hole pair. Different excited states are generated in a single QD by the number of particles in the system, and these can be defined by the electrons and holes confined in the dots. For example, one electron and hole make an exciton (X^0), two excitons form a biexciton (XX), and two electrons and one hole form a negative trion (X^-).

In QDMs, charges can be distributed spatially in a number of different ways. In vertically stacked InAs/GaAs QDMs, the two QD layers have varying size, composition, and strain, resulting in distinct confined energy states. Thus, electrons and holes are likely to confine in the individual dots. Direct and indirect excitons are characterized by the spatial coexistence of electron and hole wavefunctions in the individual QD or distinct QDs in a QDM [13]. With the filling of electrons and holes in QDs, these form direct or indirect excitons depending on the distance between the QD layers. When an electric field is applied to induce resonance in, direct excitons and indirect excitons; coherent tunnel coupling results in the formation of symmetric and antisymmetric molecular states. These molecular orbitals generate energy level anticrossings that can be observed as a function of the electric field. These are the symmetric and antisymmetric states, which are also referred to as bonding and antibonding orbitals, respectively. Bonding orbitals have the lowest energy and are thus the most stable. The quantum-confined Stark effect changes in response to applied electric fields due to the various spatial arrangements of electrons and holes. Anticrossings are characteristics of bonding and antibonding orbitals and thus offer strong evidence of tunnel coupling [82]. Anticrossings are avoided energy level crossings caused by Pauli's exclusion principle, which states that two particles cannot share the same quantum state. The energy difference between the two molecular states is defined as the anticrossing gap. The extent of this gap is determined by the tunnel coupling, which is governed by the barrier layer's parameters. The extent of this gap is governed by the tunnel coupling, which is defined by the properties of the barrier layer between the dots. The carrier tunnelling depends on the substrate doping and the respective heights of QDs in the two layers [84]. The tunneling of the carriers, electron or hole, varies significantly and occurs at different rates due to their different effective masses.

Additionally, holes exhibit a spin-orbit interaction, which can significantly alter tunnel coupling [85].

CHAPTER 3

3 Experimental techniques

This chapter describes the experimental techniques used to grow and characterize the nanostructures studied in this dissertation. The first section describes the MBE system used to grow the QD samples. Various MBE growth factors, such as substrate temperature growth and growth rate, were optimized to obtain optimal growth conditions. The second section provides the ex-situ characterization processes. Atomic force microscopy (AFM) was used to analyze the surface morphology. Optical characterization of QD samples was done with PL setups. Further investigation of the PL and electrical measurements was carried out at Finley group, TU Munich.

3.1 Molecular beam epitaxy system and growth process

In this work, the heterostructures were grown using a solid source III-V MBE system from Dr. Eberl MBE-Komponenten. Figure 3.1 shows a schematic of the MBE system. The system comprises of four main chambers: (i) growth chamber, (ii) preparation chamber, (iii) transfer chamber, and (iv) load-lock. All the chambers and pumps are interconnected via gate valves, which allows the separation of each chamber. The system is pumped by a combination of a closed-cycle cryopump, ion gettering, and titanium sublimation pumps (IGP/TSP), enabling the system to operate in the UHV regime with a base pressure of less than 10^{-10} mbar at all times, except for load-lock. The growth chamber is surrounded by liquid nitrogen-filled cryo shrouds that prevent condensable contaminants like H_2O from condensing.

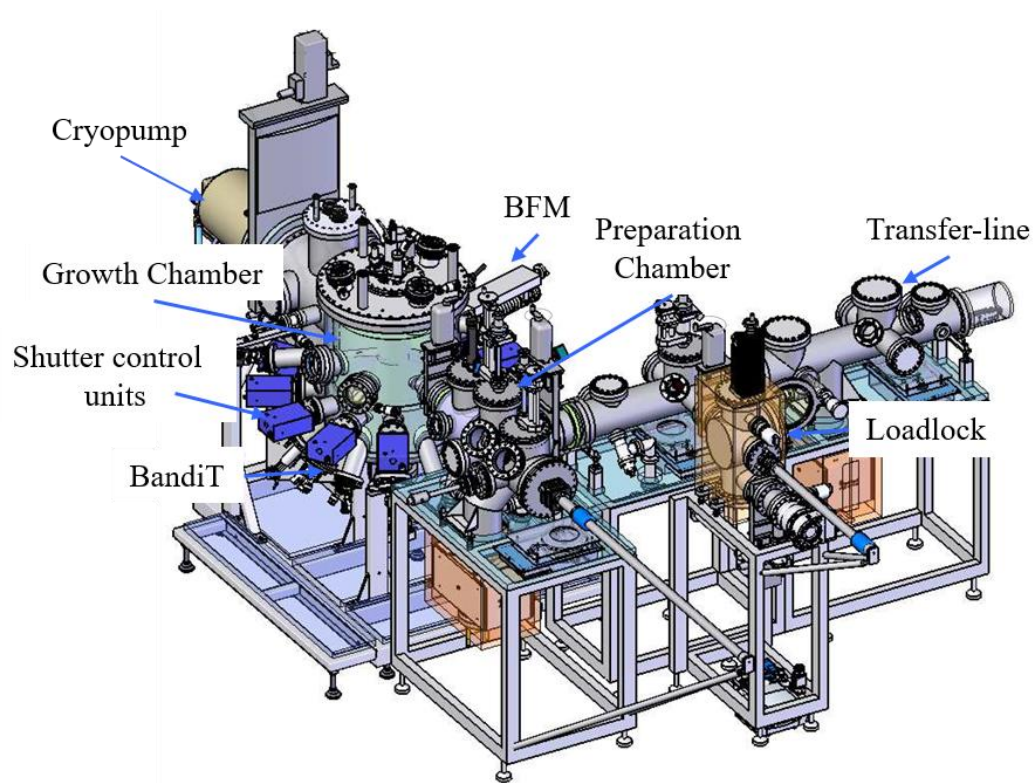


Figure 3.1: The schematic representation of the III-V MBE system employed in this thesis (MBE Komponenten).

Material sources are a critical component of MBE because they work at high temperatures and generate molecular beams of extremely high purity and uniformity over the substrate. The growth chamber contains 14 solid sources for the generation of molecular beams of Ga, Al, In, As, Sb, Si, and C, as shown in *Fig. 3.2*. These source materials (Al, Ga, In) are contained in (high purity) pyrolytic boron nitride (PBN) crucibles located in effusion cells of different capacities and placed at different positions in the growth chamber. In contrast, group V materials (As, Sb) are placed in valved cracker cells, which generate molecular beams with quick response and high precision. The temperature of the As cracking region balances the As species (As_2 or As_4) produced by the cracker cell. The silicon and carbon cells are composed of Si wire and a pyrolytic graphite wire, respectively, heated by direct current flow. As an n-type dopant, Si is employed, while C is used as a p-type dopant. These material sources are heated with a tungsten filament to achieve the appropriate material flux for growth. Each cell has a mechanical shutter that allows the beams to be turned on and off in fractions of a second. All the cells

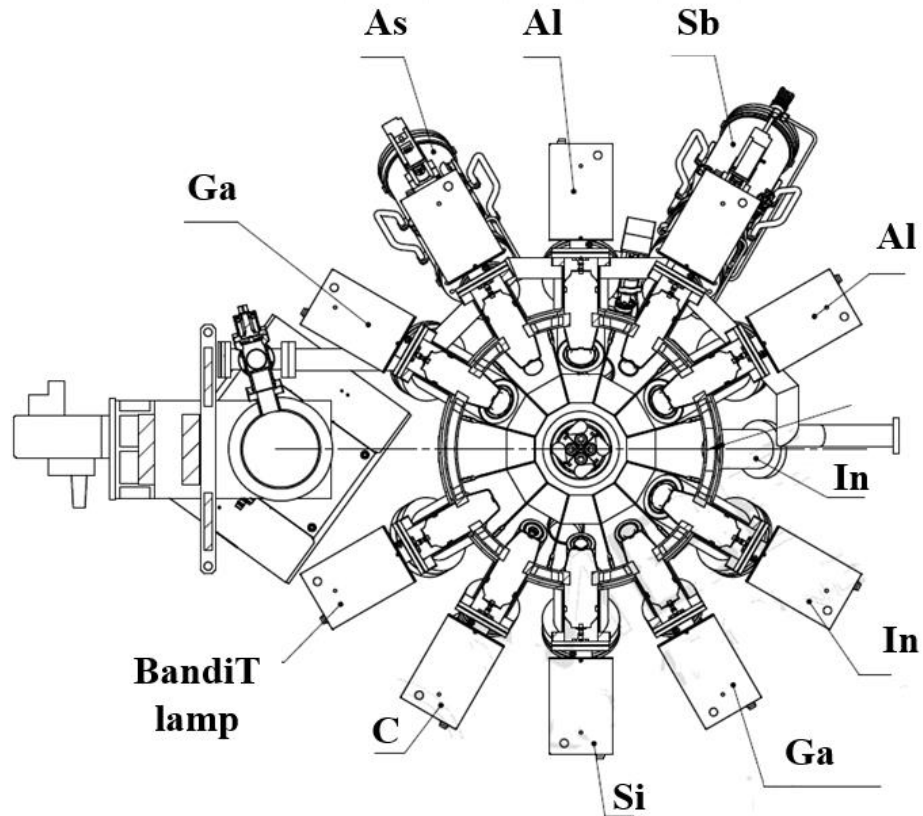


Figure 3.2: The configuration of different cells attached to the MBE (MBE Komponenten).

are connected to external water cooling tubes to help minimize the thermal load from the chamber. The background particles are monitored using a quadrupole mass spectrometer. This allows to monitor the contaminants in the growth chamber. An electron gun to study electron diffraction (RHEED) to characterize the sample and regulate the growth parameters. The substrate holder is attached to a substrate manipulator that rotates around a perpendicular axis to the chamber axis. The substrate is heated and monitored using a radiative heater with a thermocouple (T_c). The beam fluxes are measured using a beam flux monitor (BFM) placed in front of the substrate, which measures the BEP using an ion gauge and measurement of the growth rates obtained by analyzing RHEED oscillations. The substrate temperature is also measured using a BandiT band-edge thermometry system that measures the optical absorption edge. During epitaxial growth, the substrate manipulator is typically rotated at 10 rpm to

achieve more uniformity during the epitaxial layer deposition and heating of the substrate.

Wafers are introduced in and out from the system through a separately pumped load-lock chamber, ensuring that all other chambers are always under UHV. The pumping in the load-lock is maintained by the turbopumps and achieves the pressure of 5×10^{-8} mbar. This is equipped with a six-way magazine that simultaneously loads up to six wafers. The preparation chamber is equipped with a degassing heating station that allows wafers and wafer holders to be degassed before being placed in the growth chamber.

In this thesis, semiconductor heterostructures are grown on semi-insulating 3" or $\frac{1}{4}$ 3" GaAs (100) wafers from Wafer Technology Ltd. The wafers are epi-ready and used without any further chemical processing. The wafers are cleaved along [110] direction into quarters and placed upside down on a molybdenum sample holder in load-lock. The wafers are held in place by gravity. The sample preparation goes through the following steps after introduction in the MBE system:

- i) The wafers are loaded into the load-lock and are pumped via a turbo-molecular pump in order of pressure of 10^{-7} - 10^{-8} mbar. The wafers are degassed for 8 hours at 120 °C to desorb condensed water and impurities into the system. Once the pressure reaches 10^{-8} mbar, the wafers can be transferred to the transfer chamber.
- ii) After that, the substrate is transported via the transfer chamber to the preparation chamber. They are further degassed at a heating station at 200 °C for at least 1 hour or until degassing pressure spikes significantly. During degassing of GaAs(100) wafers, the chamber pressure increases typically from 10^{-10} to 10^{-8} mbar. Chamber pressure decreases to 5×10^{-9} mbar after one hour of degassing.
- iii) The substrate is transferred into the growth chamber when the pressure in both the preparation chamber and the growth chamber is less than 5×10^{-9} mbar. Growth chamber temperatures are generally 300 °C, and As flux is zero in the growth chamber when introducing the substrate. Then the metal fluxes (Ga, Al, and In) are measured, and then As flux at different values opens with BFM.

- iv) The substrate is then heated in the presence of As overpressure (2.2×10^{-5} mbar) to prevent the breakdown of GaAs. The substrate temperature was then increased to 620 °C to produce a streaky RHEED pattern, indicating surface oxide desorbed. Desorption of oxide on a GaAs surface is typically observed at 590 to 600 °C. After deoxidation, the surface is annealed to smoothen the surface. Further, the growth parameters are optimized using RHEED and substrate temperature using Bandit.

Following these stages, the different parameters are updated in the growth recipe in Epicad software to reflect updated values, growth of the required sample heterostructure can be commenced.

3.1.1 Substrate Temperature Control

The substrate temperature is one of the critical parameters during the epitaxial growth in MBE. The surface mobility of adsorbed atoms varies with temperature. Different material properties like surface roughness and carrier mobilities are strongly induced by the substrate temperature during the epitaxial growth. The growth of high purity GaAs generally takes place in the temperature range of 600-630°C. However, reliable temperature measurement of the substrate is not trivial. In our MBE system, the substrate temperature is measured using thermocouple (T_c), and band-edge (BandiT). Each method varies in terms of precision, reproducibility, and applicability:

- The T_c is positioned underneath the substrate manipulator close to the sample heater and has no physical contact with the substrate manipulator. The measurement is reproducible and covers the entire range of interest. As a result, it is ideally suited for temperature management. However, the temperature measurement can be considerably different from the temperature at the substrate surface.
- BandiT determines the temperature by measuring semiconductors' optical absorption edge shift as a function of temperature. It is based on light absorption as it passes through a semiconductor material. The absorption edge's wavelength in the observed spectrum can be attributed to a specific temperature. Optical bandgap measurement is the most accurate and reliable method used nowadays.

Recently, there has been interest in monitoring temperature utilizing the substrate's bandgap. The E_g decreases with increasing temperature in semiconductors given by the Varshni formula (Section 2.1). The bandgap can

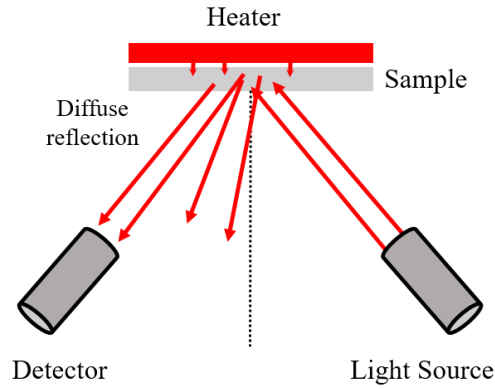


Figure 3.3: The schematic of BandiT configuration.

be evaluated by analyzing the spectrum of substrate heater radiation transmitted through the substrate or by analyzing the radiance of a specifically mounted filament light source. The light transmitted through the substrate and diffusely reflected from the rough rear surface is collected and examined spectrally in a monochromator.

In our MBE, the band-edge spectroscopy system by kSA BandiT is installed to measure the temperature via band edge thermometry. For semiconductors with a smaller E_g , such as GaAs, the near-IR spectral range between 800 and 1400 nm is suitable for detecting the absorption edge. The measurement can be done when the sample is illuminated by the heater radiation or external light source, as shown in *Fig. 3.3*. Light enters the substrate and is scattered at the unpolished backside of the wafer before passing through it. When light with an energy greater than the bandgap energy passes through the semiconductor, it is significantly absorbed, whereas light with lower energy is transmitted almost completely. The temperature-dependent bandgap induces spectral shifts in semiconductors. BandiT can also measure black body Pyrometry. This is one of the methods for measuring temperature using a BandiT.

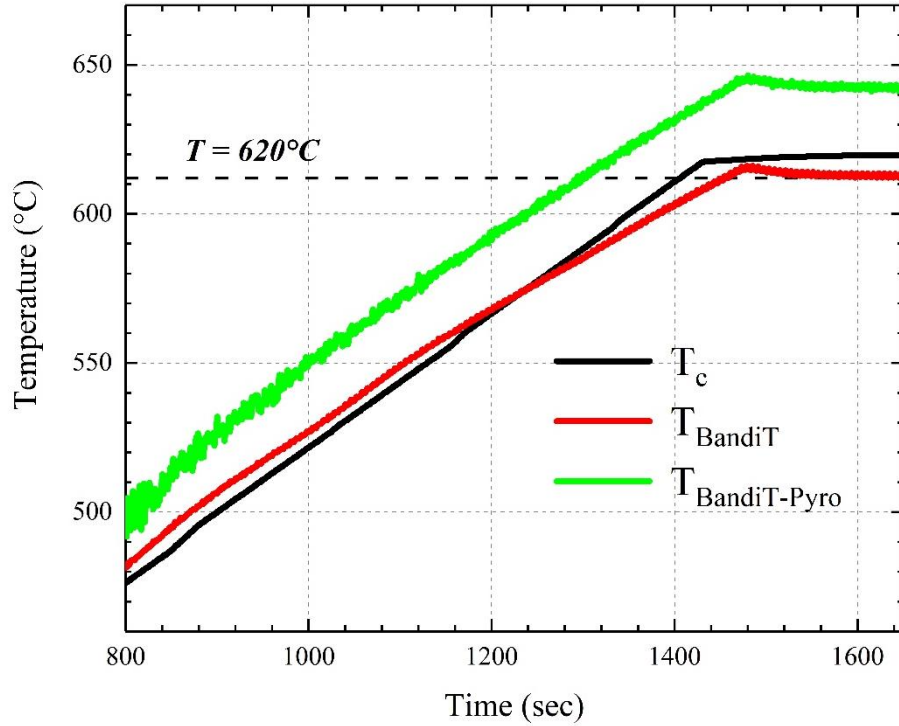


Figure 3.4: The different temperature measurements while ramping the substrate temperature.

All temperatures given in this work are BandiT readings. The BandiT temperature reading was used to reference the T_c , which is employed in the control loop. The bandit system does not refer to the theoretical band-edge but rather to the manufacturer's reference data. The substrate's material, thickness, doping type, level of doping, and manufacturer are mentioned in the references. The reference with the closest thickness and doping level to the actual wafer was chosen as the best match. The BandiT system measures real-time measurements and calculates the temperature from each spectrum. During the rotation of the sample manipulator, the spurious variation of the calculated temperature is $\pm 1^\circ\text{C}$. The band-edge temperature is more reliable based on the physical properties of the sample material than the thermocouple or pyrometer, which are strongly influenced by the chamber geometry. Figure 3.4 shows the different temperature measurements while ramping the substrate temperature to software set-point of 620°C .

3.1.2 RHEED and surface reconstructions

RHEED is an essential apparatus in the MBE system that allows us to analyze structural information of the surface crystallography at the atomic level during epitaxy. It allows in-situ monitoring of growth processes of thin-film during growth. In RHEED, a finely collimated electron beam with energies of 10-50 KeV is directed at grazing angle on the substrate, and diffraction patterns are detected on the fluorescent screen and captured using a CCD camera. The RHEED gun in our MBE system is a Staib instrument, which we run at 10 KeV. The incidence angle is small $1-3^\circ$ with respect to the surface so that the penetration depth of the beam into the surface is restricted to a few monolayers of the sample. Figure 3.5 depicts a schematic representation of RHEED. The diffraction pattern can be explained by Ewald's construction in the reciprocal lattice. After undergoing diffraction, the elastically scattered electrons interfere constructively. According to the Laue condition, for diffraction, the difference between the incident and diffracted wavevectors must be equal to the reciprocal lattice vector [24]. The diffraction pattern depends on the crystallographic orientations of the diffracting surface and the arrangement of surface atoms. Figure 3.6 illustrates the schematic representation RHEED pattern corresponding to different kinds of epitaxial surfaces. The transition from amorphous to the ordered surface condition can be recognized from the RHEED pattern from diffuse scattering to a diffraction pattern according to a structured surface. The RHEED pattern on the smooth surface generally consists of elongated streaks that are normal to the surface [86].

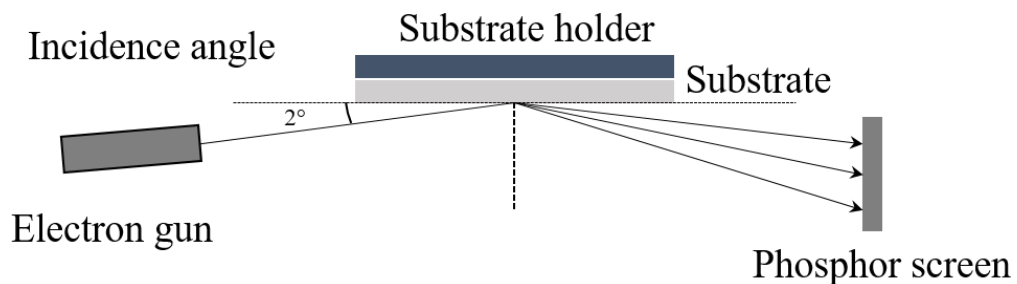


Figure 3.5: The schematic of the RHEED diagram showing the incidence angle with respect to substrate and detector.

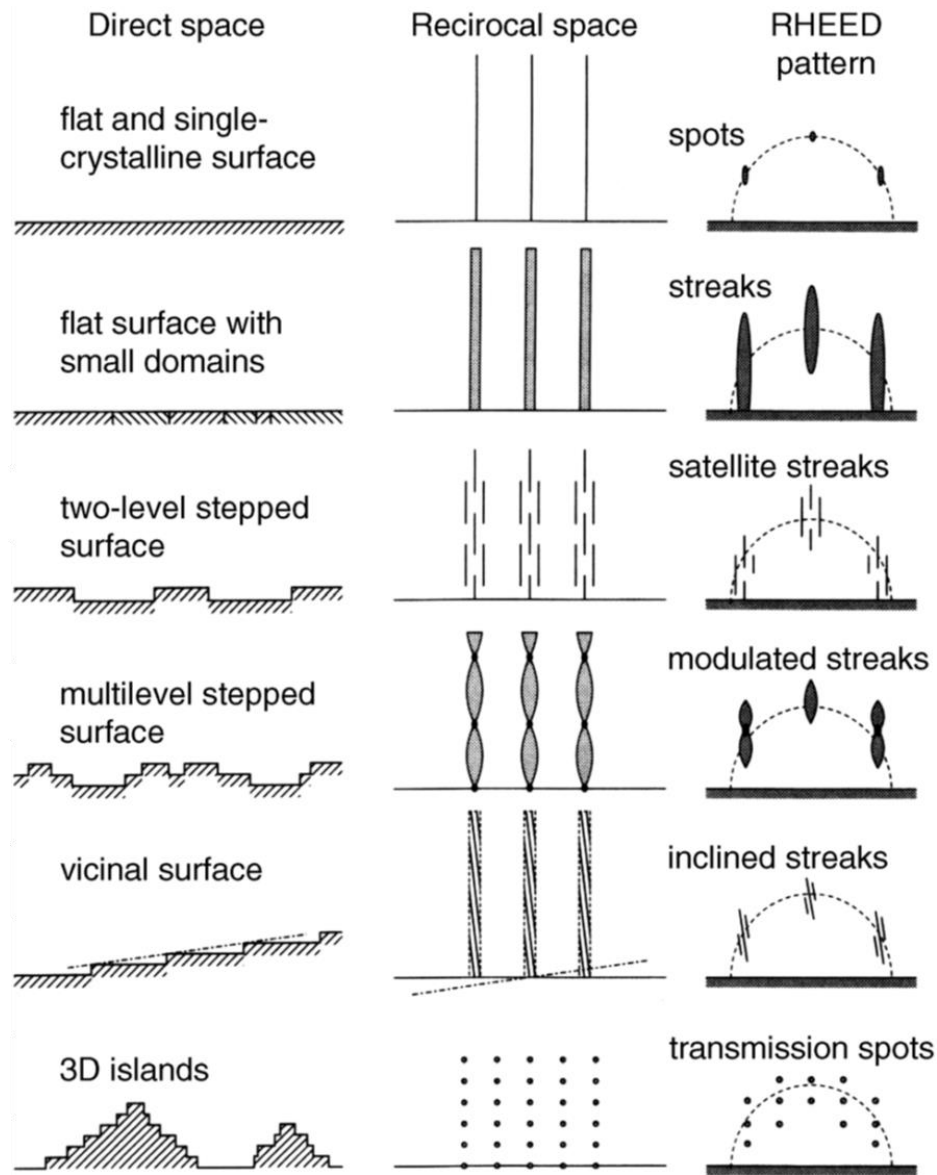


Figure 3.6: Schematic of different kinds of epitaxial surfaces and the corresponding pattern as observed in RHEED [87]

For RHEED analysis, GaAs wafers are aligned in the $[110]$ direction, and the rotation is stopped to record the RHEED oscillation and image. The diffraction pattern displays a spotty pattern following removal of oxides after thermal deoxidation of the GaAs(100) surface. Depending on RHEED intensity oscillations, we can analyze the growth mode via island nucleation or step flow (no oscillations). The oscillations period corresponds to the time required during the deposition of one ML of GaAs. By examining the time

evolution and shape of diffraction patterns in RHEED, one may track the growth of GaAs in MBE.

The stoichiometry of III/V materials is influenced by a number of growth parameters, including substrate temperature, impinging fluxes, and the III/V flux ratio. The surface energy of the system is affected by the dangling bonds that form at the boundary between solid and ambient during the deposition. Therefore, in order to acquire a more stable structure, surface atoms of groups III and V reorganize themselves to minimize the surface energy of the deposited layer. This rearrangement of surface atoms is known as surface reconstruction. When grown in ambient conditions on a GaAs(100) surface, a phase diagram consisting of many surface reconstructions can be found [88] and are represented in Figure 3.7, for different growth temperatures and As_4 to Ga BEP flux ratios. For atomically smooth GaAs surface, one observes $c(4 \times 4)$ or (2×4) reconstruction depending on the As flux and substrate temperature [89]; these are most stable in the temperature range of 500–620°C and 400–500°C respectively, in moderately or severely arsenic-rich environments. For example, as illustrated in Figure 3.7 the low growth temperatures and high As_4 to Ga ratios lead to (2×4) reconstructions which

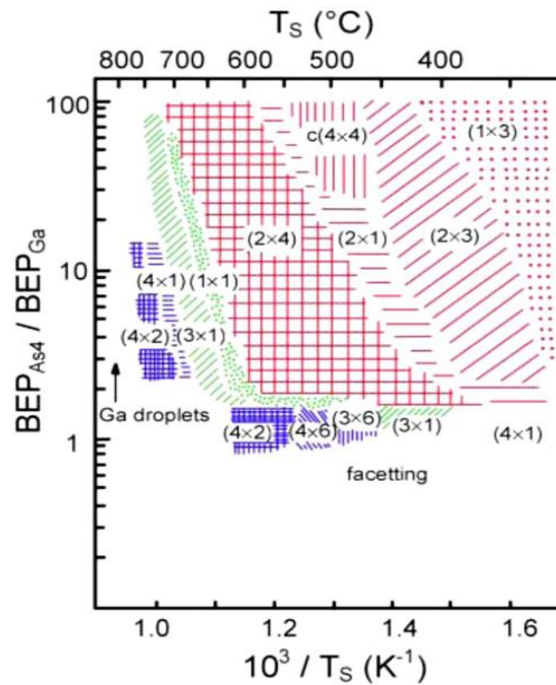


Figure 3.7: Surface phase diagram for the epitaxial growth of GaAs from Ga and As_4 beams on GaAs (100) substrate [88].

are also called As rich (or As-stabilized) conditions [86]. In contrast, (4x2) reconstructions are an indication of Ga-rich (or Ga-stabilized) circumstances, which are defined by high growth temperatures and low As₄ to Ga ratios. Several other transition structures arise in relatively narrow development circumstances between the primary (2x4) and (4x2) structures. The growth of GaAs at 600°C, surface 2x4 reconstructed surface is observed, which gives smooth surface with surface roughness of 0.3nm.

3.1.3 Calculation of growth rate

In MBE, the precise calculation of growth rates (beam fluxes) is significantly important for the growth of compound materials and for the attainment of high-quality heterostructures for various applications, such as the growth of GaAs/AlAs superlattices. In our MBE system, the growth rate of these materials can be determined using RHEED intensity oscillations and BandiT's pyrometric oscillations. These are described in detail below:

- RHEED intensity oscillations provide a fast and most accurate way to determine the 2D material growth rate. These oscillations are produced by the periodic shift in surface topography that occurs as a result of the deposition of epitaxial layers on the surface. These oscillations occur due to the periodic shift in surface roughness that occurs with the deposition of epitaxial layers. With material deposition, the RHEED intensity increases or decreases with depositing layers, and corresponding oscillations are observed with a period oscillation equal to one ML thick layer. However, there could be uncertainty in the measurement due to beam positioning error and flux transients, with up to ~ 2 % error [90].
- In BandiT, the growth rate is determined by the pyrometric interference oscillations of the deposited film that has a different refractive index than the deposited layer or substrate beneath. When a sample reaches a sufficient temperature, blackbody radiations are emitted in all directions. The emitted radiation is reflected off the interface between the film and the substrate, interfering with radiation emitted directly from the surface. BandiT detects this interference to monitor intensity oscillations at any wavelength. Peak intensity is observed when the film's optical path length is a multiple of the wavelength of light ($\frac{\lambda}{2\eta}$) where λ is wavelength and η

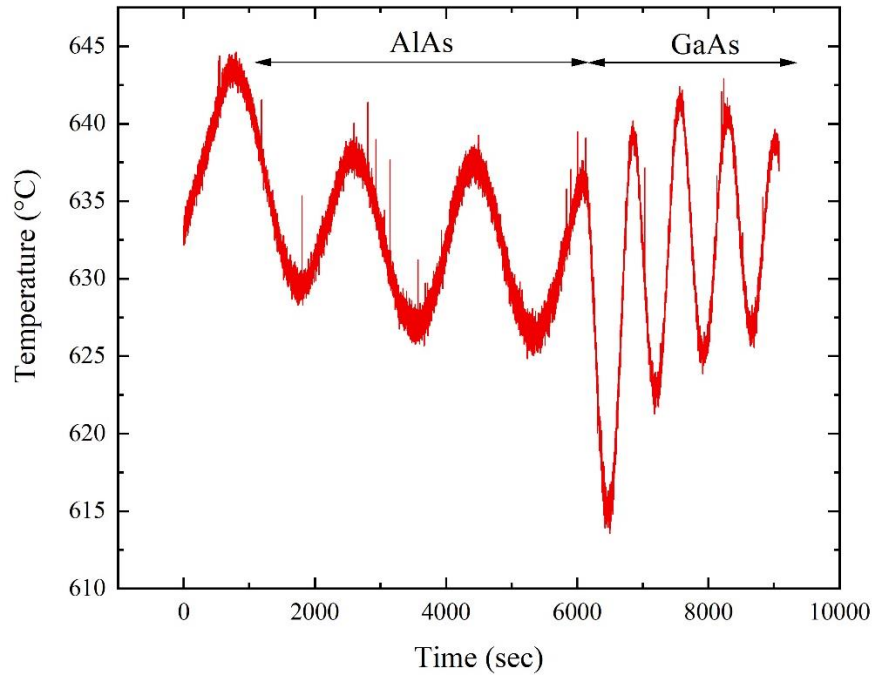


Figure 3.8: Pyrometric oscillations from BandiT pyrometry for AlAs and GaAs.

is the refractive index. Figure 3.8 illustrates the intensity oscillations during the growth of GaAs and AlAs measured at a wavelength of 1000 nm. The growth rate (G) over a period (T) can be determined using the following equation:

$$G = \frac{1}{T} \cdot \frac{\lambda}{2\eta} \quad (3.1)$$

In order to obtain the most accurate value, the growth rates of GaAs and AlAs were measured using both RHEED and BandiT pyrometry. The measurements were carried on a GaAs (100) quarter wafer. The substrate was heated to 600°C under an excess As₄ flux (2.2×10^{-5} mbar). In order to observe the RHEED patterns, the substrate rotation was stopped and aligned along [110] direction. The III to V ratio is adjusted to observe maximum oscillations, while group III flux determines the growth rate. GaAs and AlAs are typically grown at rate of 0.2 nm/sec (0.7ML/sec) and 0.1 nm/sec, respectively. Ga to As flux ratio was around 18 during the growth of atomically smooth GaAs, resulting in a smooth surface with a surface roughness of approximately 0.3 nm.

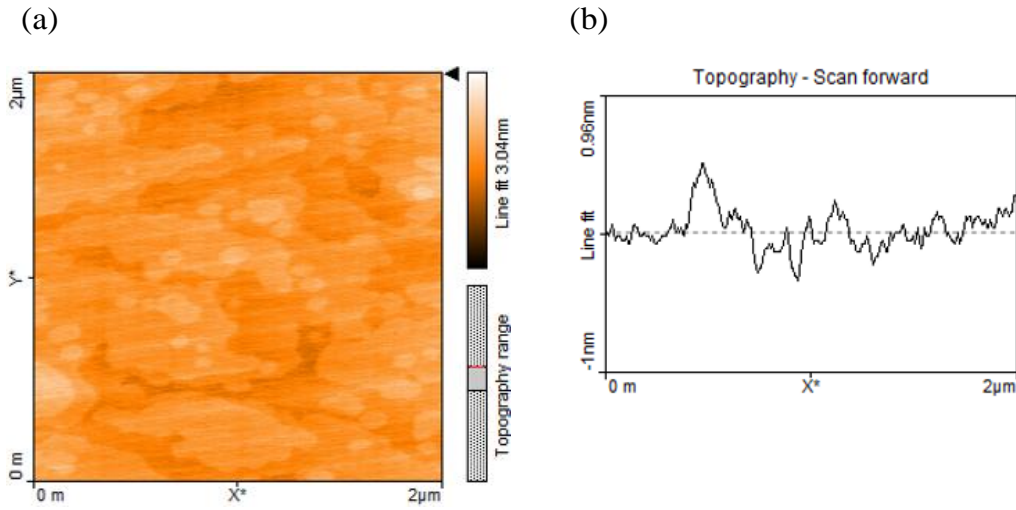


Figure 3.9: AFM image atomically smooth GaAs deposited after deoxidation with RMS roughness of 0.3 nm, b) The linescan along the image.

To observe BandiT pyrometric oscillations, 500 nm of AlAs was deposited at 600°C, followed by the deposition of 700 nm GaAs. Figure 3.8 illustrates the pyrometric oscillations measured at a wavelength of 1000 nm. The growth rate was calculated using the *eq. 3.1*. The refractive index at the growth temperature for GaAs and AlAs was adopted from [91].

Further HRXRD was performed in ω -2 θ mode to calculate the layer thickness for the sample. The different growth rates measured for the same cell temperature and under the same conditions are summarized in table 2. The growth rate measured by RHEED varied by $\pm 2\%$, possibly due to the dependence on measurement position on the wafer. The layer thickness by XRD provides the most accurate values. Based on these measurements, a factor was calculated. Further, this was used with pyrometric oscillations to

Table 2: GaAs and AlAs growth rate calculated at given cell temperature.

| Material (cell temperature) | RHEED ($\text{\AA}/\text{s}$) | Bandit Pyrometer ($\text{\AA}/\text{s}$) | HRXRD ($\text{\AA}/\text{s}$) |
|--------------------------------|---------------------------------|-----------------------------------------------|------------------------------------|
| GaAs (969.9°C) | 1.937 | 1.922 | 1.983 |
| AlAs (1143.7°C) | 1.011 | 0.950 | 0.96 |

to calculate the most accurate values during the growth of high-quality superlattices.

3.2 Atomic force microscopy

Atomic Force Microscopy (AFM) is a scanning probe microscopy technique used for surface topography imaging and surface analysis of the material's properties on a nanoscale. AFM is based on the interatomic forces that exist between the atoms at the cantilever tip and surface of a sample when they are brought very close to each other. This is the underlying principle of AFM [92]. The AFM instrument generally consists of a sample holder with x/y piezo, cantilever, a laser, a position-sensitive photodiode (PSPD), and a piezo PID controller as illustrated in Figure 3.10. AFM uses a cantilever beam with a high fine tip to scan across the sample. As the cantilever moves over the surface topography, it is deflected due to attractive or repulsive forces of the cantilever tip to the sample surface. The distance between the tip and the sample can be modulated by a piezoelectric scanner tube. The laser is reflected from the mirrored backside of the cantilever depending on its deflection. The reflected laser beam is tracked by a PSPD is used in a feedback loop to track the surface for imaging. The PSPD has a quadrant shape with four independent photodiodes. This data is transferred back to a computer, which creates a map of the topography and other desired

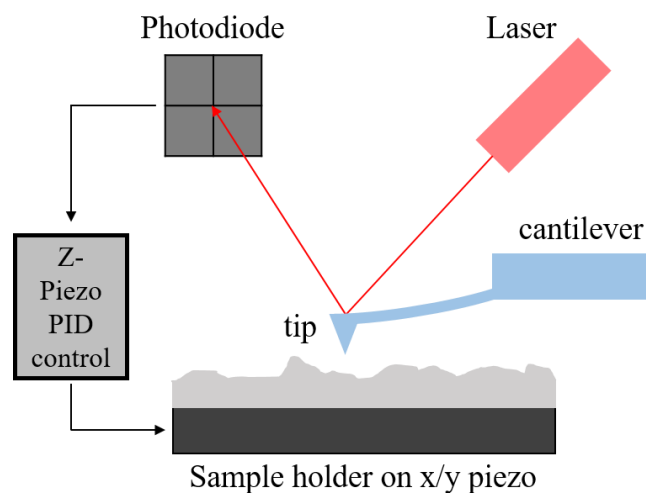


Figure 3.10: Schematic sketch of an AFM setup.

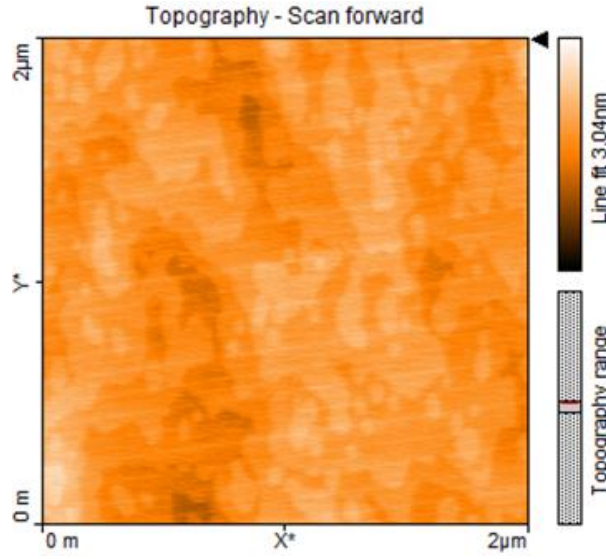


Figure 3.11: a) AFM image of GaAs surface with RMS roughness of 0.2 nm.

attributes.

In static mode (contact mode), the cantilever is moved across the sample at a constant force to maintain the deflection. The cantilever's deflection is proportional to the force exerted by the tip on the sample. This is the fundamental principle of static AFM, in which the force is estimated using Hook's law. The force can be computed using Hook's equation from the cantilever bending deflection variation.

In this work, AFM measurements were performed using the Nanosurf Mobile S AFM system. The measurements were done in static mode (contact mode) using PPP-CONTR cantilever tips from Nanosensors. The cantilevers had highly doped pyramidal silicon tips and tip radius of 7 nm and a spring constant of 0.2 Nm^{-1} . The detecting side of the cantilevers was coated with a 30 nm thick layer of Al to reflect the laser's light. The scan area varied from 0.5 μm to a maximum area of 9.8 μm^2 .

The surface topography was analyzed with regard to the root mean square (RMS), defined as

$$S_q = \sqrt{\frac{1}{N} \sum_{n=1}^n (z_i - \bar{z})^2} \quad (3.2)$$

where n represents the total number of measurements points, z_i is the height at every i measurement point, and z is the median value of the height. Figure 3.11 shows the surface of atomically smooth GaAs with roughness (S_q) of 0.2 nm.

3.3 Photoluminescence spectroscopy

Photoluminescence (PL) spectroscopy is a fundamental technique used to characterize the optical properties of semiconductor materials. It is a non-destructive and contactless method for exploring intrinsic electronic transitions across energy levels and extrinsic transitions of semiconductor impurities and defects. When a photon of energy greater than the bandgap energy of a material is incident on it, it may be absorbed, thereby exciting charge carriers (electron-hole) from the VB up to the CB across the forbidden energy gap. During photoexcitation, charge carriers have excess energy, which they lose before resting at the lowest possible energy level in the CB.

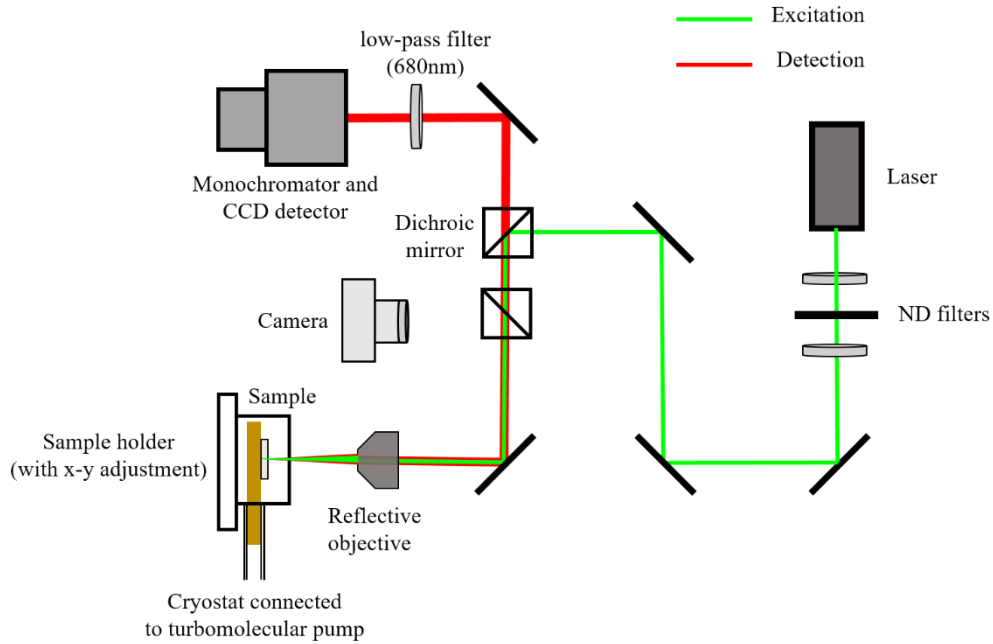


Figure 3.12: Schematic sketch of the photoluminescence setup.

The charge carriers (electron) relax by emitting a photon to the CB minimum. This process of photon excitation followed by photon emission is called photoluminescence. Thus, the photon's energy directly is a direct measure of the bandgap energy (E_g). The experimental setup for PL

spectroscopy is depicted schematically in Figure 3.12. The PL apparatus consists of an excitation laser diode, focusing optics, cryostat, monochromator, and CCD detector.

The excitation source is a continuous wave laser with 532 nm (2.33 eV), well above the bandgap of GaAs (1.42eV). The laser can operate at a maximum power of 4.5mW and be reduced by different natural density (ND) filters. The sample is mounted on a copper sample holder inside the cryostat to cool the sample for low-temperature measurements with liquid nitrogen (77K)

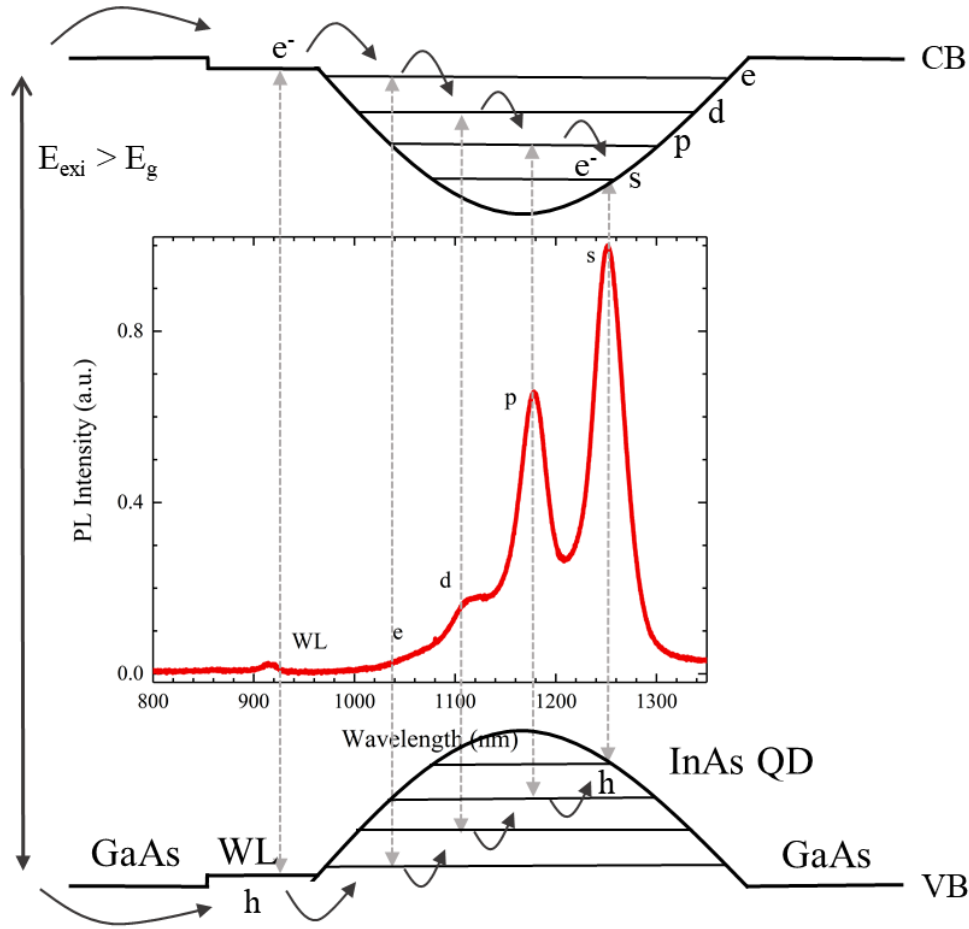


Figure 3.13: shows a room temperature of the PL spectrum of a QD ensemble with different energy states.

and liquid helium (16K). The cryostat of MicrostatHe by Oxford Instruments can be moved in x and y direction by micrometer screws. The laser is focused on the sample with a spot size of 3-4 μm using a Thorlabs LMM-15X-P01 reflecting microscope objective having a 0.30 numerical aperture. The same

microscope objective is used to collect PL signals in backscattering mode. The collected PL signal is dispersed using a monochromator Acton SP2150 from Princeton Instruments with a focal length of 0.150m and a 600mm-1 grating. The InGaAs line detector of Andor iDus DU490A-1.7 was used to detect the signal, which operates at a temperature of -60°C . The PL energy is generated by an ensemble of QDs with varied shapes, sizes, and compositions, resulting in a spectrum. The optical characteristics of self-assembled QDs can be investigated using PL. Firstly, the electron-hole pairs are generated into the bulk GaAs material, captured by the QDs through the non-radiative emission of phonons, and then relaxed in the ground state. After relaxation, the recombination takes place by emitting a photon. The typical PL spectra of an ensemble of InAs/GaAs QDs are depicted in Figure 3.13. The PL intensity represents optical quality, the PL energy depends on size and composition (ensemble of QDs), and the FWHM depicts energy that varies from dot to dot. The inhomogeneous broadening is represented by Gaussian distribution. The higher and lower energy peaks correspond to the transitions from the electron ground state (GS) to the hole GS, from the first excited electronic state to the first excited ground state, respectively.

3.4 PL imaging and electrical measurements

The optical and electrical measurements of the QD and QDM samples were carried out by Frederik Bopp in the Finley group at TU Munich.

3.4.1 PL wafer mapping and imaging setups

The wafer mapping of QD samples was carried with a low-temperature setup for spatially resolved PL. The sample is excited using a laser operating at 1.96 eV above the GaAs bandgap. The sample is mounted in a liquid helium cryostat cooled to 10 K and allows to scan a maximum sample size of 2". For mechanized measurements across the wafer, the laser is coupled with multimode fiber (TypeAFS50/125Y Thorlabs) and focused on the sample using a 10 mm focal length lens. The sample's photoluminescence emitted is collected using the same lens used for excitation, split in half by a 50:50 beam splitter, and analyzed using a grating spectrometer with an InGaAs line array detector.

Further, the investigation of QD densities was done in a PL imaging setup with a resolution allowing to identify single QDs. The PL generated by the QDs is photographed using the combination of a 63x microscope objective, a 1378 meV low energy pass filter, an $f = 400$ mm achromatic lens, and an ATIK314L+ astronomy camera that is highly sensitive for QD emission with photon energies of ~ 1300 meV. A white light source stimulates the sample, guided through a 1550 meV high-energy pass filter and a 50:50 beamsplitter. The sample is cooled to 10 K, identical to the wafer-mapper configuration.

Figure 3.14 shows wafer mapping in a false-color representation of PL recorded from the QD emission. Fig.3.14.b shows the typical QD luminescence image at one of the point QD.

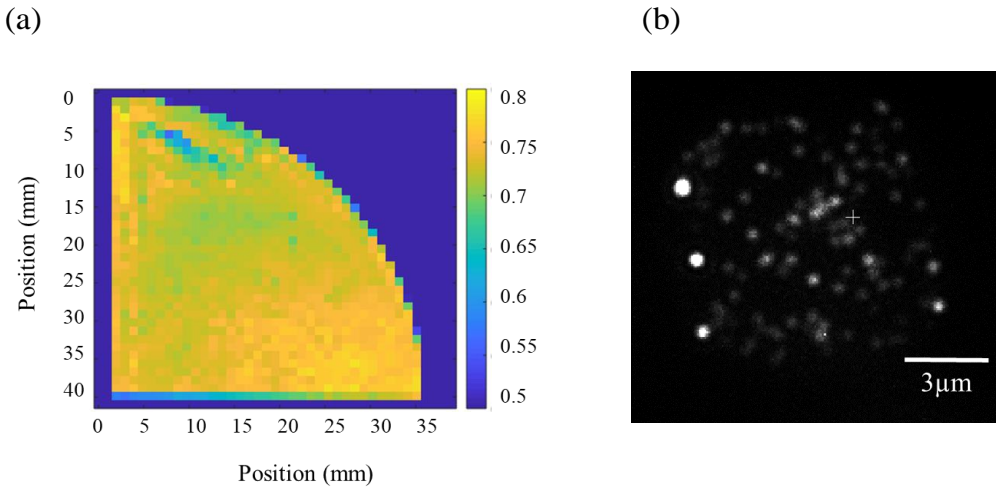


Figure 3.14: a) Wafer mapping of QD sample represented in the false-color plot. b) Shows the photoluminescence image of the same sample.

3.4.2 Electric field dependent PI setup

In order to determine the spectrum of the most energetically low orbital excited states in QDMs, electric field-dependent PL-excitation (PLE) experiments were done. The setup consists of a 1:2m long sample stick cooled to 4:2K in a liquid helium transport Dewar. A low-temperature microscope is contained in a vacuum-insulated tube on the sample stick. A tiny amount of He-exchange gas is introduced into the vacuum area and thermally coupled to the He-reservoir to cool the microscope. Low-temperature sample placement is made possible with the use of three Attocube (ANP101/RES) slip-stick piezo positioners and a high

numerical aperture microscope objective (NA=0.6). Single-mode and multimode optical fibers are used to transmit and receive optical signals in and out of the system. The sample was stimulated in the wetting layer at 1.49 eV for this PL experiment. Typical electric field-dependent PL measurements were made with field strengths ranging from 10.4 to 34.4 kV/cm.

A very detailed description of the different PL setups is given in the Doctoral thesis of Kai Muller, TU Munich [93].

CHAPTER 4

4 Results and discussion

This chapter provides a thorough discussion of the findings of this thesis. Section 4.1 describes the low-density SAQDs fabricated by SK growth mode employing two different In-deposition approaches: homogeneous deposition and In-gradient deposition approach. Section 0 covers the QD growth parameters studied and their effects on QD characteristics. The low QD densities were assessed utilizing different characterization techniques. Further, section 4.6 describes the QDM heterostructures fabricated using the low-density QD growth approach for electron and hole storage applications.

4.1 Quantum Dot Growth

In this work, low-density self-assembled InAs QDs are fabricated on GaAs(100) by MBE. The epitaxial development of low-density InAs QDs is subtle and susceptible to even small changes in MBE growth conditions such as growth temperature, the vapor pressure of As (the element ratio of III/V), growth rate and interruption mode, as well as composition and thickness of the overgrowth layer [67]. These factors affect the growth of low-density QDs, as discussed in section 2.4.

The epitaxial growth of InAs on GaAs is often done at a slightly lower temperature (400°C–550°C) than for GaAs homoepitaxy (550°C– 600°C) due to its low congruent vaporization temperature on GaAs at high temperature [94]. The InAs QDs were grown at a low growth rate of 0.017

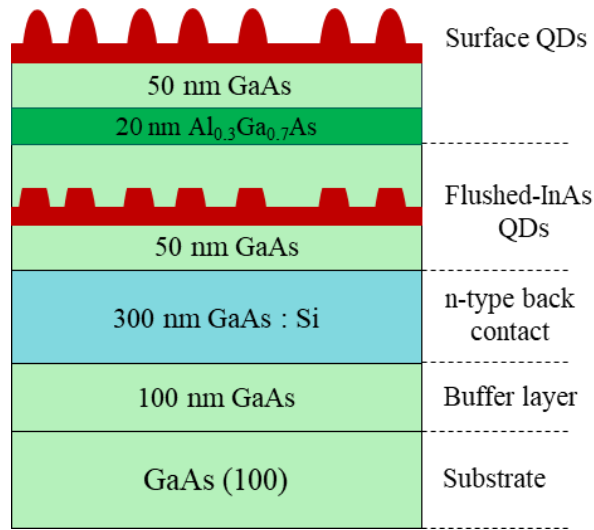


Figure 4.1: The layer sequence for the InAs QDs heterostructure.

ML s^{-1} with a corresponding In-cell temperature of 740°C . The slow growth rate reduces the size fluctuations in the QDs and allows for greater control over the growth of the QDs [16]. Also, the Ga/In intermixing during the growth process is reduced, resulting in greater In content in QDs. The growth rate of InAs is calculated with RHEED oscillations while growing the $\text{In}_x\text{Ga}_{1-x}\text{As}$.

The samples were grown on quarters and full 3" semi-insulating GaAs(100) wafers (Appendix A). The layer sequence adopted for the growth of the QD samples is sketched schematically in Figure 4.1. The samples usually contain one buried layer of QDs for PL studies emitting around 930 nm and surface QDs for AFM investigations. A 100 nm GaAs buffer layer was grown at 610°C after thermal oxide desorption at 620°C under a constant As flux of 2.2×10^{-5} mbar. The buffer layer reduces the impurity transfer from the substrate to the film and smoothens the surface. Following that, a 300 nm GaAs doped with Si ($2.0 \times 10^{18} \text{ cm}^{-3}$) is deposited as n-type back contact. Following this, the temperature of the substrate is decreased to the appropriate QD growth temperature as required for the two different In deposition approaches. The As pressure is reduced from 2.2×10^{-5} mbar to 1.5×10^{-5} mbar during the QD growth.

SAQDs are grown using the growth interruption method where InAs are deposited in cycles, with 4 seconds of deposition and 4 seconds of breaks. This interruption of growth promotes InAs migration on the surface [95]. Generally, for the formation of QDs, 18 cycles of InAs is deposited, which

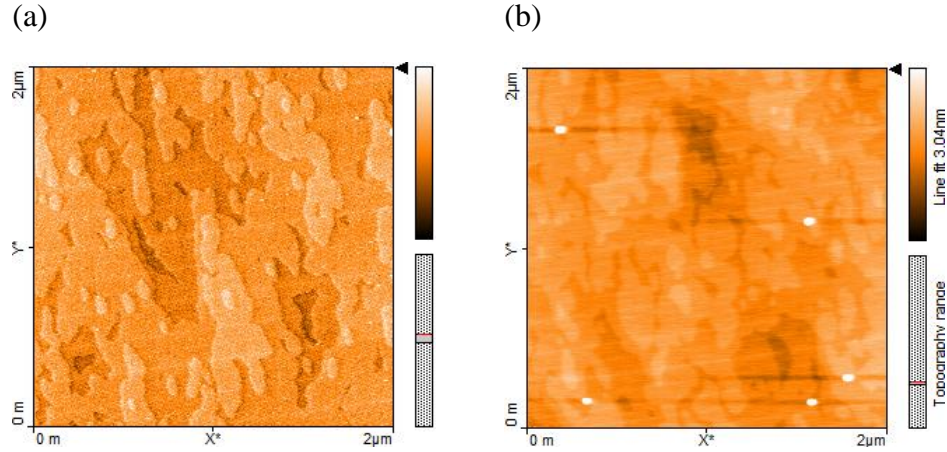


Figure 4.2: AFM images of InAs grown on GaAs(100) at 480°C substrate temperature: a) close to T_θ , atomic steps can be observed and b) InAs QDs formed with deposition above T_θ .

should be very close to critical thickness ~ 1.5 ML. Figure 4.2 shows the AFM image of InAs deposited at 480°C. The 2D islands are visible with the formation of small QDs (Figure 4.2.a) and, continue to form with subsequent deposition resulting in QDs (Figure 4.2.b).

Following the formation of QDs, the dots are completely or partially overgrown with GaAs at the same temperature. This is followed by an immediate increase of the substrate temperature to 610 °C with a temperature ramp of approximately 20 K/min. At this temperature, 90 nm GaAs is deposited, followed by 40 nm $\text{Al}_{0.3}\text{Ga}_{0.7}\text{As}$ barrier layers for the confinement of free (electron and hole) carriers. Finally, a 50 nm GaAs layer is deposited on top. The layer sequence is terminated with surface QDs grown as discussed above. A simpler layer sequence containing only surface QDs on a 100 nm GaAs-buffer layer was employed for some pure AFM studies and calibration runs.

4.1.1 Homogenous Deposition Approach

In this approach, InAs are deposited at a slightly lower substrate temperature of 480°C for the QD growth. After the deposition of the GaAs buffer layer at 610°C, the substrate temperature was decreased to 480°C within 7 minutes. This was followed by a temperature stabilization phase of approximately 5 mins, during which the software setpoint was adjusted so that the BandiT temperature was exactly $480 \pm 0.5^\circ\text{C}$. This is a crucial step and the T_c temperature had to vary within $\pm 3^\circ\text{C}$ to maintain the BandiT

temperature of 480°C. Then 50 nm of GaAs were deposited, followed by InAs deposition in a cycled mode (4s deposition, 4s break) under a constant As_4 flux (1.5×10^{-5} mbar), employing a continuous substrate rotation of 10 rpm. A slow deposition rate of 0.017 ML s^{-1} is used to deposit 18 or more In cycles for QD formation. To fine-tune the In amount, the last deposition interval of variable length was added, which was adjusted to 0.1 s. At our In-deposition rate, this amounts to an increment of 0.002 MLs. The amount of In deposited is close to the critical thickness, which should be approximately 1.5 ML as stated in [64]. After In deposition, the substrate temperature was ramped to 505 °C within 25 s and annealed at this temperature for 60 s. This annealing step results in the formation of QDs. The substrate temperature is then decreased by 15 °C in 15s. Subsequently, the samples were either cooled in 7 min to 300 °C (surface QDs) or 480 °C (buried QDs). Figure 4.3 shows the BandiT temperature profile for InAs QDs sample series grown with similar growth conditions. The QD growth temperature adjustments were done before the start every sample growth.

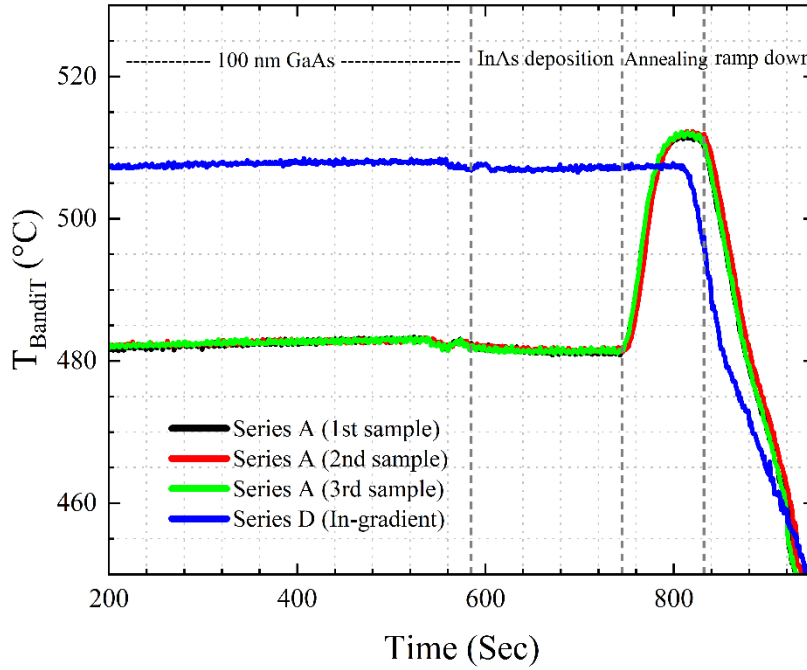


Figure 4.3: Temperature profile for InAs QD samples grown by Homogenous deposition approach (Series A with three samples) and In-gradient approach (Series D).

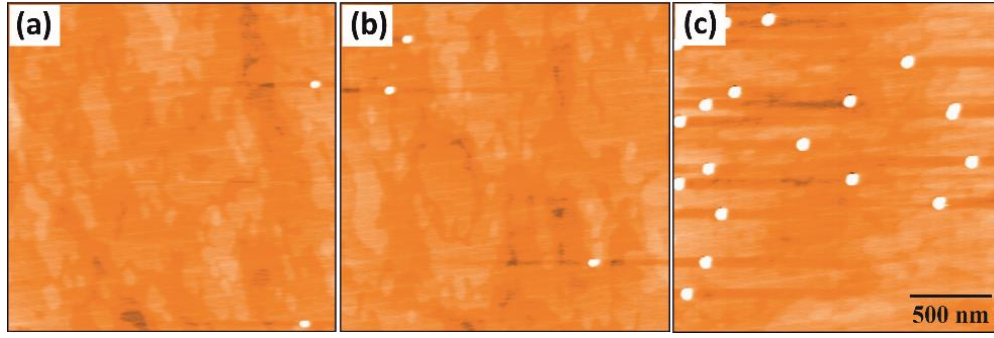


Figure 4.4: InAs QDs grown by homogenous deposition approach showing density variation with change in In amount.

Different calibration samples were grown to ascertain the correct QD density. From calibration measurements, we know that we have to deposit 18 In-cycles (~ 1.5 ML) to obtain QD densities in the range of $\sim 1 \times 10^7$ - 10^8 QDs cm^{-2} . The first sample of a growth day is a calibration sample for which we determine the density by AFM and fine-tune the In amount in steps of 0.1 s, which corresponds to 0.002 ML or ~ 0.14 % of the overall deposition time. In Table 4.1, the densities for three sample series A, B, C (not including the calibration sample) grown each on a single day without changing the temperature of the In in the cell are summarized. It can be seen that we can quite reproducibly obtain QD densities $< 10^8$ QDs cm^{-2} . Over the day, there is a tendency that the QD density decreases, which might be due to a slight decrease in the In rate. The extreme sensitivity on the In- amount, we observe, agrees with Leonard and co-workers' report, who

Table 4.1: The average InAs QDs density ($\times 10^7$ QDs cm^{-2}) for a series of samples grown by the homogenous deposition approach.

| Series A | Series B | Series C |
|-------------------|-------------------|-------------------|
| (18cycles+3.5sec) | (18cycles+4.3sec) | (18cycles+4.0sec) |
| 4.03 ± 0.13 | 3.82 ± 0.47 | 4.50 ± 0.09 |
| 1.85 ± 0.05 | 1.43 ± 0.19 | 1.56 ± 0.24 |
| 2.56 ± 0.20 | 1.10 ± 0.10 | 1.07 ± 0.02 |

observed an extreme increase of the QD density with increasing In amount once the critical thickness has been reached [9]. We found that the margin in deposition time for forming such low-density InAs QD by homogenous deposition time is in our MBE system ± 0.2 s, corresponding to 0.6 % of the overall deposition time. Leaving this window will either result in no QDs or a density larger than 1×10^8 QDs cm^{-2} . The AFM images for InAs QD samples with homogenous deposition with different In deposition are shown in Figure 4.4. To calculate QD density of the surface QDs, AFM images were taken in the center of the quarter of a 3" wafer, approximately 12 mm in x- and y-direction from the edge. For each measurement position, two images were taken a few 10 μm apart to get better statistics.

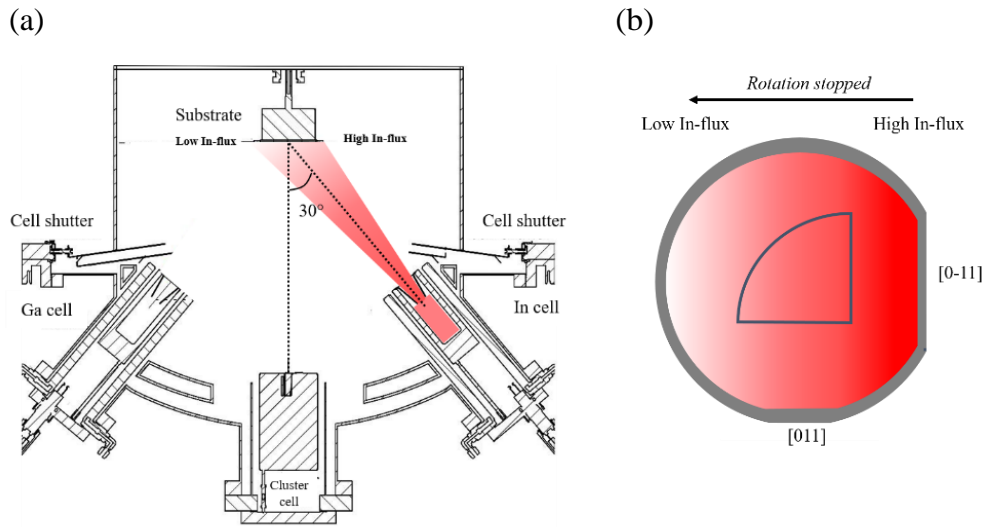


Figure 4.5: Schematic sketch of MBE growth chamber with In cell geometry (MBE Komponenten). The In-gradient on full and quarter 3" GaAs(100) substrate due to substrate rotation stop.

4.1.2 In-gradient Approach

In the In-gradient approach, the substrate temperature is decreased to 505°C for QD growth following the GaAs buffer layer at 610°C within 7 minutes. Then after the temperature stabilization, 50 nm of GaAs were deposited. Then the substrate rotation is stopped and aligned with respect to the In-cell so that the In-gradient is oriented along the [0-11] direction as shown in Figure 4.5. In our MBE system, the In-flux changes approximately 10% across a quarter

and 30% across a full 3" wafer due to the geometry of the system. After orienting the substrate along the In-cell, 19 cycles (4s deposition, 4s break) of InAs is deposited without rotation (*full-gradient*) corresponding to ca. 1.58 ML average coverage. Then after a break of 15s, the temperature is decreased by 25°C, and InAs QDs are annealed at this temperature for 30 sec. The QDs are formed during the growth interruption due to Ostwald ripening [96]. After the formation of QDs, these are partially capped with GaAs, and the substrate temperature is rapidly increased to 610°C to deposit the rest of the structure. The temperature profile for the In-gradient calibration sample series D, with only surface QDs, is shown in Figure 4.3. In the In-gradient approach, QDs are formed during the growth interruption during the InAs deposition after reaching critical thickness due to Ostwald ripening, in comparison to the Homogenous deposition approach where QDs are formed during the annealing step after depositing InAs of critical thickness. In the In-gradient approach, the QD density sharply decreases from high densities (ca. $1 \times 10^{10} \text{ cm}^{-2}$) to no QDs via a transition region with the desired low QD density. The InAs amount has to be adjusted such that the transition region is in the middle of the wafer, which results in the maximum size of the low-

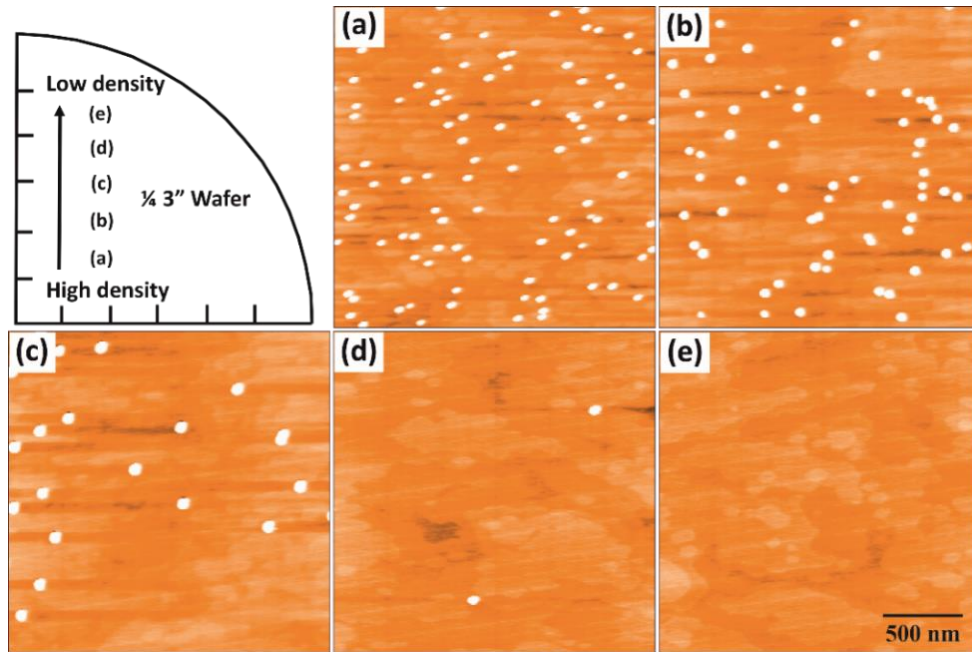


Figure 4.6: AFM images of InAs QDs grown by the In-gradient approach. Sketch of $\frac{1}{4}$ 3" wafer with marked positions (a-e) where AFM measurements have been performed.

density region. Figure 4.6 shows the AFM images at different positions along the In-gradient on a quarter wafer as marked, where position (a) and (b) correspond to a high-density region with densities in the order of $\sim 3.5 \times 10^9 \text{ cm}^{-2}$ and (c) correspond to transition region with densities $5.0 \times 10^8 \text{ cm}^{-2}$. The low-density region (d-e) with the required density lies near the edge of the wafer.

The In-gradient approach was extended in this work to further enhance the low-density areal coverage by partially stopping the rotation during the InAs deposition, called *half-gradient*. During this, the substrate rotation is stopped during deposition of the first 9 and a half cycles of InAs and restarted again with a break of 5s for deposition of the rest 9 and a half cycles of InAs. In-gradient was further investigated to achieve a shallower gradient where homogenous In deposition was increased in ratio to In-gradient deposition. The other gradients are represented as (m, n) , where m is InAs deposition without rotation and n is with rotation. The full-gradient and half-gradient described above can be expressed with this notation as $(18, 0)$ and $(9, 9)$ respectively. The different shallower gradients are $(8, 10)$, $(7, 11)$, and $(6, 12)$.

4.2 QD morphology and height distribution

The morphological characteristics such as QD height, size, and density were calculated with AFM. For the homogenous deposition approach, the images

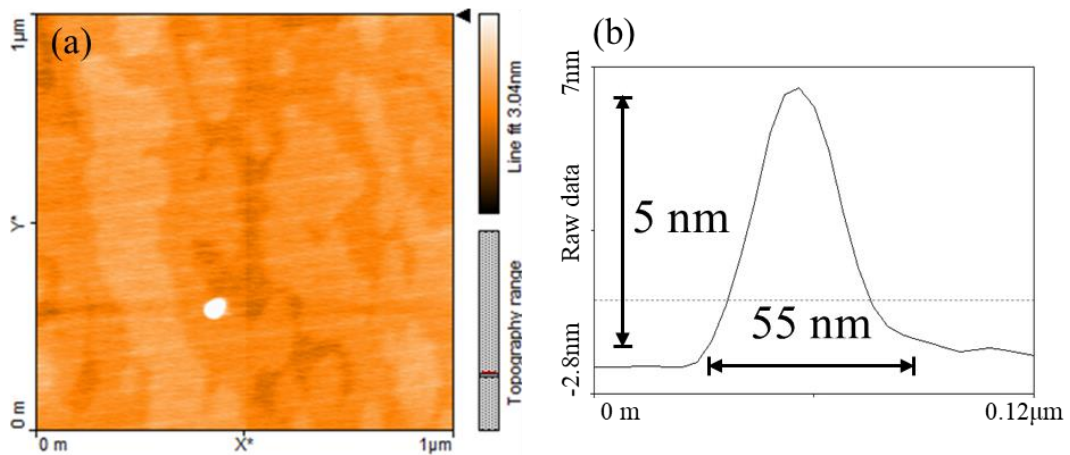


Figure 4.7: a) AFM image of InAs QD, b) The linescan show the QD height and diameter.

were taken approximately 12 mm in x- and y-direction from the edge of the quarter wafer and for In-gradient QDs along the gradient with 1 mm distance between the measurements. For each measurement position, two images were taken a few 10 μm apart to get more accurate statistical results. The statistical analysis results of the InAs QDs for the two deposition approaches were performed on several AFM images recorded from different samples.

The InAs QDs grown by both the deposition approach are randomly distributed over the surface, and no signs for clustering are found. The reason for this is probably the smooth GaAs surface on which the InAs QDs are grown. In the region without QDs, the RMS roughness is around 0.2 nm for a $1 \times 1 \mu\text{m}^2$ scan. The QDs are of lens shape as observed from AFM images as shown in Figure 4.7. The QD shape looks slightly asymmetric due to distortions from the AFM image. The QD height statistics for the two approaches were calculated for different densities with the help of Gwyddion software [97]. The AFM images

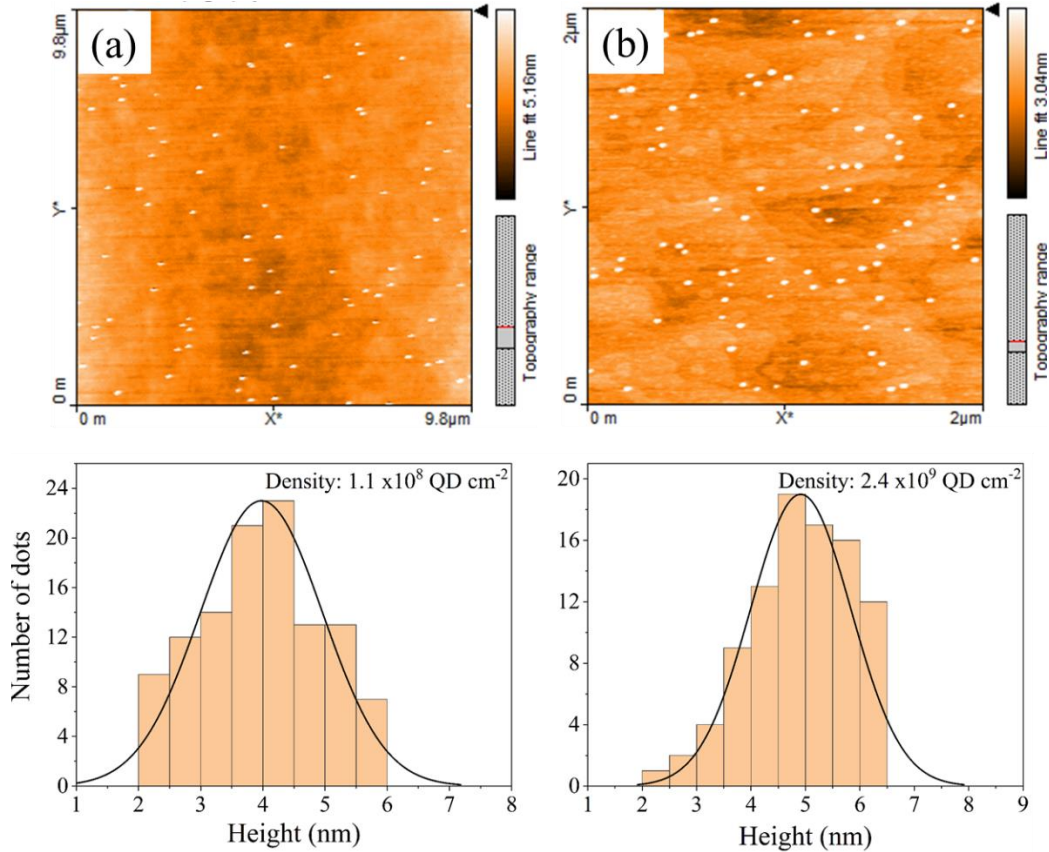


Figure 4.8: AFM images for InAs QD grown by the Homogenous deposition approach; a) low density and b) high density with height distribution for the respective densities.

were first leveled and then masked by the height threshold to calculate the height. The maximum values were taken to analyze any individual dot. Figure 4.8 shows the AFM images for low and high QD densities in the order of $1.1 \times 10^8 \text{ cm}^{-2}$ and $2.4 \times 10^9 \text{ cm}^{-2}$, respectively, for the homogenous deposition approach with their respective height histogram at the bottom. The different statistics from the AFM images reveal that the QD height and base diameter for low densities ($< 1.0 \times 10^8 \text{ cm}^{-2}$) are in the range of 2-6 nm and 40-70 nm with a standard deviation of 27 % and 22 %, respectively. However, no significant change is observed in height of QD for high-densities ($> 1.0 \times 10^8 \text{ cm}^{-2}$) with the increased InAs amount. This is probably due to the annealing step during the formation of QDs which leads to uniform dots during the 60-sec duration. The height histogram fits the Gaussian distribution function as shown.

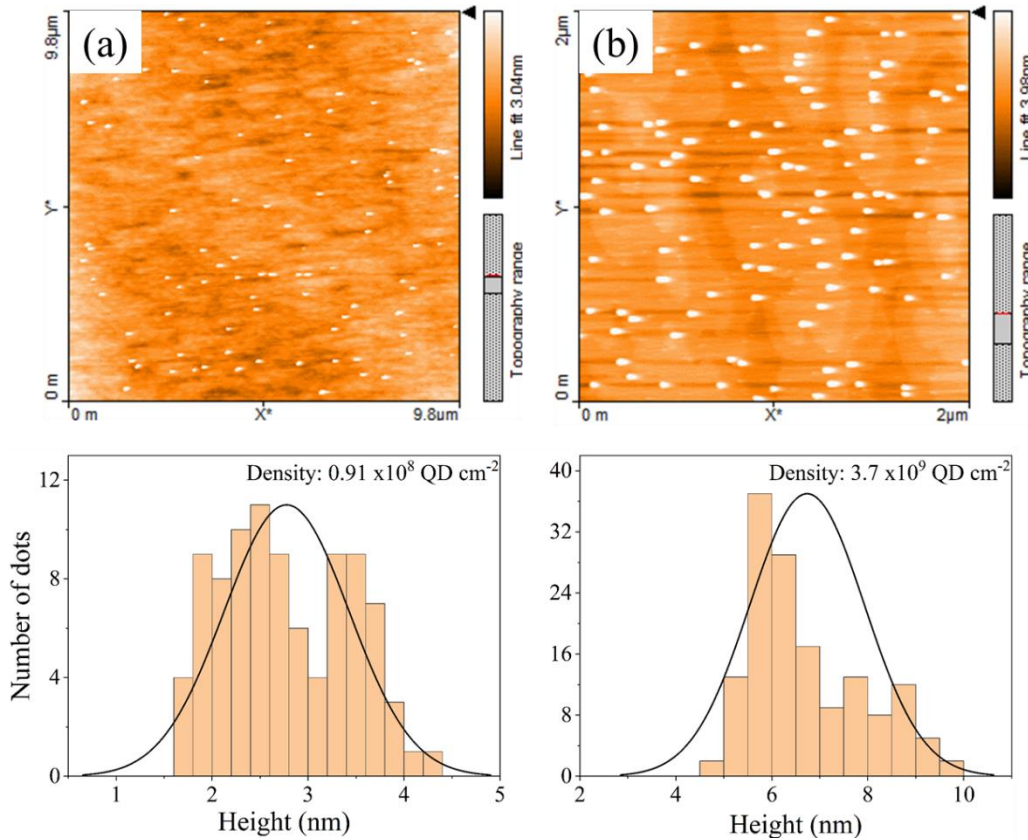


Figure 4.9: AFM images for InAs QD grown by In-gradient approach; a) low, and b) high density, respectively with respective QD height histogram.

For the In-gradient approach, an increase in the QD size is observed along the In-gradient from low QD density to high-QD density which is consistent with what is stated in different literatures [9]. Figure 4.9 shows the AFM images with low and high QD densities in the order of $0.9 \times 10^8 \text{ cm}^{-2}$ and $3.7 \times 10^9 \text{ cm}^{-2}$, respectively. The average QD height and base diameter at low density are 5.5 and 60 nm, respectively, while the high-density region is 6.8 nm and 55 nm, respectively. This can be observed from the histogram corresponding to images. The increase in QD size is due adatom migration of material to the existing islands at such temperature.

4.3 Low-density characterization

The optical characterization of QD samples was done with three different PL spectroscopy setups as described in section 3.3 and section 3.4. The low-temperature PL mapping and luminescence imaging setups with resolving the position of single QDs allowed the investigation of buried QD samples. The combination of these characterization techniques was realized to better evaluate the low-density QDs.

Figure 4.10 shows the different measurements for density characterization of a QD sample having buried and surface QDs. The (a) shows the AFM image from the center of a $5 \times 5 \mu\text{m}^2$ sample which shows the QD density in the order of $2 \times 10^7 \text{ cm}^{-2}$. Two AFM images were taken at same place to to reduce statistical error. Then low-temperature PL was performed on the same sample, which shows the emission of the wetting layer (WL) and the QDs, as shown in Figure 4.10.b. The GS of the QDs grown with 2.8 nm of GaAs partial capping layer appears at 1.35eV (930 nm) and WL emission at 1.44eV (860 nm). To create false-color PL maps from position-dependent PL measurements, the ratio I was calculated,

$$I = \frac{I_{WL}}{I_{WL} + I_{QD}} \quad 4.1$$

where I_{WL} is the area of the WL peak, and I_{QD} is the area of the QD peak. Thus, the PL maps show the color-coded intensity of the WL (area under WL peak) normalized to the total intensity (area under peak WL + area under QD peak) as shown in Figure 4.10.c. Here x and y-axis represent the size of the sample and the z-axis represents the ratio I . For example, the ration $I =$

1, implies no QD is present, and $I = 0$ corresponds to a high QD density ($> 10^9$ QDs cm^{-2}). The PL measurements for wafer mapping were performed 300 μm apart measurement points. Different high-resolution PL images were

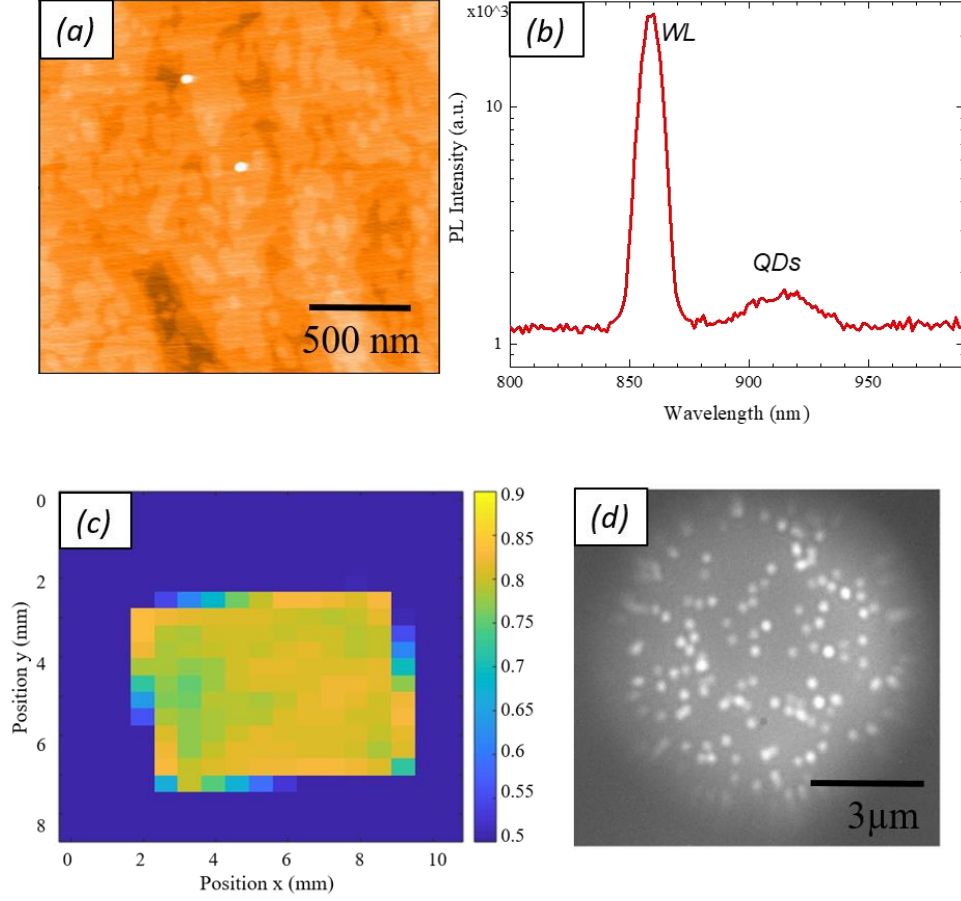


Figure 4.10: (a) AFM image showing surface QDs. (b) low-temperature PL spectrum of low-density QDs (corresponds to $I=0.7$), (c) PL map in a false-color representation of the area including the point, from which the PL spectrum in (b) was taken; (d) PL image of buried InAs QDs from the yellow region in (c) (density ~ 0.2 QDs μm^{-2}).

taken on selected areas (see Figure 4.10.d, for example), to calibrate the ratio I for low QD densities. For the employed setup, the range of 0.9 to 0.7 corresponds to the desired density range of approximately 1×10^7 to 1×10^8 QDs cm^{-2} . A comparison between the false-color plots and the luminescence images at dedicated positions showed that a ratio $I > 0.7$ corresponds to a QD density below 1 QD per μm^2 . Please note that the QDs look bigger due to the limited resolution of the setup. The PL emission from QDs

can be observed as white spots in the images. The QD density is around $1.0 \times 10^7 \text{ cm}^{-2}$, and most of the dots are separately resolvable. The density from the buried QDs is quite comparable to the surface QD density.

4.3.1 Homogenous In deposition

The PL spectra of the as-grown InAs QDs grown by the Homogenous deposition approach at room temperature (300 K) and low temperature (77 K) are shown in Figure 4.11. In PL spectra, the QD density is approximately proportional to the PL intensity of the ground state emission of QD. Therefore, QD density can be inferred from the spectrum high, due to the high intensity of QD emission in comparison to WL emission. Due to QDs of different sizes and shapes, a slightly different emission wavelength is obtained which results in QD ensemble emission and inhomogeneous broadening of PL spectra is observed.

The GS emission is observed at 1270 nm and 1190 nm at 300 K and 77 K with an FWHM of 33 meV. With lowering the measurement temperature, a

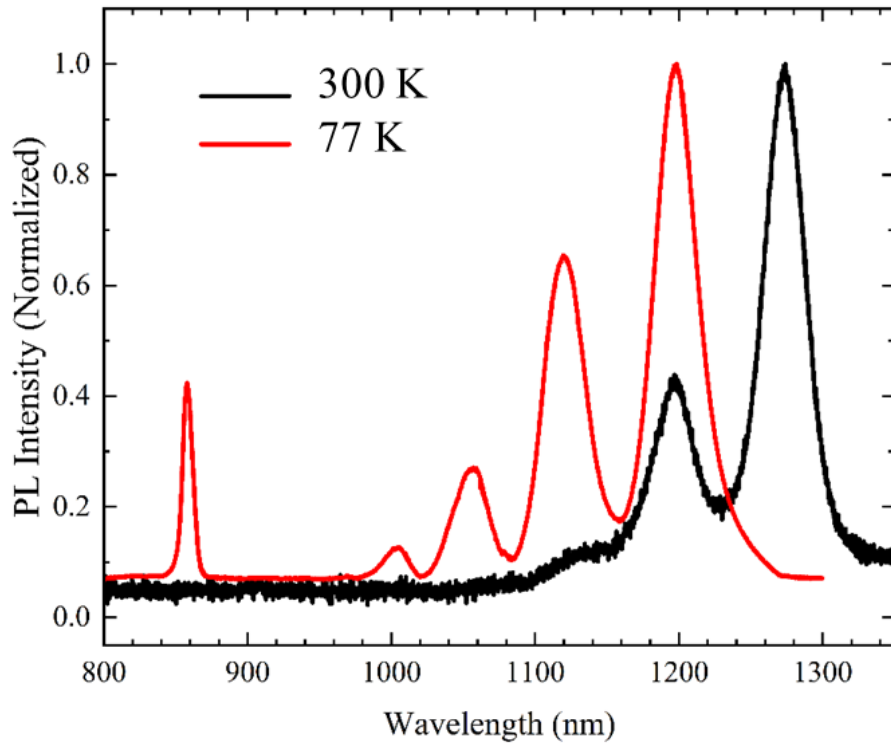


Figure 4.11: PL spectra of InAs QDs grown by homogenous deposition approach at 300 K and 77 K.

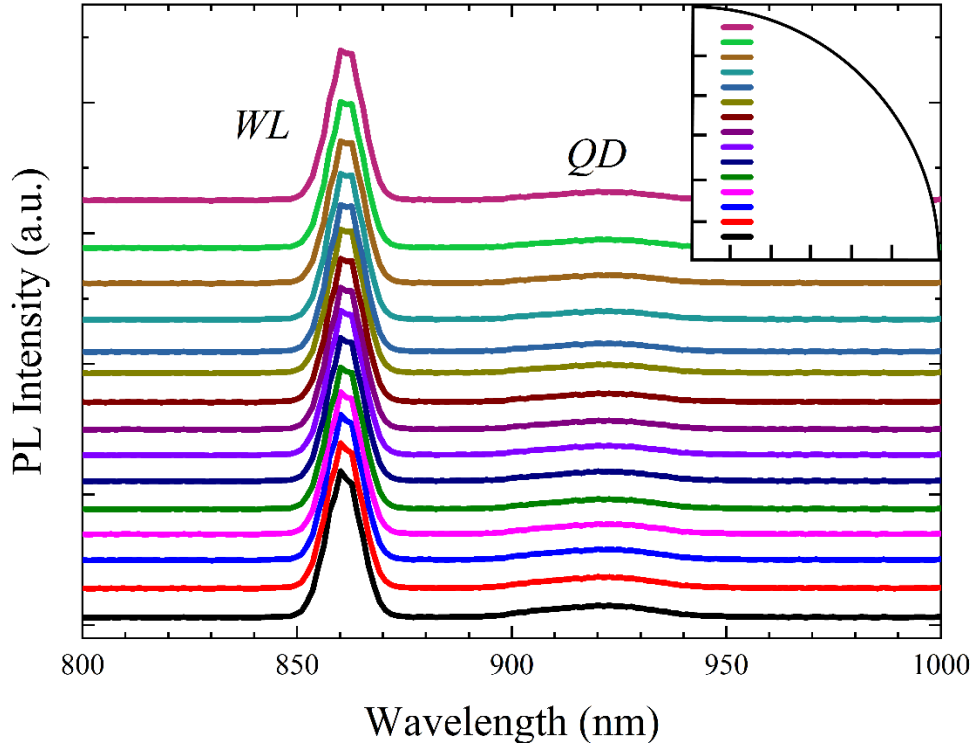


Figure 4.12: PL spectra of 2.8 nm flushed InAs QDs at 16 K, grown with Homogenous deposition approach.

blue shift in PL emission is observed due to the temperature dependence of the bandgap of InAs (section 2.1.1). However, WL emission is not observed at 300 K and only observed at 77 K with emission at 856 nm. The emission intensity is stronger at low temperatures with more clear excited states than at 300 K. The emission from different energy states (s, p, d, f..) can be observed due to lateral quantization of QD energy states.

The Figure 4.12 shows the PL spectra of 2.8 nm flushed InAs QD sample at 16 K, along a quarter wafer from a 3" wafer sample. The GS emission of 2.8 nm flushed QDs at low temperature is observed at 1.35 eV (930 nm) and WL emission at 1.44 eV (860 nm). The PL emission signal is nearly uniform across the quarter wafer. The FWHM of the GS PL emission for the QDs is in the range of 21-28 meV which indicates a small size distribution of the flushed QDs. This PL data was analyzed by employing ratio (I) of WL and WL + QD as described above. Figure 4.13, shows a false-color image of the low-temperature PL map of InAs QDs grown over a full 3" wafer by homogenous deposition approach. The wafer was cleaved into quarters to

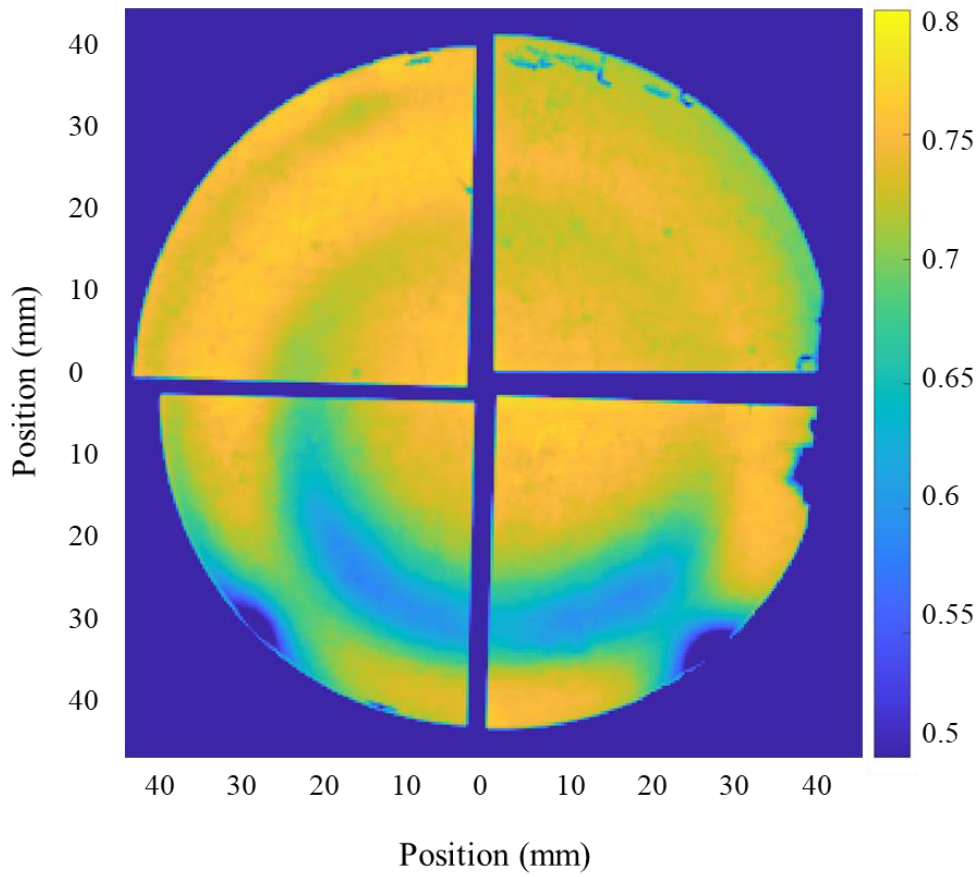


Figure 4.13: a) PL-wafer mapping for InAs QDs grown by homogenous deposition approach over 3" GaAs (100) wafer.

perform the measurements, due to the limited sample size we can mount in the PL setup. However, all the measurements were performed under similar conditions and the same integration time. From the plot, a homogenous density distribution can be observed with a larger area of the wafer having a ratio, $I > 0.7$, indicating low QD density. A quantitative analysis was carried out by calculating the wafer area having $I > 0.7$ and the total area of the wafer, which shows that over 70 % of the overall wafer exhibit the desired low QD density in the range of 1×10^7 to 1×10^8 QDs cm^{-2} . A slight variation in the QD density is observed which we attribute to inhomogeneities in the substrate temperature due to the substrate holder. QD densities by AFM images of the surface, QDs of the same sample ranged from 1.0×10^7 - 2.0×10^8 QDs cm^{-2} , which agrees well with the density range deduced from buried QDs. The densities for buried and surface QDs agrees well which also points to the relatively good reproducibility of the process.

4.3.2 In-gradient Approach

In this section, the PL results for different In-gradients, particularly the full-gradient and half-gradient, will be discussed in detail. The PL measurements were done by the PL setup described in section 3.3.

The PL spectra of as-grown InAs QDs by full-gradient approach at 300 K are shown in Figure 4.14. The PL spectra are measured at different points along the In-gradient on the quarter wafer sample as shown (a-g). The GS emission is observed at 1260 nm with subsequent excited states at 300 K. The GaAs and WL emission is observed at 880 nm and 920 nm. The points (a-c) represent the high-density region, (d) the transition region and points (e-g) correspond to the desired low density ($< 1 \times 10^8$ QDs cm^{-2}).

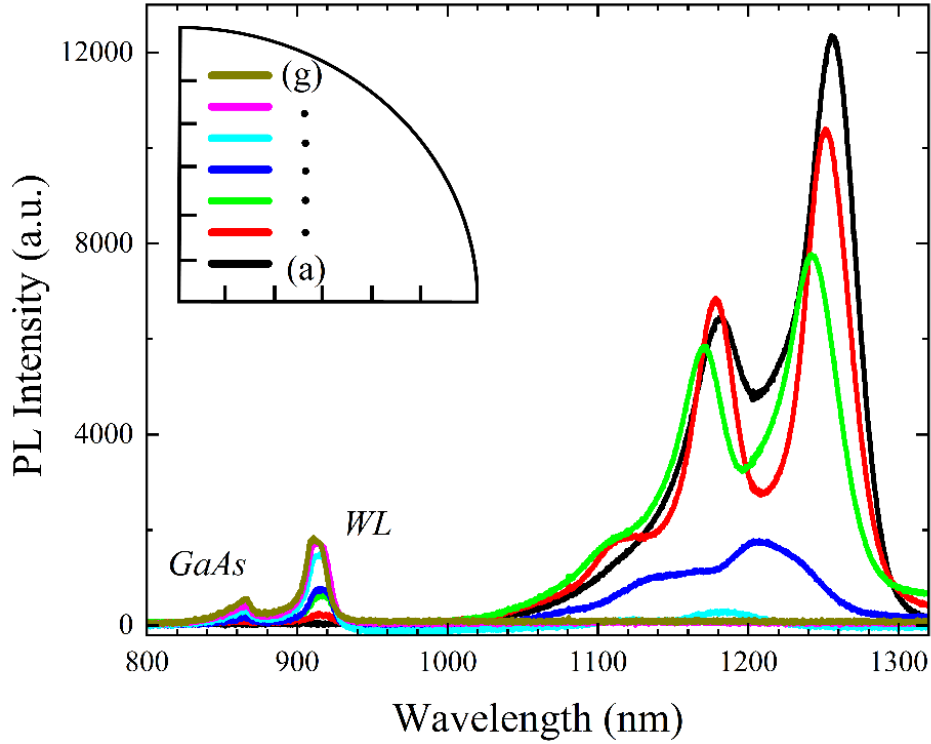


Figure 4.14: PL spectra of InAs QDs grown by In-gradient at 300 K. Inset shows the points where measurements were done.

To gain a better understanding of the density distribution, flushed InAs QDs were grown where only ground state emission is observed due to the QD size reduction. The PL spectra of 2.8 nm flushed InAs QDs grown by full-gradient approach at 16 K are shown in Figure 4.15. The QD and WL

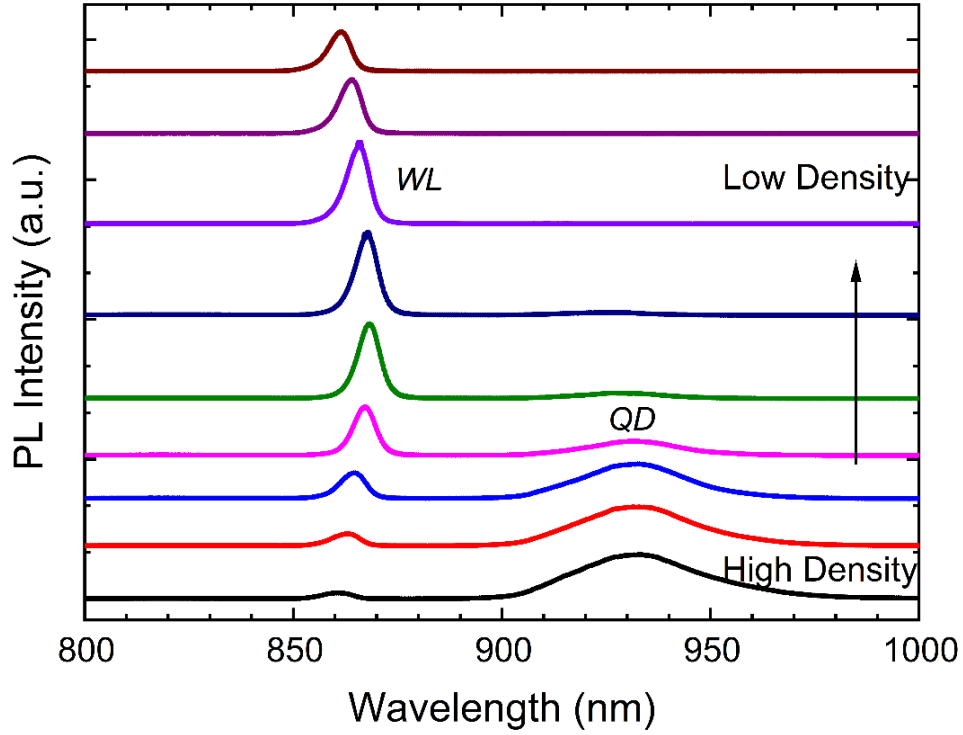


Figure 4.15: PL spectra of 2.8 nm flushed InAs QDs at 16 K grown with In-gradient approach.

emission is observed at the same wavelength i.e. 930 nm and 860 nm, as for the 2.8 nm flushed QDs grown by homogenous deposition approach. A slight blue shift of QD emission is observed along the gradient from high density to low-density region. The FWHM of the GS for the QDs varies from 25-36 meV, which is slightly larger than for the homogeneous deposition approach. The density optimization with 19 cycles of InAs results in the appropriate density from high-density region to no QD region. The PL intensity from the QDs is approximately proportional to the QD density. It can be observed decreases along the gradient direction from high-density region to low density region and vanishes at the detection limit for very low QD densities ($< 5 \times 10^5 \text{ cm}^{-2}$). As the density decreases, emission from WL and GaAs peaks increase, and the QD emission peaks diminish. The optical characteristics for half-gradients are the same as for full-gradients, other than QD density variations across the wafer which leads to change in PL intensity only. The shape and size of the QDs are observed to follow a similar pattern as those of the full gradient. Figure 4.16 and Figure 4.17 summarize the behavior of the QD densities for the full- and the half-gradient. Figure 4.16, shows the

QD densities as a function of the position for surface QDs determined from AFM images. The height of the QDs increases along the gradient direction from high density to the low-density side as described in section 4.2. For full-gradient, the QD density sharply increases to densities in the order of $\sim 1 \times 10^{10}$ QDs cm^{-2} as expected and follows the same general behavior as described in the work of Leonard and co-workers [64]. For the full-gradient, the density in the high-density region is higher than for the half-gradient. The QD density for half-gradient at high density starts at $\sim 4 \times 10^9$ QDs cm^{-2} for the same deposited InAs material (1.58 ML) and QD density transition slope reduces to half in comparison to

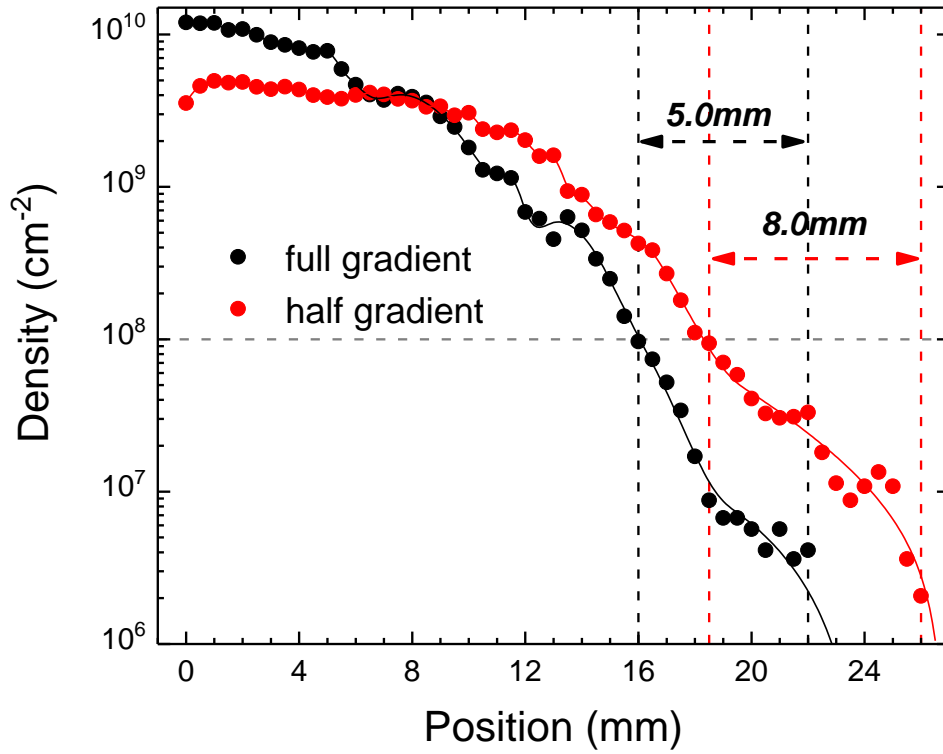


Figure 4.16: The graph shows the density vs. position plot for the full-gradient and half-gradient deposition approach calculated from AFM images for the surface QDs.

full-gradient. This is just due to the higher In amount deposited in this region for the full-gradient in comparison to half-gradient. It can be observed that the width of the transition region with a density starting at 1×10^8 QDs cm^{-2} and decreasing to the detection limit of $\text{ca. } 5 \times 10^6$ QDs cm^{-2} is $\text{ca. } 5$ mm for the full-gradient and approximately 8 mm for the half-gradient. Thus, for the

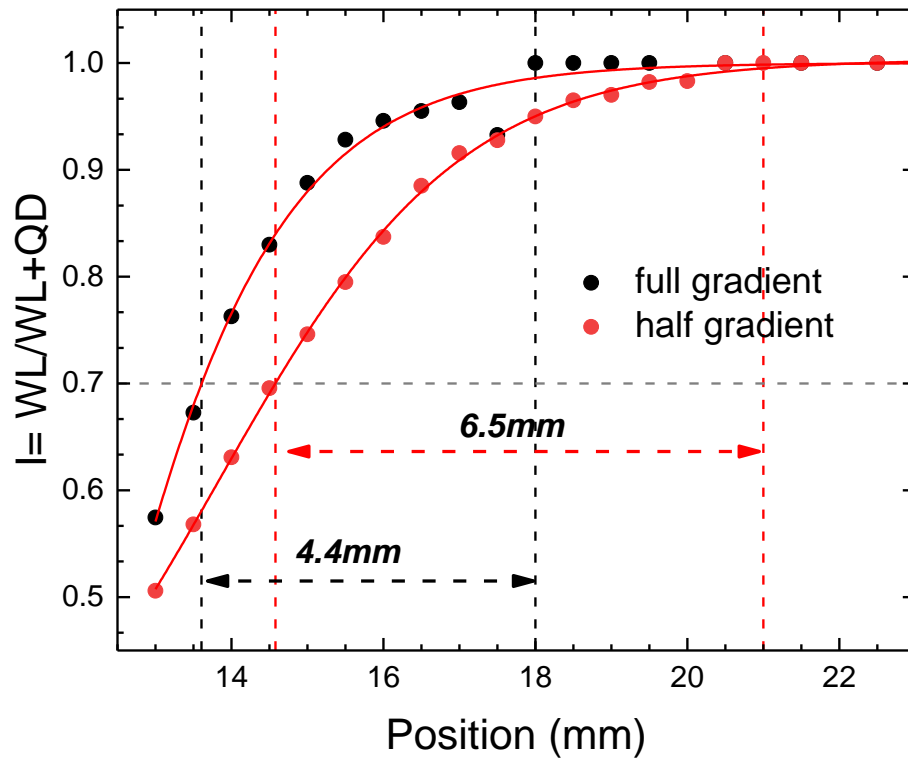


Figure 4.17: Graph showing ratio I , the WL intensity normalized to total intensity (peak WL+ QD), vs. position on the wafer. The ratio above 0.7 corresponds to a density $< 10^8 \text{ cm}^{-2}$.

half-gradient, the transition region is significantly larger. Similar behavior is observed for the buried QDs, as shown in Figure 4.17, where the ratio I is shown as a function of the position. Here the transition region is defined from $I > 0.7$ to the first point, where $I = 1$. For the full-gradient, the transition region is $\sim 4.4 \text{ mm}$ along the gradient, whereas for the half-gradient it is approximately 6.5 mm . For both cases, the length of the transition region corresponds to a low-density region ($< 10^8 \text{ QDs cm}^{-2}$) This corresponds to less than 10 % of a full 3" wafer for full-gradient if the transition region is ideally in the middle of the wafer. The region is larger but still less than 15 % of the overall wafer area for the half-gradient. If the transition region is not positioned perfectly in the middle of the wafer, the fraction of the low-density region becomes even smaller. Although the half- gradient results in a larger transition region, the position of the transition region on the wafer varies stronger, which makes the process slightly less reproducible.

Shallower In-gradient

Different other shallower gradients of (8, 10), (7, 11), and (6, 12) other than half-gradient are grown as described in section 4.1.2, to observe the QD density variation over the quarter wafer. The same InAs amount as used for full-gradient is deposited in 19 cycles, with varying the amount deposited without rotation and with rotation. The last InAs cycle amount was varied equally between the two. Figure 4.18 shows a graph calculated from PL spectra, for the QD intensity normalized with respect to GaAs emission peak, as a function of position for different shallower gradients. For the shallower gradient, a significant decrease in the density is observed from the PL data at the high-density side and a slight increase in the transition region. However we observe that this becomes less reproducible with the increase in the will increase if one makes the gradient even shallower, e.g., using only a quarter gradient.

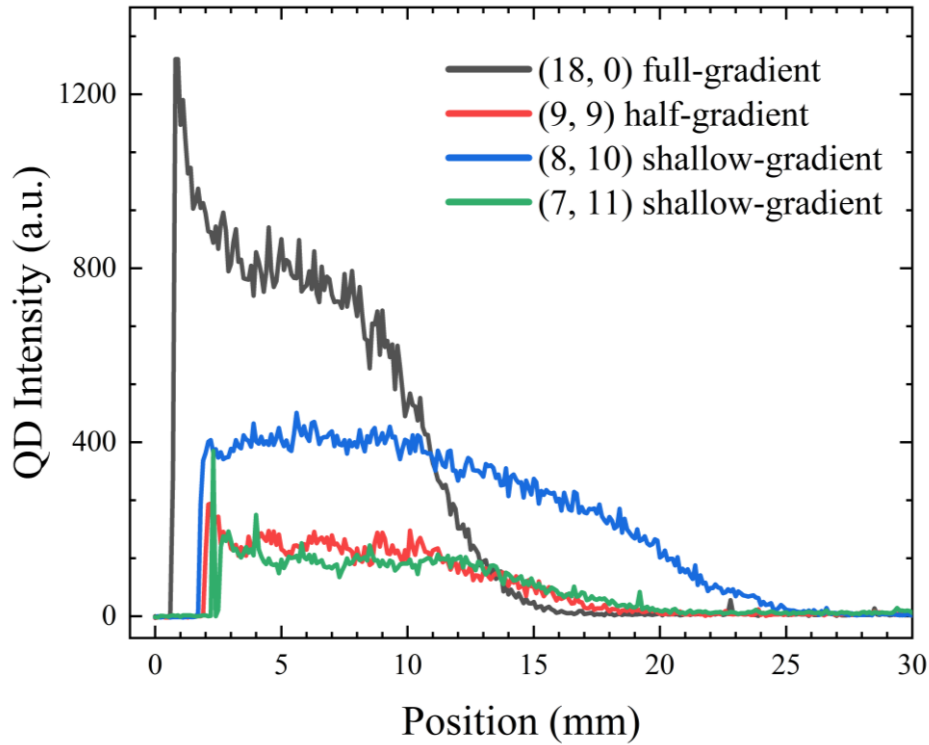


Figure 4.18: The PL intensity of InAs QDs grown by Shallower In-gradient approach given with respect to position on the quarter of 3" wafer.

4.4 Comparison of two In deposition approaches

Using the two deposition approaches that is homogeneous In-deposition followed by an annealing step and deposition with an In-gradient, respectively we achieved low QD densities in the range of 10^7 - 10^8 QDs cm^{-2} . The In-gradient approach, results in a small area of the sample, generally less than 90 mm^2 (transition region less than 5 mm), with a very low dot density (less than 1 dot per μm^2), which is ideal for optical spectroscopy experiments of single QDs, and a larger region with a significantly greater dot density (more than 50 dots per μm^2). For the half-gradient, the transition region extends approximately 7 mm, which corresponds to less than 15 % of the overall wafer area, in case the transition is ideally at the middle of the wafer. By optimizing the conditions for the Homogenous deposition approach, It is possible to use a greater area of the wafer ($> 900 \text{ mm}^2$) for single QD studies resulting in dot densities of 2–4 dots per μm^2 . However, to achieve this the In amount and the substrate temperature are needed to be controlled very precisely.

A half-gradient seems a good compromise between Homogenous deposition and full-gradient deposition approach, resulting in reproducible QDs with slightly greater transition region and the variability of the position of the transition region so that, in general, no dedicated calibration samples are required.

4.5 QD Size modification/ Emission energy tuning

SAQDs formed by the S-K growth mode leads to the formation of randomly distributed QDs of different size and shape. These characteristics of QDs have a significant influence on determining the different optical and electrical properties of QDs. The different sizes of the QDs lead to shifting in the quantization energy of a QD which results in a change in transition energy. Modifications to these QD characteristics, such as size and shape, are possible by changing various growth parameters during the QD fabrication process and also by utilizing various post-QD formation techniques. During the fabrication of QDs, the growth temperature, In-flux (growth rate), growth interruption time, and InAs coverage can be generally used to modify QD properties and following the formation of QDs, different methods which are used are the In-flush technique [98], In-Ga intermixing [99], rapid thermal annealing [100], and $\text{In}_x\text{Ga}_{1-x}\text{As}$ capping layer [101].

In this work, InAs QDs are grown at different low growth rates (LGR), QD growth temperatures, and growth interruption time to study the morphological properties and emission wavelength modification of QDs. And In-flush technique is used to tune the QD height (emission wavelength) after the QD formation. The samples were grown on a quarter GaAs (100) wafer using the same growth structure (Figure 4.1), as described in section 4.1. InAs QDs were grown utilizing the In-gradient approach as described in section 4.1.2 as it allows for a more detailed examination of the QDs varying from high density to low-density region. Following the formation of InAs QDs, QDs were capped with 20 nm GaAs for buried QDs (for PL) and uncapped surface QDs for density and morphological studies.

4.5.1 Low growth rate QDs

At a lower growth rate (LGR), the nucleation probability dominates the growth process. The rate of nucleation rises with an increase in growth rate, which leads to an increased QD density; However, the rate of nucleation approaches an equilibrium state at a high growth rate, which results in the saturation of the QD density [102]. An LGR reduces the strain during the formation of InAs QDs. This decrease in strain within the QDs results in an increase in QDs size, which leads to a redshift of the InAs QDs' emission [103].

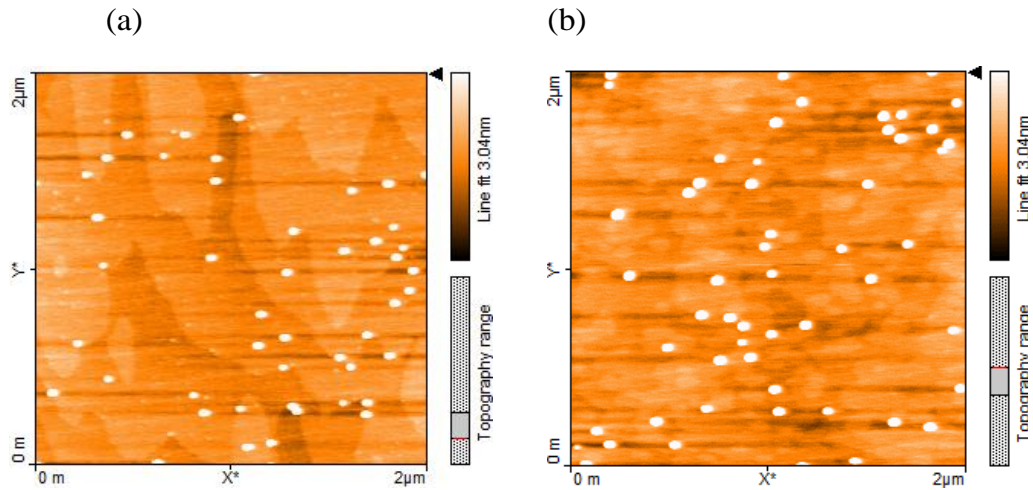


Figure 4.19: AFM images of InAs QDs grown with growth rate of 0.017 ML s^{-1} and 0.008 ML s^{-1} .

The conventional LGR InAs QDs were grown at 505°C substrate the temperature at the rate of 0.017 ML s⁻¹ (740°C), as described in section 4.1. Further, the InAs QDs were grown at the same temperature at significantly lower LGR of 0.008 ML s⁻¹, 0.005 ML s⁻¹, and 0.001 ML s⁻¹ with a corresponding In cell temperature of 720°C, 702°C, and 658°C, respectively. The InAs QDs were grown deposited using cycled growth of 19 cycles (1.58 ML) at a deposition rate of 0.017 ML s⁻¹ results in the QD density gradient with average QD height and diameter of 5 nm and 50 nm respectively at high-density sides. At room temperature, the GS emission of InAs QD is observed at 1260 nm with emission linewidth with an FWHM of 30 meV. Then WL emission is observed at 920 nm. Higher energy peaks from the first and second excited states are observed at low growth rates. Figure 4.19 shows the AFM images of InAs QDs grown at two different growth rates of 0.017 ML s⁻¹ and 0.008 ML s⁻¹, with average QD height of 5 nm and 8 nm respectively. When using an LGR of 0.008 ML s⁻¹, 38 cycles of In were deposited to achieve the same QD density gradient over the

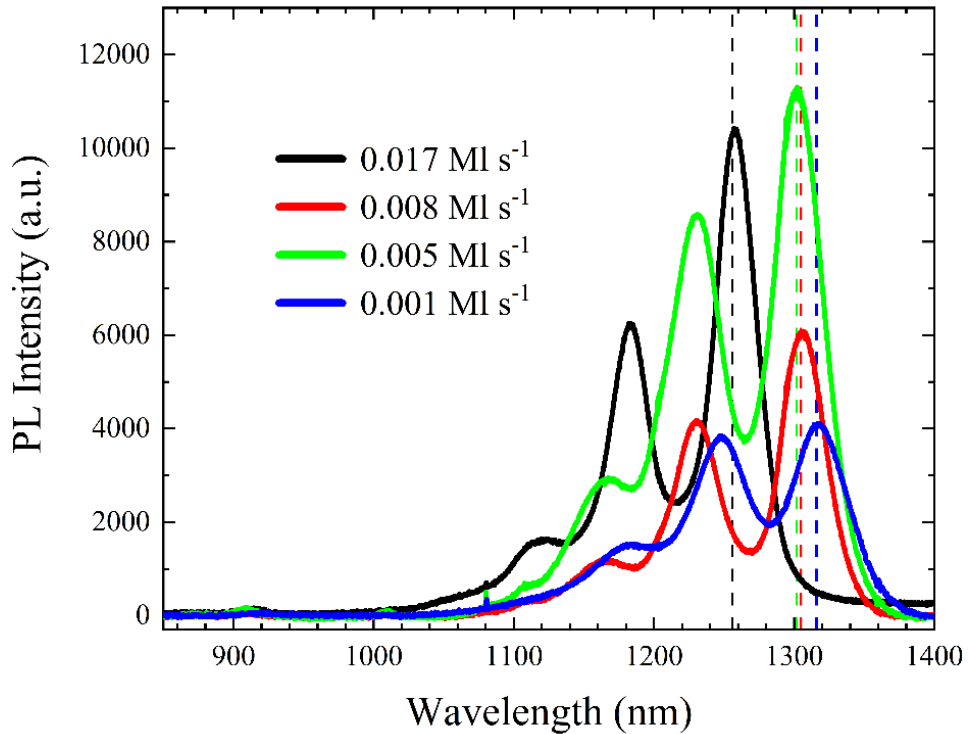


Figure 4.20: PL spectra at 300 K for InAs QDs grown with different In LGRs.

quarter wafer area. A slight increase of QD size is observed in the order of 4-8 nm with a diameter of 40-70 nm, which results in a significant redshift of ~ 50 nm with GS emission at 1310 nm with an FWHM of 38 meV. Further decreasing the growth rate has no discernible effect on the QDs' size and the corresponding emission energy, which may be due to the thermodynamic equilibrium size correlated with the substrate temperature. Figure 4.20 shows the PL spectra of InAs QDs grown at different growth rates. With an LGR of 0.005 ML s^{-1} and 0.001 ML s^{-1} , 58 cycles and 100 cycles of InAs were deposited for QD formation. Due to significant desorption during the long growth process at a slower LGR, more materials were deposited for the QD formation. The GS emissions of 1305 nm and 1320 nm with FWHM of 41 meV and 33 meV respectively were observed for the two growth rates. The QDs grown at LGR have a slightly larger height and are more uniform as can be observed from the narrow linewidths in the order of 30-40 meV.

4.5.2 QD growth at different temperature

The epitaxial growth of InAs QDs on GaAs is generally done in the temperature range of 450-540°C. At higher temperatures ($>500^\circ\text{C}$), In adatoms' increased mobility makes it easier for them to adhere to existing islands rather than forming new islands. As a result, the island size increases, and a few large islands are observed at high temperatures, whereas several small islands are formed at low temperatures.

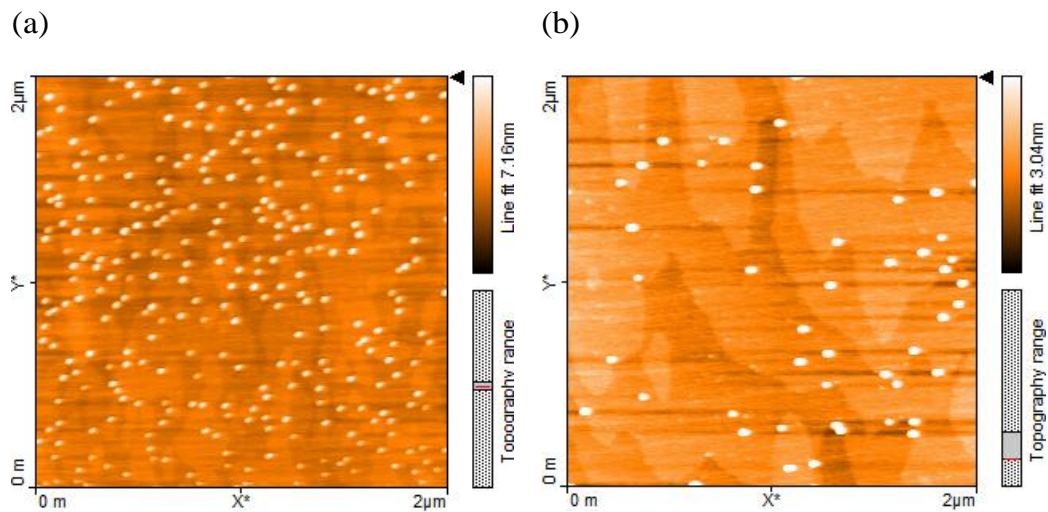


Figure 4.21: InAs QDs grown at 470°C and 505°C.

InAs QDs were grown at a different substrate temperature in the range of 470°C and 510°C with an interval of 5 or 10 °C between them. For this InAs were deposited at a low In growth rate of 0.008 ML s⁻¹ as determined to be optimal from LGR QDs experiments. At a lower substrate temperature (470°C, 480°C, and 490°C), 38 cycles (4sec deposition, 4sec break) of InAs were deposited for QDs formation with correct density gradient across the wafer. AFM images reveal the QD height to be significantly smaller in the range of 2-4 nm. This is probably due to the lesser mobility of In adatoms at lower temperatures. The ground state emission from PL for QD was grown at 470°C, 480°C, and 490°C at 1130 nm, 1168nm, and 1180nm, respectively. The increase in PL emission is a due small increase in QD size, which is also observed from AFM images, however, a high FWHM linewidth of 68 meV, 66 meV, and 89 meV, respectively is observed, which indicates the inhomogeneous broadening due to QDs of varying size. The PL spectra of QDs grown at a different temperature in a high-density region are shown in Figure 4.22. With further increase of substrate temperature, above 500°C, In

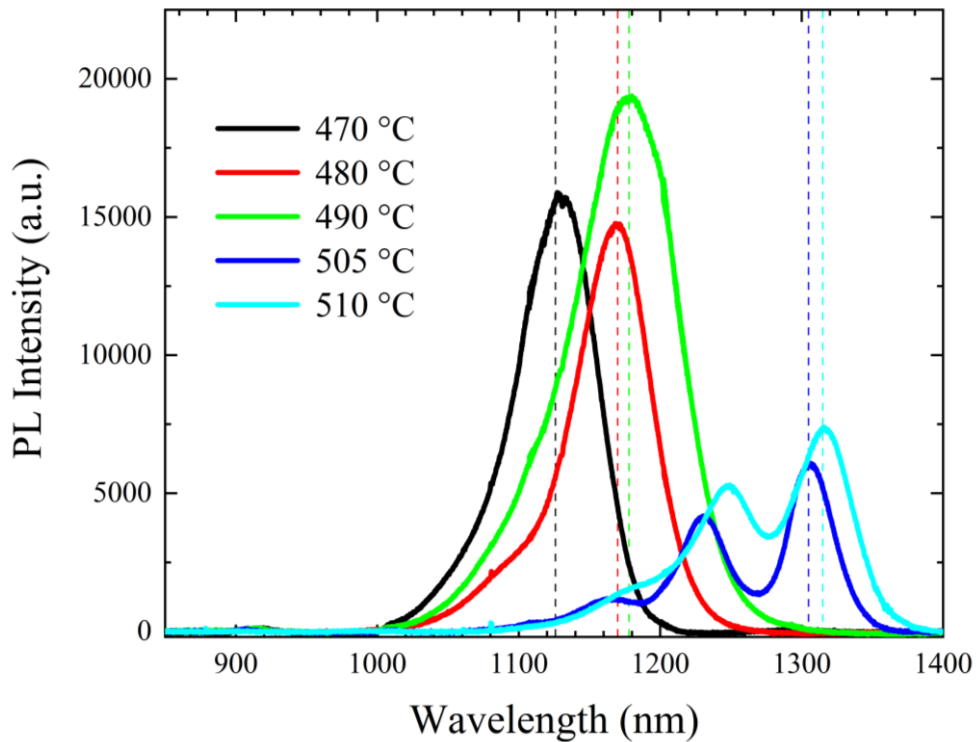


Figure 4.22: PL spectra for InAs QDs grown at QD growth temperature at 300 K.

desorption significantly increases and higher In amount was required to obtain the same QD density. Increasing the QD growth temperature decreases the nucleation rate of the QD, resulting in a drop in dot density and 9.5 nm, respectively. The bigger-sized QDs result in a significant redshift in the E_0 emission to 1310 nm and 1315 nm with an FWHM of 30 meV and 40 meV. Growing QDs at a further higher temperature may result in slight increase in dot density while simultaneously increasing the size of the dot. The AFM images of InAs QDs grown at a substrate temperature of 470°C and 505°C with the deposition of 30 cycles and 38 cycles of InAs are shown in Figure 4.21. The AFM images were taken at the high-density region where QD density is in the order of $1 \times 10^9 \text{ cm}^{-2}$ or above. For the InAs QDs grown at 505°C and 510°C, the QD height significantly increases to average 8 nm QD sizes but it significantly increases the In desorption. As a result, an optimum temperature of 505°C was chosen for further experiments.

4.5.3 Different growth interruption time

In the SK growth mode, the formation of QDs takes place by material transport under partially strained conditions. When a growth interruption is introduced, the QDs are given more time to rest in an energetically favorable environment and more time to interact with the QDs in their immediate surroundings. QDs exhibit a ripening behavior under these conditions. Thereby, the addition of a growth break can significantly have an impact on the sample's shape and structure. Several studies examined the influence of growth interruption in the InAs/GaAs QD system that the increase in the growth interruption time results in the formation of bigger QDs, which leads to redshift [104]. The InAs QDs were grown at low In LGR of 0.008 ML s^{-1} at a substrate temperature of 505°C. InAs is generally deposited by the growth interruption process where it is deposited in cycles of 4-sec deposition and 4-sec break for the formation of QDs. This growth interruption (break) time was varied during the growth of InAs QDs samples in the interval of 4 sec. For the QDs grown with a 4-sec break, the average QD height and diameter are 6.5 nm and 63 nm respectively, which gives the GS emission of 1304 nm at room temperature. With an initial increase in growth interruption time from 4 sec to 8 secs, an increase in the average height of QDs was observed from 6.5 nm to 8.4 nm. For this PL emission of

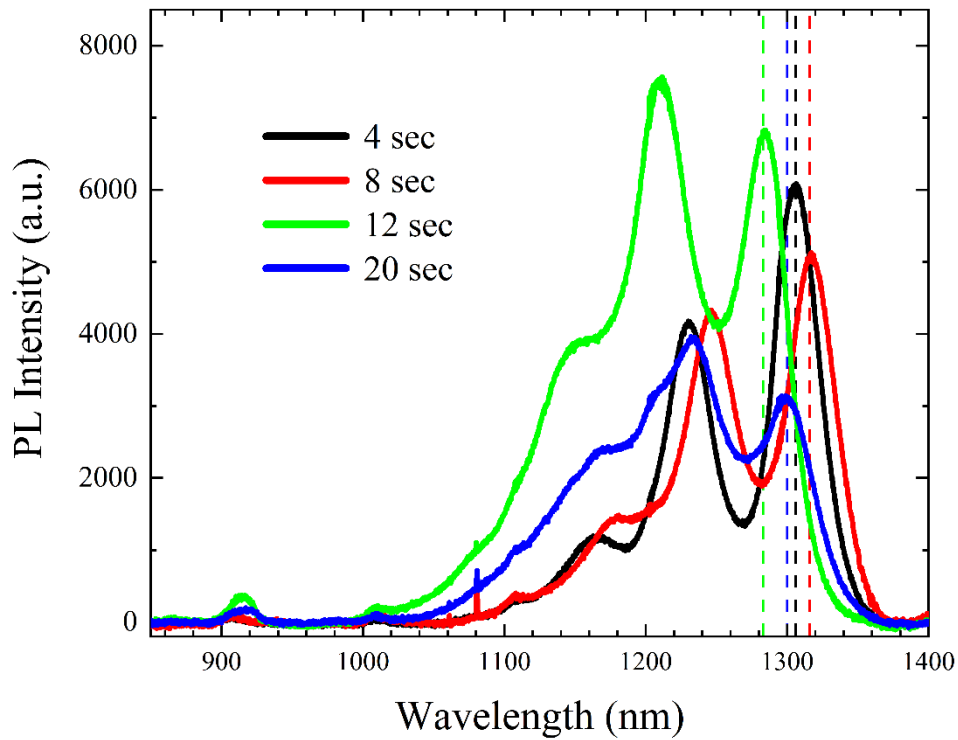


Figure 4.23: PL spectra for InAs QD grown with different growth interruption times at 300 K.

InAs QDs shifts to a higher wavelength of 1317 nm due to the average increase in QD size. A further increase of growth interruption time from 8 sec to 12 sec and 20 sec did not result in a significant increase in the QD size. Figure 4.23 shows the PL spectra at room temperature for InAs QDs grown with different growth interruption times. The average QD observed for 12 and 20 sec interruption time are 6.8 nm and 7.4 nm with corresponding QD emission at 1285 nm and 1298 nm respectively. The PL from the QDs grown with various growth interruption times exhibit FWHM broadening from 30 to 55 meV with increasing growth interruption time up to 20 sec, which is probably due to the indium desorption that decrease the dot size uniformity and subsequently the PL line width increases [105].

4.5.4 Comparison of these parameters

The different QD growth parameters that have been examined for the growth of InAs QDs results in QDs of various sizes, which leads to a change of

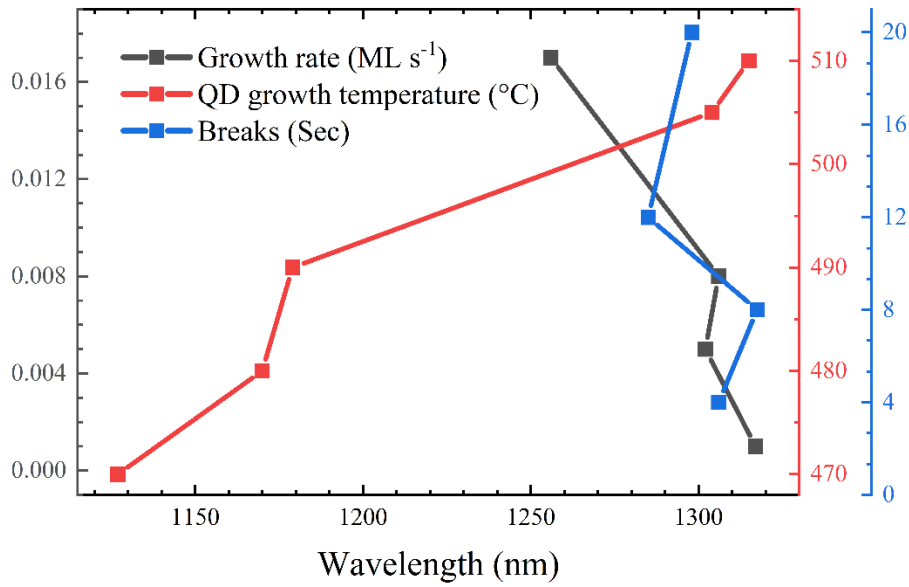


Figure 4.24: The comparison of different QD parameters with respect to the emission wavelength of GS.

emission energy of the QDs. These parameters can be used to alter the QD emission wavelength and can be used accordingly for use in various applications. The different QD growth parameters studied are summarized and shown in Figure 4.24. The use of LGR of In significantly redshifts the QD emission. To obtain a higher emission wavelength greater than 1300 nm, one can use LGRs of In, substrate temperature $> 500^{\circ}\text{C}$, and longer growth interruption time.

4.5.5 In-flushed technique

The size, shape, and composition of InAs QDs influence their optical and electronic properties as described in previous sections. Conventional InAs SAQDs have GS emission around 1200-1300 nm at room temperature with a very large linewidth due to differences in QD sizes. Generally for single dot spectroscopy, Si-detectors are used due to their high sensitivity which has a spectral range of below 1000 nm. As a result, the ground-state emission must be blue-shifted in order to be detected by these detectors. This tuning of emission energy of the QDs can be accomplished with the use of the Indium-flush (In-flush) technique [98,106–108]. In this technique, controlled re-

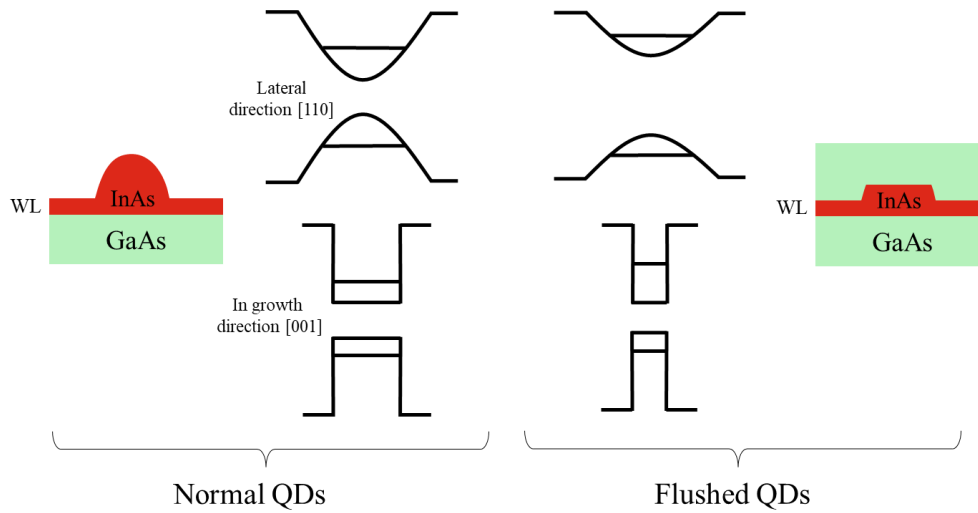


Figure 4.25: Schematic diagram of the modification in confinement potential of InAs QDs due to the In-flush technique in both directions [001] and [110].

evaporation removes the excess InAs particles, thus narrowing the particle size and therefore allows for more precise adjustment of the QD height [109]. Figure 4.25 depicts the confinement potential of normal and in-flushed QDs in both lateral and growth directions. This narrowing of the confinement potential in growth direction blue shifts the QDs' transition wavelength, and the confinement potential's height limits the energy states.

In-flushing is done in three steps, as shown in Figure 4.26. In general, first InAs are deposited at desired substrate temperature for the formation QDs as described in Section 4.1. Then the substrate temperature is decreased by 25°C to minimize any In desorption. This is followed by the second step of the QD overgrowth by deposition of GaAs layer of desired thickness d , smaller than the height of the QDs. After then, a brief 30-sec pause is introduced to allow for In segregation and redistribution on the GaAs surface. In the last step, the substrate temperature is rapidly increased to 610°C, with a temperature ramp of approximately 20 K/min (in 2 min) to desorb In at higher growth temperature ($> 540^\circ\text{C}$), from the uncapped part of InAs QDs. The exposed InAs is evaporated due to their low sticking coefficient at such high temperature [110]. This leads to the formation of smaller truncated dots, with a slight intermixing when Ga diffuses into the InAs layer. During the whole process, including the desorption of In, the As

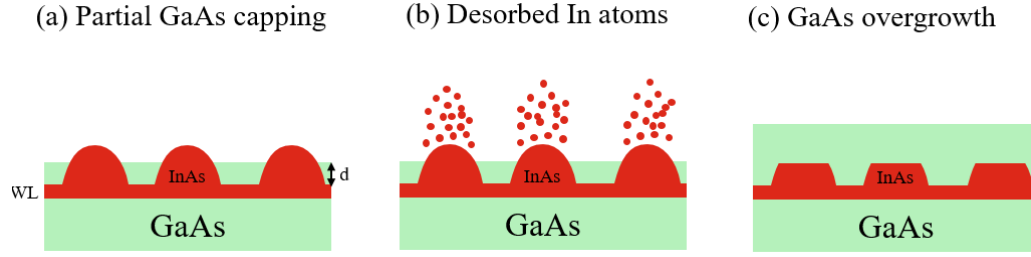


Figure 4.26: The schematic of the In-flush technique.

pressure is kept constant at 2.2×10^{-5} mbar. At last, a GaAs layer is deposited at 610°C with the rest of the heterostructure. These flushed QDs have provided strong carrier confinement and controlled the emission of the QD ensemble. The PL measurement of InAs QDs grown as-grown and flushed at 16 K is shown in Figure 4.27. The GS emission wavelength for uncapped QDs is observed at 1160 nm at 16 K with an FWHM of 34 meV. The other states observed are the s and p peaks and the WL at 860 nm. In this work, fabricated QDs were tuned to have a GS emission wavelength of 930 nm at low temperatures, allowing them to be used efficiently Si-detectors for single dot

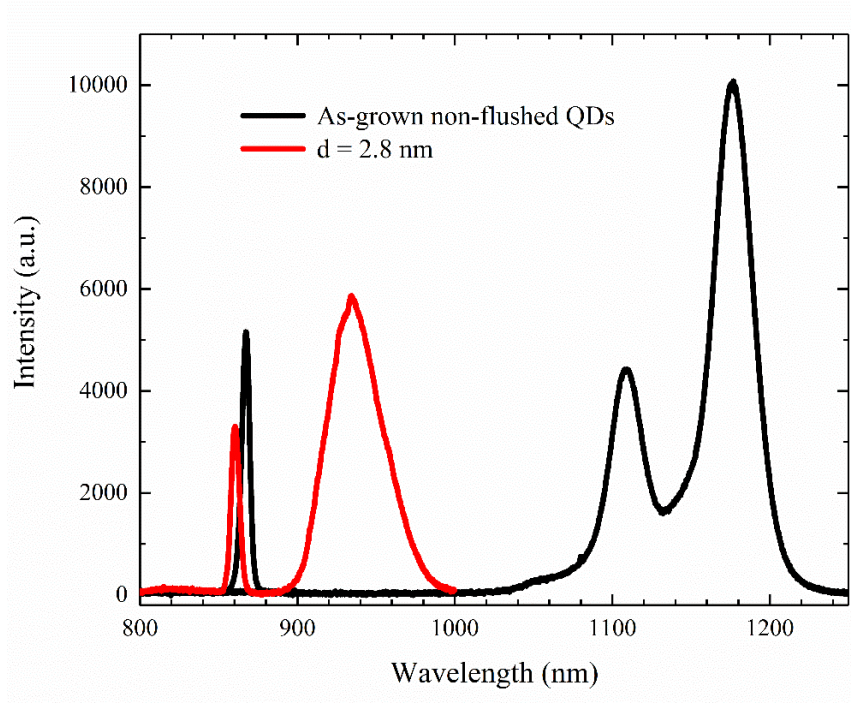


Figure 4.27: PL spectra of InAs QD ensemble grown without flushing (as-grown) and with flushing at 16 K.

minimum blue shift of 5- 10 nm with a variation of 0.05 nm of GaAs. For the flushed QDs with 2.8 nm capping, ground-state emission appears at 930nm with an FWHM 30 nm. Additionally, the WL signal shifts to 860 nm for 2.8 nm flushed QDs in contrast to 870 nm for unflushed QDs, indicating that the In-Ga intermixing occurs during the flushing step. Figure 4.28 shows the PL spectra for flushed QDs grown by the In-gradient approach. A slight blue shift of QD emission is observed along the gradient from high density to low-density region.

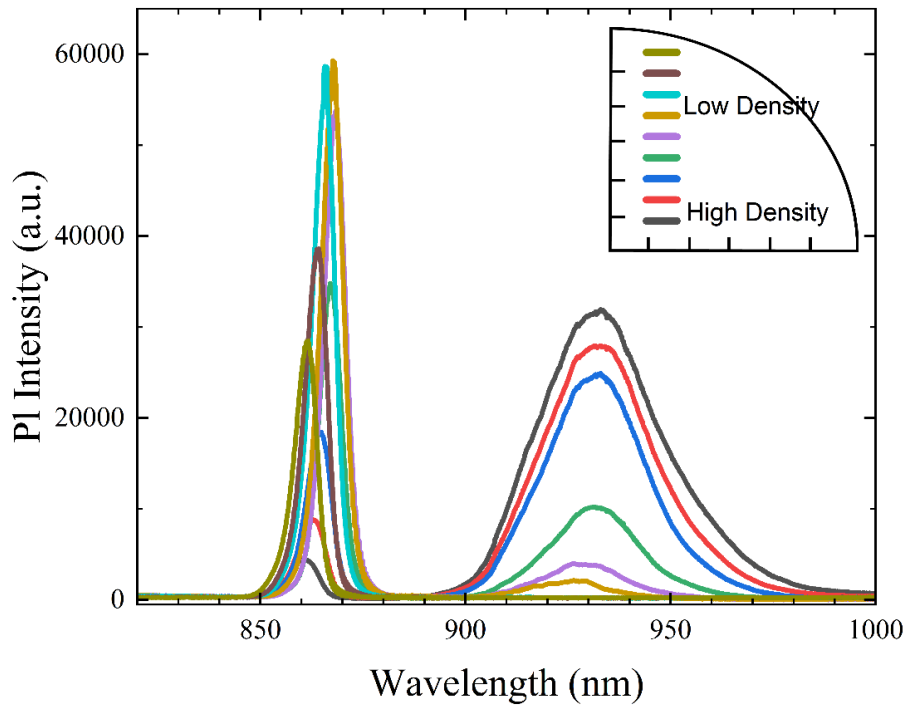


Figure 4.28: PL spectra of 2.8 nm flushed QDs along the In-gradient at 16 K

experiments. QD samples with a partial GaAs capping of 2.7 nm, 2.75 nm, and 2.8 nm were grown to optimize the required emission, which leads to a

4.6 Quantum dot Molecules

Optically addressable QDMs fabricated by the self-assembly process have emerged as an exciting new area of fundamental research and application in quantum technologies such as quantum computing and quantum cryptography. In an individual QD, we can generate charge carriers i.e. electrons and holes, manipulate their spins, create entangled photon states,

and induce spin–photon entanglement which is used to accomplish these quantum computing applications [7]. On the other hand, QDMs formed by coherent tunneling of the electrons or holes between the two QD layers allow for different new ways of manipulating quantum states in the coupled system. Due to this QDMs have opened new ways to implement quantum computing [19], quantum repeaters, and quantum communication [111].

The stacked InAs QDMs formed by coherent tunneling of the electrons or holes between the two QD layers can be used to generate entangled photon sources. The entangled photons generated by the electron or hole spins in individual quantum dots can serve as a quantum memory with the significant advantage that their spin can be modified and read-out using optical techniques.

In this work, QDM heterostructures for electron and hole storage are studied and fabricated for quantum memory applications, the basic working principle to which can be described as follows: the spin states in the two QD layers can be initialized in an electrically tunable structure by i) optical excitation and tuning of tunnel coupling, then ii) the generation of two-electron (two holes) entangled state by voltage change in QD, iii) the spin states are then spatially separated and entangled by applying voltage, iv) optical excitation induces the emission of spin entangled photon pairs and further v) entanglement distribution via Bell state measurements on two-spin states.

4.6.1 Electron/ Hole storage for quantum memory

The entangled states of electrons or holes in a QDM can be used to store information, however, each has its distinct advantage and limitations in terms of its implementation. Electrons, due to the relatively small effective mass, resulting in relatively large quantization energies in the QDs such that the ground state of the QD can be excited even with short laser pulses, ensuring that no higher levels are excited in the QDs. Using electron spin simplifies the implementation of the for reading in and reading out of the quantum memory. However, a highly asymmetric tunneling probability is required to store optically driven electrons in QDMs. To prevent electrons from tunneling from QDs and being stored, a barrier layer ($\text{Al}_x\text{Ga}_{1-x}\text{As}$) needs to be embedded beneath the InAs QDMs. Another important

parameter is the electronic coupling between the two QDs, which depends on the composition and thickness of the layer between them.

On the other hand, a quantum memory based on hole spins can interact less strongly with the nuclear spins, allowing for longer storage times in principle. However, due to the greater effective mass of holes, the energy levels in the valence band for the QDs are much closer together. As a result, the reading in and out of the quantum memory based on hole spin becomes complicated than reading and writing in electron storage. The position of the barrier layer in contrast to electron storage structures needs to be placed above the QDM layers. Because of the holes' higher effective mass, the electronic coupling decreases; as a result, the thicknesses and composition between quantum dot layers should be tuned relatively.

In this thesis, QDM heterostructures for electron and hole storage are fabricated. Although the growth and results for hole storage samples are discussed in detail. Here we emphasize the critical nature of precisely controlling the InAs deposition for the formation of low-density QDMs and optimizing InAs amount in the top QD layer to almost match the coverage in the lower layer to create QDMs with a similar energy structure for the constituent dots.

4.7 Heterostructure design

In order to study QDMs for quantum storage applications, field-controllable Schottky diode structures were fabricated which allows for precise control of their coupling and charge state. Figure 4.29 illustrates a basic structure of InAs QDMs embedded in a Schottky diode structure with the energy band diagram of the structure. The structure generally consists of highly n-doped GaAs as back contact to investigate CB states, which act as a source of electron gas, whereas for VB state investigations, a p-type layer is used. The InAs QDs layers are sandwiched by undoped GaAs, which act as a tunneling barrier, and $\text{Al}_x\text{Ga}_{1-x}\text{As}$ acts as a current blocking layer which prevents charge carriers from tunneling due to large bandgap. The thickness of each layer depends on specific experiments. The detailed layer sequence is described in the growth section. When the electric field is applied, electrons move from the back contact to the QD and the QD confines a typically small number of electrons. The external voltage modulates the QD energy levels

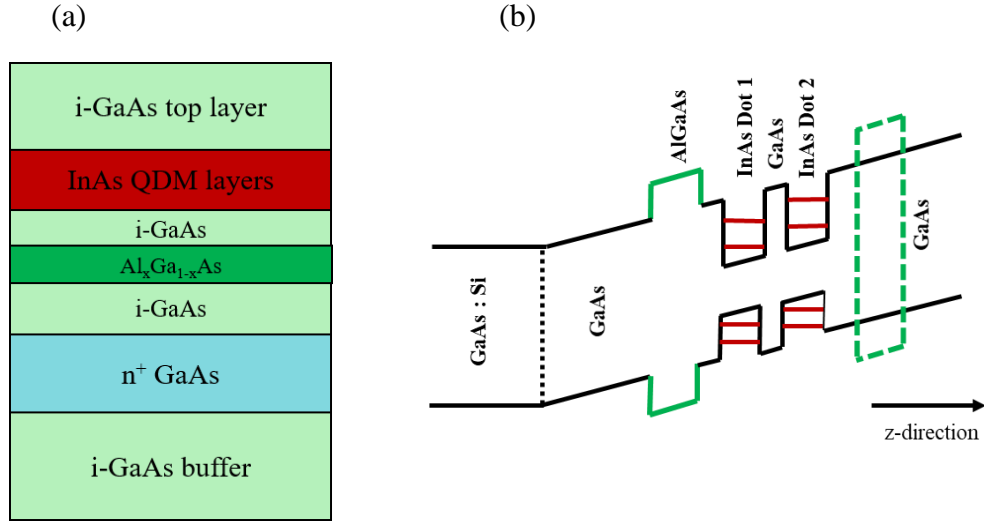


Figure 4.29: (a) Shows the growth structure. (b) The energy band profiles to Schottky diode structures to implement electron and hole storage. The AlGaAs layer (green color) for hole structures is placed above the QDM layers.

in the n-doped GaAs substrate in respect to the Fermi Sea of the n-doped layer. As a result of external voltage via the gate voltage, the electronic states of the two dots can be tuned into resonance.

4.7.1 Enhancing extraction efficiency

The extraction of photons generated by QDs is complicated by the high refractive index (η) of GaAs ($\eta = 3.54$ at room temperature). For most of the QD emission, the photon extraction efficiency decreases due to the internal reflection of the photons because of the refractive index difference between the QD matrix and air. This QD photon efficiency can be improved by embedding a mirror-like structure called Distributed Bragg Reflector (DBR), just below the doped layer in the sample.

A DBR is a stack of alternating semiconductor layers with a high refractive index difference that acts as mirrors over a range of wavelengths. The difference in the refraction index at each interface results in Fresnel reflections, which all add up constructively depending on the layer thickness. DBRs amplify the emitted light from the dots by multiple beam reflection and constructive interference at the required wavelength where the phase

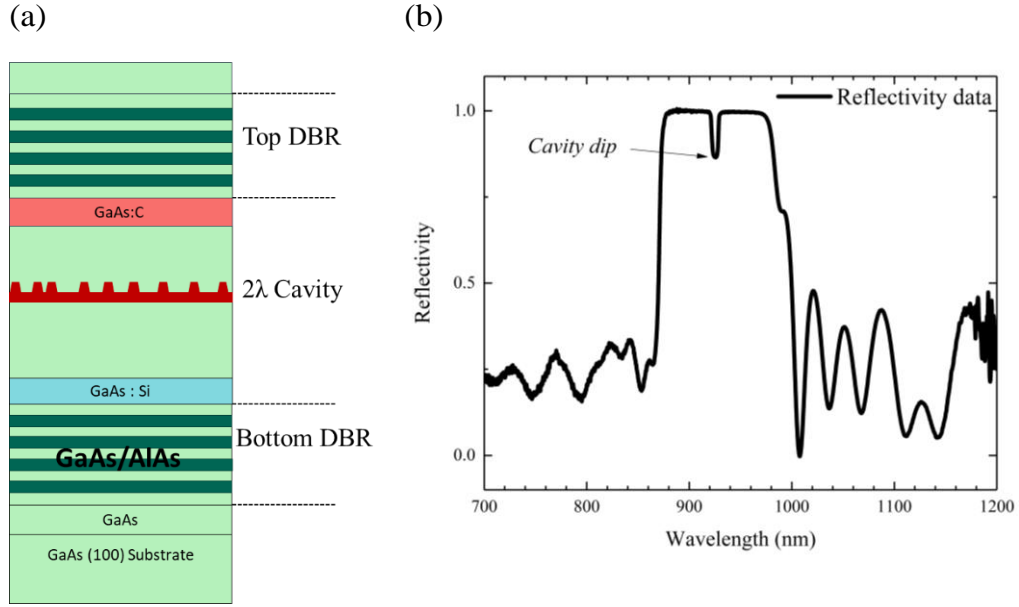


Figure 4.30: pin diode structure grown with AlAs/GaAs DBR. b) The reflectivity measurements at room temperature for the corresponding cavity structure.

difference ($\Delta\phi = \frac{2\pi}{\lambda} d \cdot \lambda$) at the interface of each layer from reflections, must be an integer of π for one of the layers in the pair.

In this work, AlAs/GaAs DBRs are fabricated because of their high refractive index and low lattice mismatch between them. A pin diode structure with top and bottom DBR was fabricated. The schematic of the fabricated structure is shown in Figure 4.30.a. The cavity thickness for λ -cavity with stopband centered around 940 nm at room temperature was 550 nm. Flushed InAs QDs grown using a homogenous deposition approach were embedded in the λ -cavity structure to observe the PL emission. A total of 16 pairs bottom and 10 pairs of top DBRs were grown with AlAs and GaAs thickness of 68 nm and 81 nm, respectively. The growth rates of GaAs and AlAs were precisely measured (described in section 3.1.3) to obtain correct layer thicknesses for DBR structures. The characterization of cavity structures was carried with the assistance of Dr. Viktoriya Zolatanosha. Figure 4.30.b shows the reflectivity measurement done in the reflectivity mode of the FTIR instrument. The stopband and the cavity dip can be observed at 930 nm at room temperature, slightly blue-shifted possibly due to variations in the layer thicknesses. Different samples were grown in a loop with the calculation

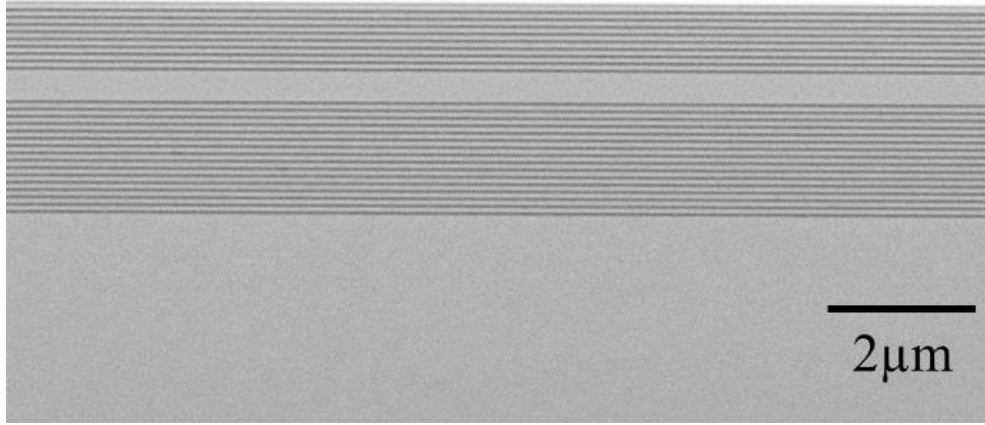


Figure 4.31: SEM image of cavity sample showing 16 and 10 pairs of AlAs/GaAs DBR layers for the bottom and top respectively.

of growth rate measurements considering growth factor, the fractional change in growth rate during the growth over a more extended period. We were able to grow DBR structures with appropriate cavity dip and stopbands, still, a more comprehensive understanding of different related factors is needed to achieve a

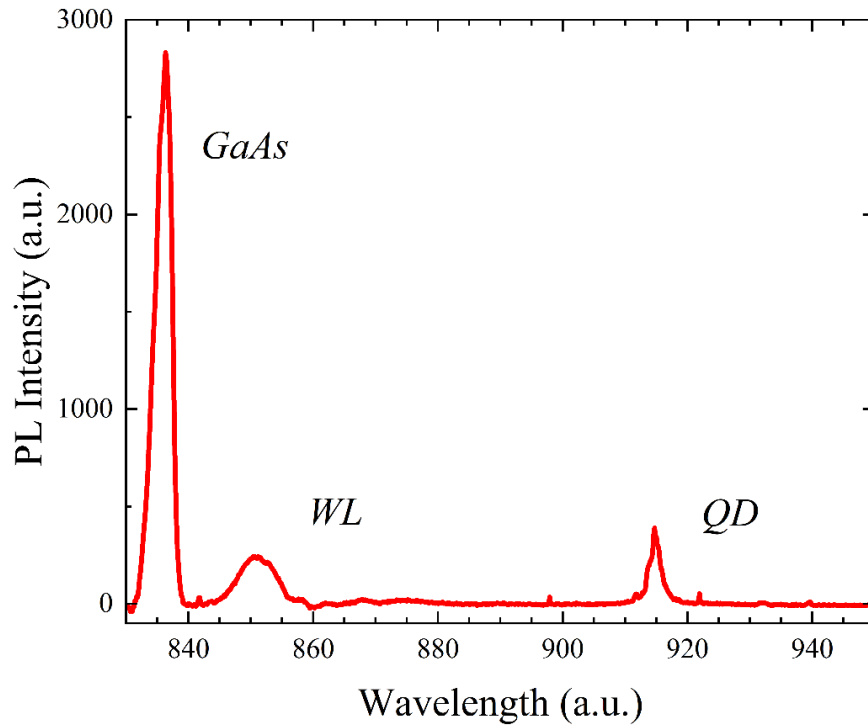


Figure 4.32. The PL spectra of InAs QDs observed in the pin cavity structure at low temperatures.

really good DBR structure for maximum efficiency.

DBR structures were observed by scanning electron microscopy (SEM) to have very fine AlAs/GaAs layers. Figure 4.31 shows the SEM image of the AlAs/GaAs DBR structure with 10 and 16 pairs in the top and bottom, respectively. The PL spectra of InAs QDs of the cavity heterostructure sample are shown in Figure 4.32. PL measurements of this 2.5 nm flushed InAs QDs grown by homogenous approach shows the QD and WL emissions around 916 nm and 850 nm, respectively at low temperature. This significantly implies that QDs grown by homogenous deposition approach can be used and integrated into more complex heterostructures for different applications.

4.6 Growth of quantum dot molecules

The samples were grown on 3" semi-insulating GaAs(100) wafers (Appendix A). The layer sequence, consisting of Schottky diode (pi) devices, was fabricated for initial optimization as illustrated in Figure 4.33.a. The heterostructure layer sequence starts with the growth of 100 nm GaAs at 610°C to smoothen the surface, followed by 30 pairs of a 2 nm AlAs/ 2 nm GaAs superlattice which suppresses the propagation of dislocations across the surface [112]. After that, the growth of the main layer sequence is initiated. A 300 nm thick GaAs buffer layer is grown at 610°C followed by a 100 nm thick GaAs doped with Si ($2.0 \times 10^{18} \text{ cm}^{-3}$) as n-type back contact. During this, the As flux was maintained at 2.2×10^{-5} mbar. Further, 100 nm GaAs were deposited while ramping down the substrate temperature to 480°C and As pressure to 1.5×10^{-5} mbar for QD growth. The InAs SAQDs were grown by a Homogenous In-deposition approach, as discussed in section 4.1.1. After carefully monitoring the substrate temperature, the bottom InAs layer was deposited using 18 cycles (4s deposition, 4s break) of InAs with continuous substrate rotation. The last deposition interval of variable length was added, to fine-tune the In amount, which was adjusted to 0.1 s. The QD emission was tuned using the In-flushed technique as described in section 4.4. The QDs were partially capped with 2.8 nm GaAs followed by an immediate increase of the substrate temperature to 610 °C with a ramp of approximately 20 K/min.

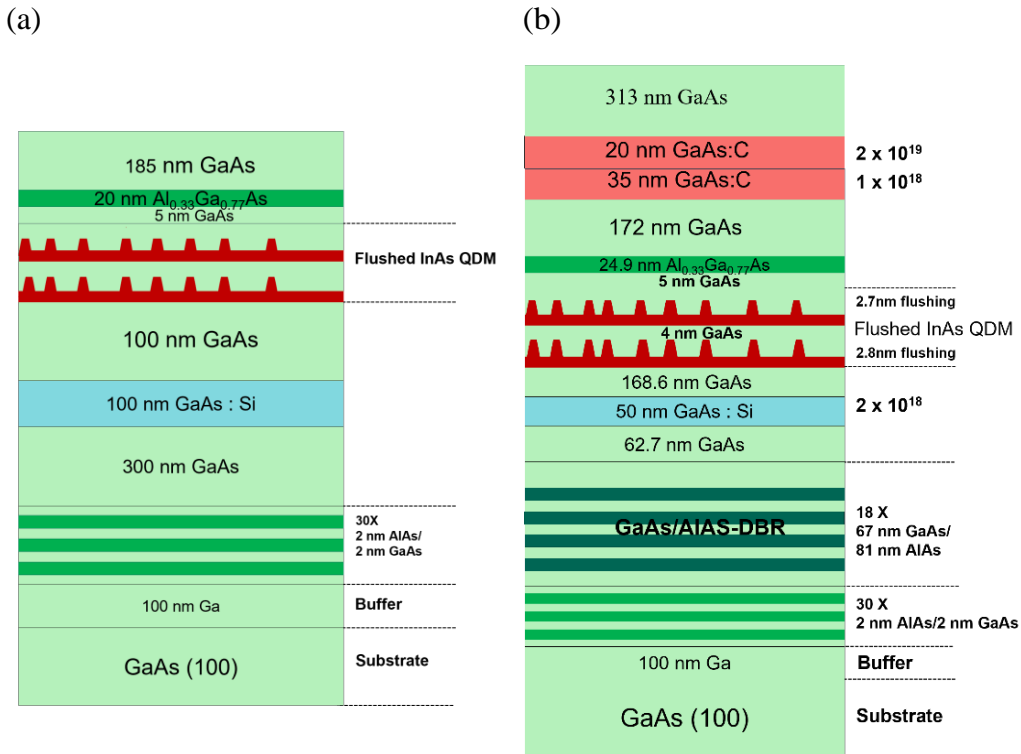


Figure 4.33: Basic layer sequences of hole storage QDM heterostructure; a) pi-Schottky diode structure and b) pin diode structure.

Then after a thin GaAs barrier, 8 nm was deposited at 610°C, before ramping down the substrate temperature to deposit the second InAs layer. The top InAs layer was deposited a cycle less (17 cycles). The In amount in the top layer was varied in a series of samples to match the ground state emissions of the two layers in the required way. The second QD layer was overgrown with the 2.8 nm GaAs and employed with the In-flush approach. The QD in the second layer nucleates directly above the first QD layer due to the strain field from the first. After that grown with 5 nm GaAs at 610°C. At this temperature, a 20 nm $\text{Al}_{0.3}\text{Ga}_{0.7}\text{As}$ layer was deposited, and finally, 185 nm GaAs were deposited. After the growth of the full structure, the substrate temperature was lowered to 300°C and taken out of MBE for ex-situ measurement. The flushed technique was used to obtain ground state emission around 930 nm.

With optimization of QDM properties such as QD density, emission energy tuning, and coupling between the QD layers, QDMs were embedded in pin diode structures with DBRs to improve the extraction efficiency, as shown

in Figure 4.33.b. The layer sequence starts with 19 pairs of AlAs/GaAs DBRs with a thickness of 81 nm and 68 nm, respectively, with a 2λ cavity emitting at 930 nm at low temperature. This is followed the layer sequence described above with slightly different layer thicknesses. Such as the barrier thickness between the QD layers was reduced 5 nm from 8 nm. After the QD layers, C- doped GaAs layers with different thicknesses and doping ($1.0 \times 10^{18} \text{ cm}^{-3}$, $2.0 \times 10^{19} \text{ cm}^{-3}$) are grown. Finally, a thick 300 nm GaAs layer was grown for performing fabricating contacts.

4.8 Characterization

The QDM samples were characterized by surface and optical characterization techniques as described in chapter 3. The results described in the next sections are from sample structure grown and illustrated in Fig. 4.33.a. The different growth parameters were evaluated and tailored to achieve the optimum QDM structure parameters. The QDM density was optimized due to the first-time implementation of a homogenous deposition approach for growing QDMs. This was done by carefully monitoring the growth temperature and depositing optimum material in the top QD layer to match the lower layer. The detailed results are described below:

4.8.1 Low-density optimization

Low-density QDMs are grown using In Homogenous deposition approach, and density optimization is a significantly important step when growing by

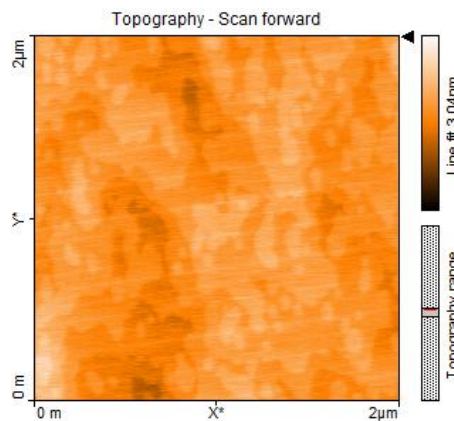


Figure 4.34: AFM image of the QDM sample surface with RMS roughness of 0.5 nm.

the Homogenous deposition approach. Different calibration samples were grown before growing the QDM sample to ascertain the low QD density and fine-tune the In amount in steps of 0.1 s, which corresponds to 0.002 ML of the overall deposition time. For calibration experiments, 18 In-cycles (1.5 ML) were deposited to achieve QD densities in the range of $\sim 1 \times 10^7$ - 10^8 QDs cm^{-2} . The In amount in the top QD layer was deposited a cycle less than the bottom layer due to the strain effect from the lower dots.

The QDM samples had a surface RMS roughness of 0.5 nm, as shown in Figure 4.34.b. The QDM samples were analyzed using low-temperature PL mapping and luminescence imaging to ascertain the density of the QDMs

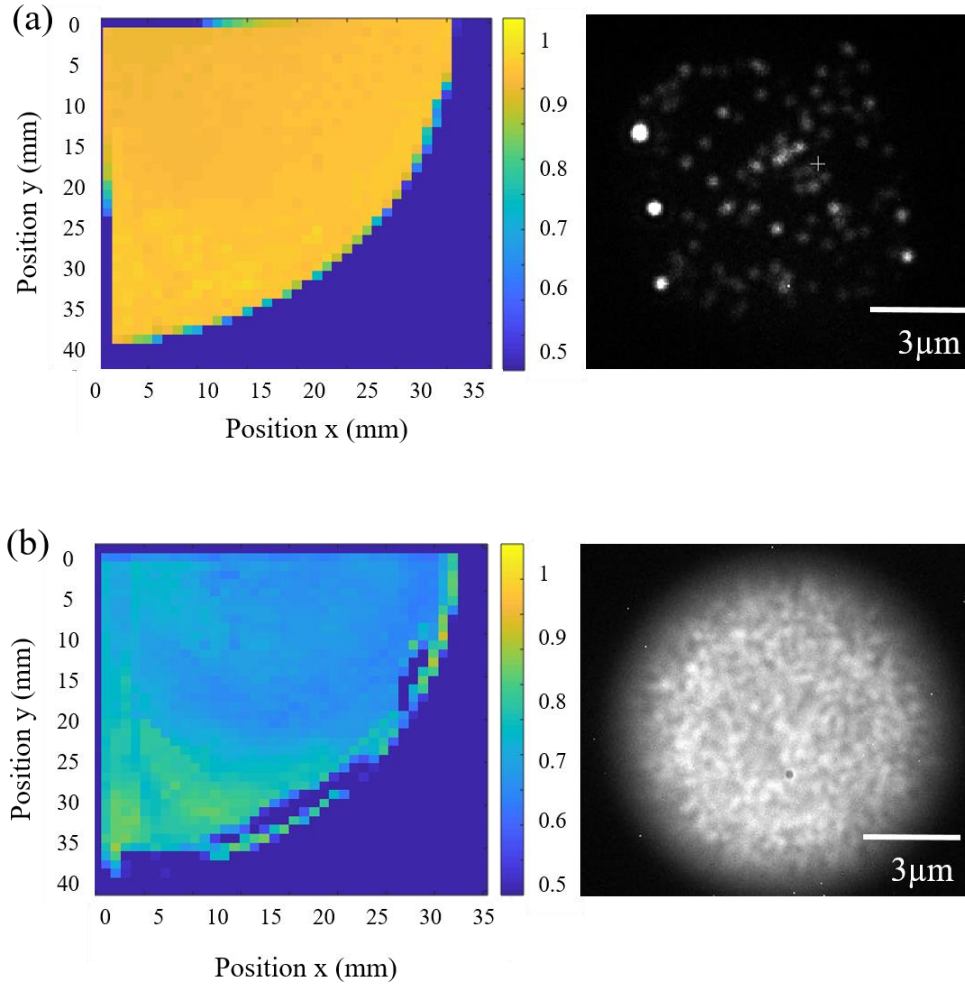


Figure 4.35: PL map in a false-color representation of QDM samples calculated from the PL spectrum with the corresponding PL image of buried InAs QDM in the right.

embedded in the heterostructures. The characterization of densities based on the false-color plot and the pl image is described in detail in section 4.3. Figure 4.35 shows the false-color plot for the QDM samples with corresponding luminescence images at the center of the wafer. The PL maps show the color-coded intensity represented by the ratio (I) (eq. 4.2), where $I = 1$, implies that no QD are present and $I = 0$ corresponds to a high QD density ($>10^9$ QDs cm^{-2}). QDM samples with InAs deposition of 1.50 Ml and 1.502 Ml corresponding to 18 and 18.2 cycles for the bottom layer, respectively, show a significant variation of the density with a change of 0.2 seconds of deposition. Figure 4.35.a shows a homogenous QDM density over the entire quarter of a 3" wafer. The QDM density of less than 1×10^8 QDs cm^{-2} is observed from the PL image at the center of the wafer. While the second QDM sample (Figure 4.35.b) shows a high QDM density ($>10^9$ QD cm^{-2}), the density cannot be resolved with the used setup. The QDM density can be approximated using the calibration of the QDM samples and the ratio I calculated from the PL spectrum.

4.8.2 Emission energy tuning

The best available semiconductor light sources for single-photon sources and entangled photon pairs have wavelengths in the range of 900-940 nm. Therefore, for QDM heterostructures, the ground state-emission of the QDM was tuned to emit around 925 nm at low temperatures. The top QD was slightly red-shifted (~ 1 nm) to be able to distinguish ground state emission between the QD layers. The emission energy of QD layers was tuned employing the In-flush technique (section 4.5.4) to obtain emit around 925 nm. The amount in the top QD layer was carefully optimized with respect to the bottom QD layer to get the ground state emissions of the two layers separately. Different samples were grown with a slightly varying amount of material in the top layer concerning the bottom QD layer. Figure 4.25 shows PL spectra of QDM samples at 10 K with 2.8 nm, 2.85 nm, and 2.9 nm flushing. Both the top and bottom QDs were flushed with the same overgrowth thickness. The QDM emission for these samples was around 930 nm and WL emission at 860 nm. The ensemble QDM emission

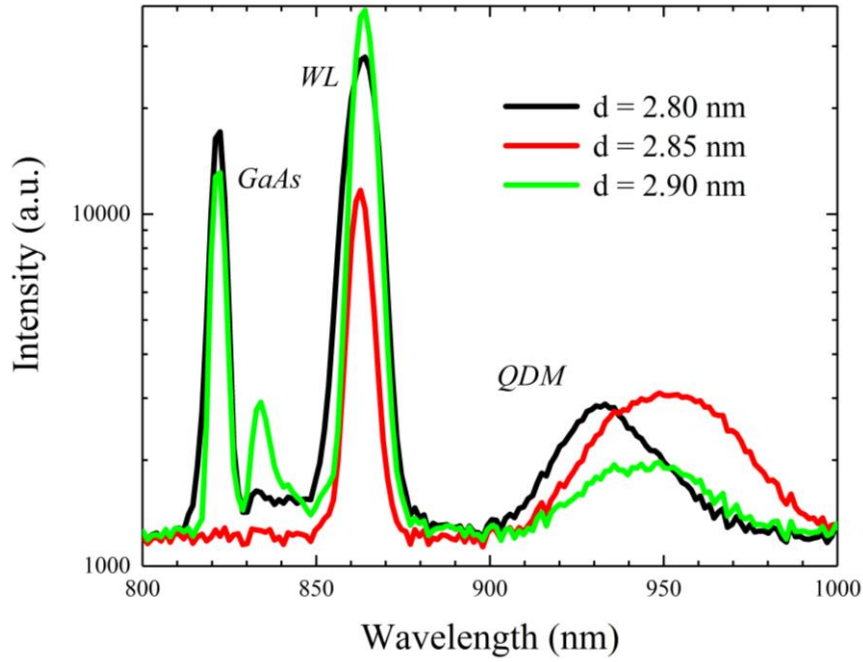


Figure 4.36: PL spectra of flushed QDMs for the low-density region at 10 K.

corresponding to ground state emission was 930, 948, and 952 nm for flushed dots with 2.8 nm, 2.85nm, and 2.9nm overgrowth, respectively, at low temperatures. In the QDMs samples with 2.8 nm flushed QDs we were able to obtain the wavelength of 925 nm. Further in μ -pl measurement, were able to see single dot spectra for the QDM samples as shown in Figure 4.37. The two separate PL peaks at 910 nm and 908 nm corresponding to QD in the top and bottom can be observed. The QD emission of bottom QD slightly is blueshifted with respect to the top QD, as objected which is due to variation In amount in the two layers. [70]

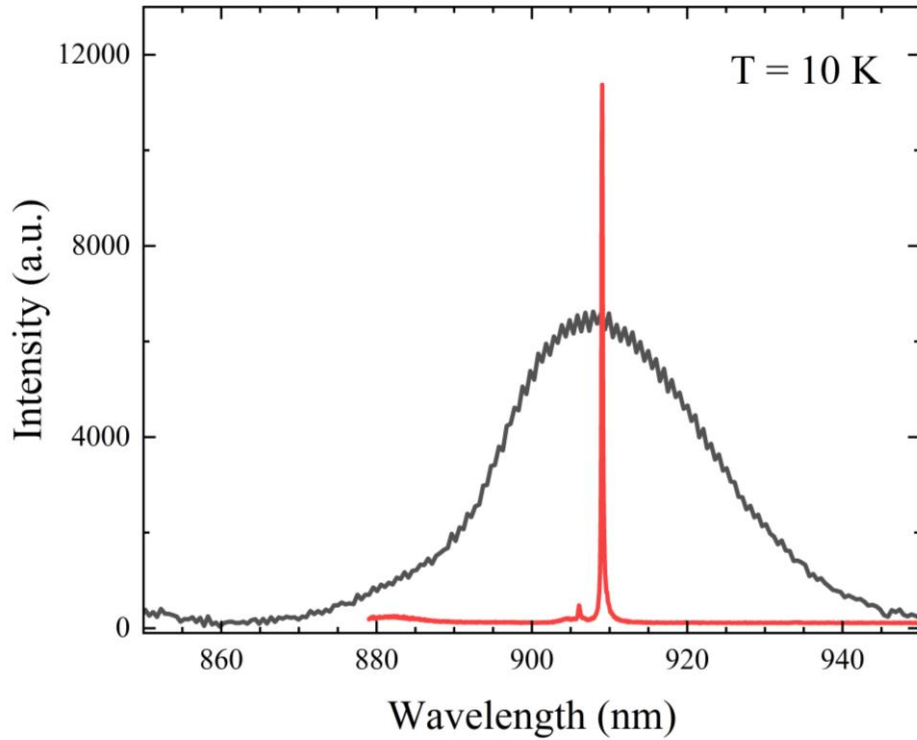


Figure 4.37: PL spectra of an ensemble of QDMs (black) and μ PL for single QDM (red) at 10 K.

4.8.3 Electrical characterization

In this work, the QDM samples were fabricated, and the electrical (electric field dependent PL) measurements were performed on fabricated InAs QDM samples in TU Munich. The results of hole storage samples are presented in this section.

The pi-Schottky diode heterostructures of InAs QDM grown (described in Section 4.6) were fabricated using a conventional technique like optical lithography. The InAs QDM samples were fabricated to form ohmic back contacts that enable charge flow freely across the conductor. On the top of the structure, semi-transparent metallic gates were fabricated to that allow for low-density QDs characterization. By changing the voltage between the

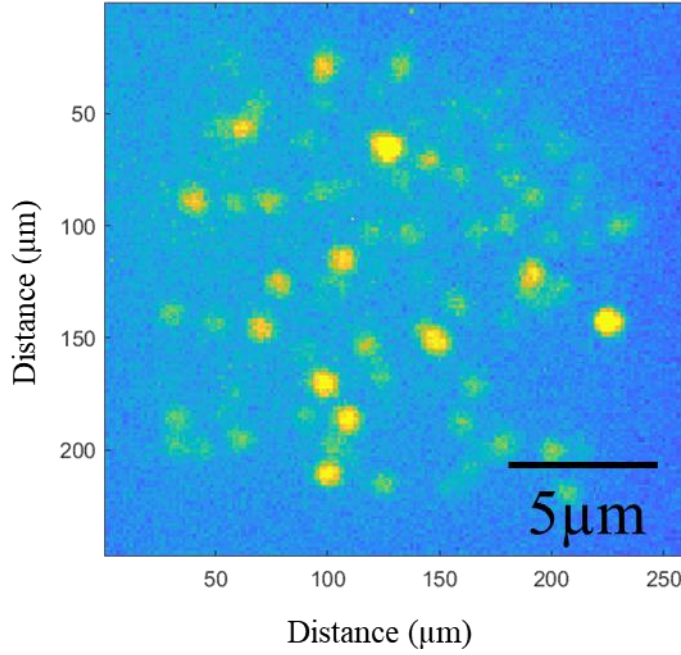


Figure 4.38: μ PL image of contacted InAs QDM sample at 0 V illuminated with 850 nm laser.

front contact and the Ohmic back contact modulate the electric field around the QDs. A detailed description of the methods involved in the fabrication of the metallic top contact and back contacts are given in [94]. After the fabrication of contacts, μ PL measurements were performed to confirm and identify the low-density QDM. Figure 4.38 shows the μ PL image of the fabricated hole storage InAs QDM sample at zero voltage. It can be observed that most of the dots are separately resolvable. The dot density and emission wavelength were best met with this sample.

The electric field-dependent PL measurements for hole storage QDM sample having GaAs barrier layer thickness of 10 nm are shown in Figure 4.39. For the electric field-dependent, PL experiments the electric field was varied between 2 and 23 kV/cm. We can observe multiple lines with differing, weak, and strong Stark shifts that are detected, each of which corresponds to a particular transition state. Due to the randomized nature of optical charging, spectra show several charge states. Moreover, different crossing lines are evident but only a few anticrossing are seen. Direct excitons (electron and hole in the same QD) result in weak Stark shifts while indirect excitons occur when an electron and a hole coexist in separate dots of a

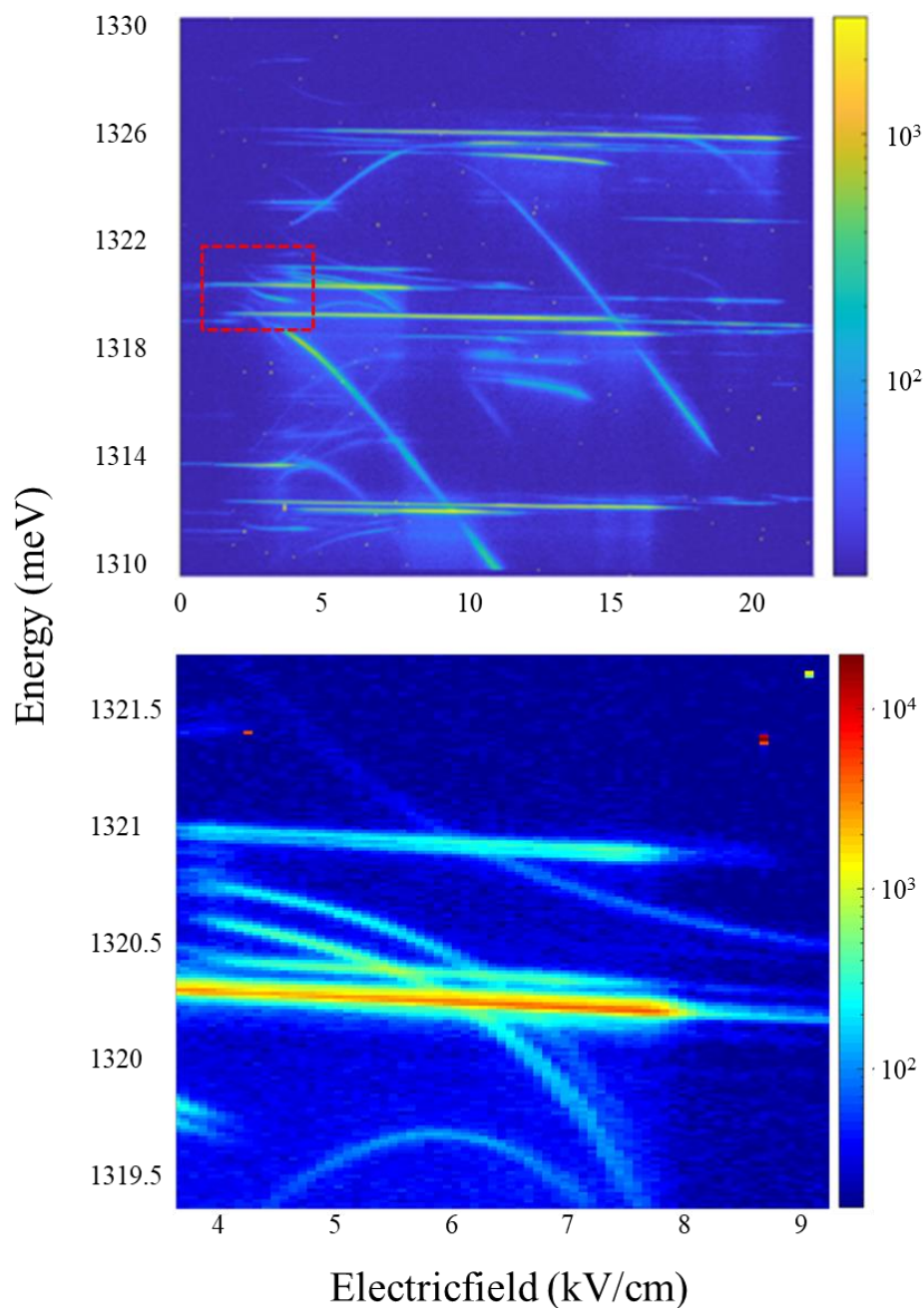


Figure 4.39: Electric field-dependent PL measurements for a hole storage QDM sample having barrier thickness of 10 nm (top). A magnified image of the marked part shows the anticrossing peaks (bottom).

QDM. These can be tuned into and out of resonance by the electric field resulting in anticrossing of the molecular states. The molecular behavior of QDM is mostly revealed through the observation of anticrossings [82,113]. While the PLE data presented in Figure 4.39 (top) shows a lot more

information and is rather intricate, in the magnified image (bottom) we can observe the anticrossing resulting from a single QDM. The splitting of anticrossing is found to be 1.5 meV in this sample. With our interdot distance of 10 nm and comparing it with that given in the literature [84,114], we see that the data are in agreement for the given dot spacing, however, we observe electron tunneling. Generally for hole tunneling with 5-10 nm barrier layer thickness the coupling energy should be in the order of 10-20 meV as stated in different literatures [84,114]. Therefore, to be able to observe hole tunneling in the QDM samples different heterostructure changes were made based on these observations. The top QD were made smaller to be able to have a transition at higher energies. In addition, it was observed that dots currently most likely couple to the back contact. To prevent this the QD was grown ~100 nm away from the back contact. The barrier layer thickness was reduced to 8 nm, which increases the probability for molecules to form. Based on these findings QDM heterostructures with modified layer thicknesses and barrier layer thicknesses were grown for hole storage structures.

This page has been intentionally left blank

CHAPTER 5

5 Summary and Outlook

In summary, the most significant accomplishment of this thesis is the fabrication of low-density InAs QDs and QDMs on GaAs(100) substrates by the MBE technique. This low-density QD in the order of ~ 1 QDs per μm^2 was employed for the fabrication of QDM heterostructures.

We achieved low InAs QD densities in the range of 10^7 - 10^8 QDs cm^{-2} by employing two different In deposition schemes: homogeneous In-deposition and In-gradient approach respectively. For the homogeneous deposition, a continuous InAs deposition was employed with an annealing step for QD formation. This results in at least 70 % of a 3" wafer area ($> 900 \text{ mm}^2$) in dot densities of 1-2 dots per μm^2 if the In amount and the substrate temperature is controlled very precisely. With inhomogeneous In-deposition via growing without sample rotation, we obtained low QD densities reproducible on a small fraction of the wafer surface. For a full-gradient, i.e., depositing the full In amount without rotation, the low-density area amounts in the best case to 10 % of the overall wafer surface, generally less than 90 mm^2 of a 3" wafer, with a very low dot density (less than 1 dot per μm^2) whereas for a half-gradient, i.e. only half the In amount is deposited without rotation, we have a more extended transition region (ca. 7 mm), which corresponds to less than 15 % of the overall wafer area, in case the transition is ideally at the middle of the wafer.

The homogenous deposition process gives a more low-density fraction area however is less reproducible and needs calibration samples every time due to the high sensitivity to the substrate temperature and the In amount. The half-gradient seems a good tradeoff between the length of the transition region

and the variability of the position of the transition region so that, in general, no dedicated calibration samples are required.

In the second part, the different QD growth parameters such as the InAs growth rate, the QD growth temperature, and the growth interruption were studied to observe change in structural and optical properties. The QD size modification leads to a shift in the QD emission energy. The use of LGR and high growth temperatures ($> 500^{\circ}\text{C}$) with slightly high growth interruption time (< 20 sec) for QD growth leads to the formation of uniform QDs with significant redshift of emission wavelength to 1318 nm.

In the third part, low-density InAs QDM heterostructures were fabricated for electron and hole storage applications using homogenous deposition approach. Schottky diode structures were grown to optimize several parameters such as QD density, emission energy tuning, and tunnel coupling for QDM samples. Homogenous deposition approach was successfully implemented for the growth of two QD layers of InAs QDM. The height of QDs was varied by depositing slightly different amount in both the layers, which determines the energies of the lowest confined states, and energy levels. This can be controlled by applying an electric field in the growth direction in the Schottky diode structure.

The results present a promising approach for the fabrication of low-density InAs QDs grown by S-K growth mode. Using a homogeneous deposition approach the InAs QDs fabricated were used in the QDM and pin cavity heterostructures with DBRs for the first time. Half-gradient seems a reasonable compromise for extending low density transition region and reproducible low-density areal fraction in comparison to other two. We gained a better understanding of the secondary purpose of investigating InAs QDs growth factors which can be implemented further for different studies. InAs QDM heterostructures were grown for quantum storage applications with most of important parameters being optimized.

Bibliography

- [1] R. Kumar Mishra, A. G. Vedeshwar, and R. P. Tandon, *The Role of Glass-Viscosity on the Growth of Semiconductor Quantum Dots in Glass Matrices*, J. Appl. Phys. **111**, 094315 (2012).
- [2] L. L. Chang, L. Esaki, and R. Tsu, *Resonant Tunneling in Semiconductor Double Barriers*, Appl. Phys. Lett. **24**, 593 (1974).
- [3] P. H. Holloway and T. J. Anderson, editors, *Compound Semiconductors: Growth, Processing, and Devices* (CRC Press, Boca Raton, Fla, 1989).
- [4] M. Reed, J. Randall, R. Aggarwal, R. Matyi, T. Moore, and A. Wetsel, *Observation of Discrete Electronic States in a Zero-Dimensional Semiconductor Nanostructure*, Phys. Rev. Lett. **60**, 535 (1988).
- [5] L. Goldstein, F. Glas, J. Y. Marzin, M. N. Charasse, and G. Le Roux, *Growth by Molecular Beam Epitaxy and Characterization of InAs/GaAs Strained-layer Superlattices*, Appl. Phys. Lett. **47**, 1099 (1985).
- [6] K. Nishi, *Device Applications of Quantum Dots*, in *Semiconductor Quantum Dots*, edited by Y. Masumoto and T. Takagahara (Springer Berlin Heidelberg, Berlin, Heidelberg, 2002), pp. 457–480.
- [7] P. Michler, editor, *Quantum Dots for Quantum Information Technologies* (Springer International Publishing, Cham, 2017).
- [8] R. M. Stevenson, R. J. Young, P. Atkinson, K. Cooper, D. A. Ritchie, and A. J. Shields, *A Semiconductor Source of Triggered Entangled Photon Pairs*, Nature **439**, 179 (2006).
- [9] G.-C. Shan, Z.-Q. Yin, C. H. Shek, and W. Huang, *Single Photon Sources with Single Semiconductor Quantum Dots*, Front. Phys. **9**, 170 (2014).
- [10] S. T. Moroni, T. H. Chung, G. Juska, A. Gocalinska, and E. Pelucchi, *Statistical Study of Stacked/Coupled Site-Controlled Pyramidal Quantum Dots and Their Excitonic Properties*, Appl. Phys. Lett. **111**, 083103 (2017).

- [11] L. Wang, A. Rastelli, S. Kiravittaya, M. Benyoucef, and O. G. Schmidt, *Self-Assembled Quantum Dot Molecules*, Adv. Mater. **21**, 2601 (2009).
- [12] R. C. Ashoori, *Electrons in Artificial Atoms*, Nature **379**, 413 (1996).
- [13] Z. M. Wang, editor, *Self-Assembled Quantum Dots* (Springer, New York, 2008).
- [14] K. Yamaguchi, K. Yujobo, and T. Kaizu, *Stranski-Krastanov Growth of InAs Quantum Dots with Narrow Size Distribution*, Jpn. J. Appl. Phys. **39**, L1245 (2000).
- [15] P. B. Joyce, T. J. Krzyzewski, G. R. Bell, B. A. Joyce, and T. S. Jones, *Composition of InAs Quantum Dots on GaAs(001): Direct Evidence for (In,Ga)As Alloying*, Phys. Rev. B **58**, R15981 (1998).
- [16] P. B. Joyce, T. J. Krzyzewski, G. R. Bell, T. S. Jones, S. Malik, D. Childs, and R. Murray, *Effect of Growth Rate on the Size, Composition, and Optical Properties of InAs/GaAs Quantum Dots Grown by Molecular-Beam Epitaxy*, Phys. Rev. B **62**, 10891 (2000).
- [17] M. Faraday, *Experimental Researches in Electricity. Fourth Series*, Philos. Trans. R. Soc. Lond. **123**, 507 (1833).
- [18] M. Grundmann, *The Physics of Semiconductors: An Introduction Including Devices and Nanophysics* (Springer, Berlin ; New York, 2006).
- [19] J. Koenigsberger and J. Weiss, *Über die thermoelektrischen Effekte (Thermokräfte, Thomsonwärme) und die Wärmeleitung in einigen Elementen und Verbindungen und über die experimentelle Prüfung der Elektronentheorien*, Ann. Phys. **340**, 1 (1911).
- [20] 2524035.Pdf, (n.d.).
- [21] I. Saïdi, S. Ben Radhia, and K. Boujdaria, *Band Parameters of GaAs, InAs, InP, and InSb in the 40-Band $K\cdot p$ Model*, J. Appl. Phys. **107**, 043701 (2010).
- [22] P. Y. Yu and M. Cardona, *Introduction*, in *Fundamentals of Semiconductors* (Springer Berlin Heidelberg, Berlin, Heidelberg, 2010), pp. 1–15.
- [23] Y. P. Varshni, *Temperature Dependence of the Energy Gap in Semiconductors*, Physica **34**, 149 (1967).
- [24] U. W. Pohl, *Epitaxy of Semiconductors* (Springer Berlin Heidelberg, Berlin, Heidelberg, 2013).
- [25] S. J. Moss, A. Ledwith and A. L. S. J. Moss, *The Chemistry of the Semiconductor Industry* (Springer, 1987).
- [26] I. Vurgaftman, J. R. Meyer, and L. R. Ram-Mohan, *Band Parameters for III–V Compound Semiconductors and Their Alloys*, J. Appl. Phys. **89**, 5815 (2001).

-
- [27] L. Vegard, *Die Konstitution der Mischkristalle und die Raumfüllung der Atome*, Z. Für Phys. **5**, 17 (1921).
 - [28] J. A. Van Vechten and T. K. Bergstresser, *Electronic Structures of Semiconductor Alloys*, Phys. Rev. B **1**, 3351 (1970).
 - [29] M. A. Herman, W. Richter, and H. Sitter, *Epitaxy: Physical Principles and Technical Implementation*, Vol. 62 (Springer Berlin Heidelberg, Berlin, Heidelberg, 2004).
 - [30] P. Capper and M. Mauk, editors, *Liquid Phase Epitaxy of Electronic, Optical, and Optoelectronic Materials* (Wiley, Chichester, England ; Hoboken, NJ, 2007).
 - [31] G. W. Cullen, E. Kaldis, and R. L. Parker, *Vapour Growth and Epitaxy: Proceedings of the Third International Conference on Vapour Growth and Epitaxy, Amsterdam, The Netherlands, 18-21 August 1975*. (Elsevier Science, Amsterdam, 2014).
 - [32] R. F. C. Farrow and R. F. C. Farrow, *Molecular Beam Epitaxy: Applications to Key Materials*. (Elsevier Science, Burlington, 1995).
 - [33] T. Kääriäinen, D. Cameron, M.-L. Kääriäinen, and A. Sherman, *Atomic Layer Deposition: Principles, Characteristics, and Nanotechnology Applications*, 2nd Edition (Scrivener Publishing, Beverly, MA, 2013).
 - [34] E. Bauer, *Phänomenologische Theorie Der Kristallabscheidung an Oberflächen. I*, Z. Für Krist. **110**, 372 (1958).
 - [35] D. Bimberg, editor, *Semiconductor Nanostructures* (Springer Berlin Heidelberg, Berlin, Heidelberg, 2008).
 - [36] E. Borovitskaya and M. Shur, editors, *Quantum Dots* (World Scientific, River Edge, N.J, 2002).
 - [37] M. A. Cotta, *Quantum Dots and Their Applications: What Lies Ahead?*, ACS Appl. Nano Mater. **3**, 4920 (2020).
 - [38] S. Fafard, Z. R. Wasilewski, C. N. Allen, K. Hinzer, J. P. McCaffrey, and Y. Feng, *Lasing in Quantum-Dot Ensembles with Sharp Adjustable Electronic Shells*, Appl. Phys. Lett. **75**, 986 (1999).
 - [39] V. M. Ustinov, E. R. Weber, S. Ruvimov, Z. Liliental-Weber, A. E. Zhukov, A. Yu. Egorov, A. R. Kovsh, A. F. Tsatsul'nikov, and P. S. Kop'ev, *Effect of Matrix on InAs Self-Organized Quantum Dots on InP Substrate*, Appl. Phys. Lett. **72**, 362 (1998).
 - [40] L. Friedman, G. Sun, and R. A. Soref, *SiGe/Si THz Laser Based on Transitions between Inverted Mass Light-Hole and Heavy-Hole Subbands*, Appl. Phys. Lett. **78**, 401 (2001).
 - [41] T. Lundstrom, W. Schoenfeld, H. Lee, and P. M. Petroff, *Exciton Storage in Semiconductor Self-Assembled Quantum Dots*, Science **286**, 2312 (1999).

- [42] M. C. Bödefeld, R. J. Warburton, K. Karrai, J. P. Kotthaus, G. Medeiros-Ribeiro, and P. M. Petroff, *Storage of Electrons and Holes in Self-Assembled InAs Quantum Dots*, Appl. Phys. Lett. **74**, 1839 (1999).
- [43] P. Schittenhelm, *Self-Assembled Ge Dots: Growth, Characterization, Ordering, and Applications*, J. Vac. Sci. Technol. B Microelectron. Nanometer Struct. **16**, 1575 (1998).
- [44] R. Soref, *Applications of Silicon-Based Optoelectronics*, MRS Bull. **23**, 20 (1998).
- [45] N. H. Bonadeo, J. Erland, D. Gammon, D. Park, D. S. Katzer, and D. G. Steel, *Coherent Optical Control of the Quantum State of a Single Quantum Dot*, Science **282**, 1473 (1998).
- [46] S. Birudavolu, N. Nuntawong, G. Balakrishnan, Y. C. Xin, S. Huang, S. C. Lee, S. R. J. Brueck, C. P. Hains, and D. L. Huffaker, *Selective Area Growth of InAs Quantum Dots Formed on a Patterned GaAs Substrate*, Appl. Phys. Lett. **85**, 2337 (2004).
- [47] N. N. Ledentsov, V. A. Shchukin, M. Grundmann, N. Kirstaedter, J. Böhrer, O. Schmidt, D. Bimberg, V. M. Ustinov, A. Yu. Egorov, A. E. Zhukov, P. S. Kop'ev, S. V. Zaitsev, N. Yu. Gordeev, Zh. I. Alferov, A. I. Borovkov, A. O. Kosogov, S. S. Ruvimov, P. Werner, U. Gösele, and J. Heydenreich, *Direct Formation of Vertically Coupled Quantum Dots in Stranski-Krastanow Growth*, Phys. Rev. B **54**, 8743 (1996).
- [48] C. Pryor, *Eight-Band Calculations of Strained InAs/GaAs Quantum Dots Compared with One-, Four-, and Six-Band Approximations*, Phys. Rev. B **57**, 7190 (1998).
- [49] H. Fu, L.-W. Wang, and A. Zunger, *Excitonic Exchange Splitting in Bulk Semiconductors*, Phys. Rev. B **59**, 5568 (1999).
- [50] D. Leonard, M. Krishnamurthy, C. M. Reaves, S. P. Denbaars, and P. M. Petroff, *Direct Formation of Quantum-sized Dots from Uniform Coherent Islands of InGaAs on GaAs Surfaces*, Appl. Phys. Lett. **63**, 3203 (1993).
- [51] A. J. Ptak, *Principles of Molecular Beam Epitaxy*, in *Handbook of Crystal Growth* (Elsevier, 2015), pp. 161–192.
- [52] J. R. Arthur, *Interaction of Ga and As₂ Molecular Beams with GaAs Surfaces*, J. Appl. Phys. **39**, 4032 (1968).
- [53] T. E. Bell, *Alfred Yi Cho [Biography]*, IEEE Spectr. **31**, 70 (1994).
- [54] A. Madhukar, *Far from Equilibrium Vapour Phase Growth of Lattice Matched III–V Compound Semiconductor Interfaces: Some Basic Concepts and Monte-Carlo Computer Simulations*, Surf. Sci. **132**, 344 (1983).
- [55] G. Shan, X. Zhao, M. Hu, C.-H. Shek, and W. Huang, *Vertical-External-Cavity Surface-Emitting Lasers and Quantum Dot Lasers*, Front. Optoelectron. **5**, 157 (2012).

-
- [56] D. L. Huffaker, G. Park, Z. Zou, O. B. Shchekin, and D. G. Deppe, *1.3 Mm Room-Temperature GaAs-Based Quantum-Dot Laser*, Appl. Phys. Lett. **73**, 2564 (1998).
 - [57] J. X. Chen, A. Markus, A. Fiore, U. Oesterle, R. P. Stanley, J. F. Carlin, R. Houdré, M. Illegems, L. Lazzarini, L. Nasi, M. T. Todaro, E. Piscopiello, R. Cingolani, M. Catalano, J. Katcki, and J. Ratajczak, *Tuning InAs/GaAs Quantum Dot Properties under Stranski-Krastanov Growth Mode for 1.3 Mm Applications*, J. Appl. Phys. **91**, 6710 (2002).
 - [58] J. Phillips, K. Kamath, and P. Bhattacharya, *Far-Infrared Photoconductivity in Self-Organized InAs Quantum Dots*, Appl. Phys. Lett. **72**, 2020 (1998).
 - [59] N. Yasuoka, K. Kawaguchi, H. Ebe, T. Akiyama, M. Ekawa, S. Tanaka, K. Morito, A. Uetake, M. Sugawara, and Y. Arakawa, *Demonstration of Transverse-Magnetic Dominant Gain in Quantum Dot Semiconductor Optical Amplifiers*, Appl. Phys. Lett. **92**, 101108 (2008).
 - [60] X.-Q. Li and Y. Arakawa, *Single Qubit from Two Coupled Quantum Dots: An Approach to Semiconductor Quantum Computations*, Phys. Rev. A **63**, 012302 (2000).
 - [61] D. Bimberg, M. Grundmann, and N. N. Ledentsov, *Quantum Dot Heterostructures* (John Wiley, Chichester, [Eng.]; New York, 1999).
 - [62] J. M. Moison, F. Houzay, F. Barthe, L. Leprince, E. André, and O. Vatel, *Self-organized Growth of Regular Nanometer-scale InAs Dots on GaAs*, Appl. Phys. Lett. **64**, 196 (1994).
 - [63] A. Madhukar, Q. Xie, P. Chen, and A. Konkar, *Nature of Strained InAs Three-dimensional Island Formation and Distribution on GaAs(100)*, Appl. Phys. Lett. **64**, 2727 (1994).
 - [64] D. Leonard, K. Pond, and P. M. Petroff, *Critical Layer Thickness for Self-Assembled InAs Islands on GaAs*, Phys. Rev. B **50**, 11687 (1994).
 - [65] M. Grundmann, editor, *Nano-Optoelectronics* (Springer Berlin Heidelberg, Berlin, Heidelberg, 2002).
 - [66] D. J. Eaglesham and M. Cerullo, *Dislocation-Free Stranski-Krastanow Growth of Ge on Si(100)*, Phys. Rev. Lett. **64**, 1943 (1990).
 - [67] J. Wu and P. Jin, *Self-Assembly of InAs Quantum Dots on GaAs(001) by Molecular Beam Epitaxy*, Front. Phys. **10**, 7 (2015).
 - [68] W. L. Barnes, G. Björk, J. M. Gérard, P. Jonsson, J. A. E. Wasey, P. T. Worthing, and V. Zwiller, *Solid-State Single Photon Sources: Light Collection Strategies*, Eur. Phys. J. - At. Mol. Opt. Phys. **18**, 197 (2002).

- [69] P. Michler, editor , *Single Quantum Dots: Fundamentals, Applications, and New Concepts* (Springer-Verlag, Berlin ; New York, 2003).
- [70] J. Sun, P. Jin, and Z.-G. Wang, *Extremely Low Density InAs Quantum Dots Realized in Situ on (100) GaAs*, *Nanotechnology* **15**, 1763 (2004).
- [71] K. H. Schmidt, G. Medeiros-Ribeiro, U. Kunze, G. Abstreiter, M. Hagn, and P. M. Petroff, *Size Distribution of Coherently Strained InAs Quantum Dots*, *J. Appl. Phys.* **84**, 4268 (1998).
- [72] P. Jin, X. L. Ye, and Z. G. Wang, *Growth of Low-Density InAs/GaAs Quantum Dots on a Substrate with an Intentional Temperature Gradient by Molecular Beam Epitaxy*, *Nanotechnology* **16**, 2775 (2005).
- [73] H. Z. Song, T. Usuki, Y. Nakata, N. Yokoyama, H. Sasakura, and S. Muto, *Formation of InAs/GaAs Quantum Dots from a Subcritical InAs Wetting Layer: A Reflection High-Energy Electron Diffraction and Theoretical Study*, *Phys. Rev. B* **73**, 115327 (2006).
- [74] L. N. McCabe and J. M. O. Zide, *Techniques for Epitaxial Site-Selective Growth of Quantum Dots*, *J. Vac. Sci. Technol. A* **39**, 010802 (2021).
- [75] T. J. Krzyzewski and T. S. Jones, *Ripening and Annealing Effects in InAs/GaAs(001) Quantum Dot Formation*, *J. Appl. Phys.* **96**, 668 (2004).
- [76] D. M. Schaadt, D. Z. Hu, and K. H. Ploog, *Stress Evolution during Ripening of Self-Assembled InAs/GaAs Quantum Dots*, *J. Vac. Sci. Technol. B Microelectron. Nanometer Struct.* **24**, 2069 (2006).
- [77] M. Henini, editor , *Molecular Beam Epitaxy: From Research to Mass Production*, Second edition (Elsevier, Amsterdam, Netherlands ; Cambridge, MA, 2018).
- [78] G. Ortner, I. Yugova, G. B. H. von Högersthal, A. Larionov, H. Kurtze, D. R. Yakovlev, M. Bayer, S. Fafard, Z. Wasilewski, P. Hawrylak, Y. B. Lyanda-Geller, T. L. Reinecke, A. Babinski, M. Potemski, V. B. Timofeev, and A. Forchel, *Fine Structure in the Excitonic Emission of InAs / GaAs Quantum Dot Molecules*, *Phys. Rev. B* **71**, 125335 (2005).
- [79] G. S. Solomon, J. A. Trezza, A. F. Marshall, and J. S. Harris, Jr., *Vertically Aligned and Electronically Coupled Growth Induced InAs Islands in GaAs*, *Phys. Rev. Lett.* **76**, 952 (1996).
- [80] Q. Xie, A. Madhukar, P. Chen, and N. P. Kobayashi, *Vertically Self-Organized InAs Quantum Box Islands on GaAs(100)*, *Phys. Rev. Lett.* **75**, 2542 (1995).
- [81] Q. Xie, P. Chen, and A. Madhukar, *InAs Island-induced-strain Driven Adatom Migration during GaAs Overlayer Growth*, *Appl. Phys. Lett.* **65**, 2051 (1994).


-
- [82] H. J. Krenner, M. Sabathil, E. C. Clark, A. Kress, D. Schuh, M. Bichler, G. Abstreiter, and J. J. Finley, *Direct Observation of Controlled Coupling in an Individual Quantum Dot Molecule*, Phys. Rev. Lett. **94**, 057402 (2005).
 - [83] B. Legrand, J. P. Nys, B. Grandidier, D. Stiévenard, A. Lemaître, J. M. Gérard, and V. Thierry-Mieg, *Quantum Box Size Effect on Vertical Self-Alignment Studied Using Cross-Sectional Scanning Tunneling Microscopy*, Appl. Phys. Lett. **74**, 2608 (1999).
 - [84] A. S. Bracker, M. Scheibner, M. F. Doty, E. A. Stinaff, I. V. Ponomarev, J. C. Kim, L. J. Whitman, T. L. Reinecke, and D. Gammon, *Engineering Electron and Hole Tunneling with Asymmetric InAs Quantum Dot Molecules*, Appl. Phys. Lett. **89**, 233110 (2006).
 - [85] M. F. Doty, J. I. Climente, M. Korkusinski, M. Scheibner, A. S. Bracker, P. Hawrylak, and D. Gammon, *Antibonding Ground States in InAs Quantum-Dot Molecules*, Phys. Rev. Lett. **102**, 047401 (2009).
 - [86] A. Ichimiya and P. I. Cohen, *Reflection High-Energy Electron Diffraction*, 1st ed. (Cambridge University Press, 2004).
 - [87] S. Hasegawa, *Reflection High-Energy Electron Diffraction*, in *Characterization of Materials*, edited by E. N. Kaufmann (John Wiley & Sons, Inc., Hoboken, NJ, USA, 2012), p. com139.
 - [88] L. Däweritz and R. Hey, *Reconstruction and Defect Structure of Vicinal GaAs(001) and Al_xGa_{1-x}As(001) Surfaces during MBE Growth*, Surf. Sci. **236**, 15 (1990).
 - [89] D. J. Chadi, *Semiconductor Surface Reconstruction*, Vacuum **33**, 613 (1983).
 - [90] T. E. Harvey, K. A. Bertness, R. K. Hickernell, C. M. Wang, and J. D. Splett, *Accuracy of AlGaAs Growth Rates and Composition Determination Using RHEED Oscillations*, J. Cryst. Growth **251**, 73 (2003).
 - [91] N. Cherroret, A. Chakravarty, and A. Kar, *Temperature-Dependent Refractive Index of Semiconductors*, J. Mater. Sci. **43**, 1795 (2008).
 - [92] G. Binnig, C. F. Quate, and Ch. Gerber, *Atomic Force Microscope*, Phys. Rev. Lett. **56**, 930 (1986).
 - [93] K. M. Muller, *Optical Control of Quantum States in Artificial Atoms and Molecules*, 216 (n.d.).
 - [94] A. Ohtake and M. Ozeki, *In Situ Observation of Surface Processes in InAs/GaAs(001) Heteroepitaxy: The Role of As on the Growth Mode*, Appl. Phys. Lett. **78**, 431 (2001).

- [95] Y. Morishita, K. Osada, and T. Hasegawa, *Effects of Growth Interruption during Growth of InAs Wetting Layer on Formation of InAs Quantum Dots*, Jpn. J. Appl. Phys. **44**, 2925 (2005).
- [96] L. H. Li, N. Chauvin, G. Patriarche, B. Alloing, and A. Fiore, *Growth-Interruption-Induced Low-Density InAs Quantum Dots on GaAs*, J. Appl. Phys. **104**, 083508 (2008).
- [97] *Gwyddion – Free SPM (AFM, SNOM/NSOM, STM, MFM, ...) Data Analysis Software*, <http://gwyddion.net/>.
- [98] Z. R. Wasilewski, S. Fafard, and J. P. McCaffrey, *Size and Shape Engineering of Vertically Stacked Self-Assembled Quantum Dots*, J. Cryst. Growth **201–202**, 1131 (1999).
- [99] N. Perret, D. Morris, L. Franchomme-Fossé, R. Côté, S. Fafard, V. Aimez, and J. Beauvais, *Origin of the Inhomogeneous Broadening and Alloy Intermixing in InAs/GaAs Self-Assembled Quantum Dots*, Phys. Rev. B **62**, 5092 (2000).
- [100] A. Babiński, J. Jasiński, R. Bożek, A. Szepielow, and J. M. Baranowski, *Rapid Thermal Annealing of InAs/GaAs Quantum Dots under a GaAs Proximity Cap*, Appl. Phys. Lett. **79**, 2576 (2001).
- [101] F. Y. Chang, C. C. Wu, and H. H. Lin, *Effect of InGaAs Capping Layer on the Properties of InAs/InGaAs Quantum Dots and Lasers*, Appl. Phys. Lett. **82**, 4477 (2003).
- [102] C. K. Chia, Y. W. Zhang, S. S. Wong, S. J. Chua, A. M. Yong, and S. Y. Chow, *Testing the Upper Limit of InAs/GaAs Self-Organized Quantum Dots Density by Fast Growth Rate*, Superlattices Microstruct. **44**, 420 (2008).
- [103] B. Alloing, C. Zinoni, V. Zwiller, L. H. Li, C. Monat, M. Gobet, G. Buchs, A. Fiore, E. Pelucchi, and E. Kapon, *Growth and Characterization of Single Quantum Dots Emitting at 1300 Nm*, Appl. Phys. Lett. **86**, 101908 (2005).
- [104] U. W. Pohl, K. Pötschke, A. Schliwa, F. Guffarth, D. Bimberg, N. D. Zakharov, P. Werner, M. B. Lifshits, V. A. Shchukin, and D. E. Jesson, *Evolution of a Multimodal Distribution of Self-Organized InAs / GaAs Quantum Dots*, Phys. Rev. B **72**, 245332 (2005).
- [105] S. Kiravittaya, Y. Nakamura, and O. G. Schmidt, *Photoluminescence Linewidth Narrowing of InAs/GaAs Self-Assembled Quantum Dots*, Phys. E Low-Dimens. Syst. Nanostructures **13**, 224 (2002).
- [106] J. M. García, G. Medeiros-Ribeiro, K. Schmidt, T. Ngo, J. L. Feng, A. Lorke, J. Kotthaus, and P. M. Petroff, *Intermixing and Shape Changes during the Formation of InAs Self-Assembled Quantum Dots*, Appl. Phys. Lett. **71**, 2014 (1997).

-
- [107] G. Costantini, A. Rastelli, C. Manzano, P. Acosta-Diaz, R. Songmuang, G. Katsaros, O. G. Schmidt, and K. Kern, *Interplay between Thermodynamics and Kinetics in the Capping of InAs / GaAs (001) Quantum Dots*, Phys. Rev. Lett. **96**, 226106 (2006).
 - [108] Q. Gong, P. Offermans, R. Nötzel, P. M. Koenraad, and J. H. Wolter, *Capping Process of InAs/GaAs Quantum Dots Studied by Cross-Sectional Scanning Tunneling Microscopy*, Appl. Phys. Lett. **85**, 5697 (2004).
 - [109] G. D. Lian, J. Yuan, L. M. Brown, G. H. Kim, and D. A. Ritchie, *Modification of InAs Quantum Dot Structure by the Growth of the Capping Layer*, Appl. Phys. Lett. **73**, 49 (1998).
 - [110] O. Brandt, K. Ploog, L. Tapfer, M. Hohenstein, R. Bierwolf, and F. Phillipp, *Formation and Morphology of InAs/GaAs Heterointerfaces*, Phys. Rev. B **45**, 8443 (1992).
 - [111] P. Kok, W. J. Munro, K. Nemoto, T. C. Ralph, J. P. Dowling, and G. J. Milburn, *Linear Optical Quantum Computing with Photonic Qubits*, Rev. Mod. Phys. **79**, 135 (2007).
 - [112] M. Shinohara, T. Ito, and Y. Imamura, *Generation and Propagation of Defects into Molecular Beam Epitaxially Grown GaAs from an Underlying GaAs Substrate*, J. Appl. Phys. **58**, 3449 (1985).
 - [113] E. A. Stinaff, M. Scheibner, A. S. Bracker, I. V. Ponomarev, V. L. Korenev, M. E. Ware, M. F. Doty, T. L. Reinecke, and D. Gammon, *Optical Signatures of Coupled Quantum Dots*, Science **311**, 636 (2006).
 - [114] M. Scheibner, A. S. Bracker, D. Kim, and D. Gammon, *Essential Concepts in the Optical Properties of Quantum Dot Molecules*, Solid State Commun. **149**, 1427 (2009).

6 APPENDIX A

Data sheet of GaAs (100) wafers used in this work from Wafer Technology Ltd.

|  WAFER TECHNOLOGY LTD. | | | |
|----------------------------------------------------------------------------------------------------------------|-------------------------|-----------------------------|-----------------|
| Certificate of Conformance: Single Crystal Materials | | | |
| Customer | UNIVERSITY OF PADERBORN | Ingot/lot no. | WV 23757/Un |
| Customer specification | QT102542 | Quantity | 30 Slices |
| Customer order number | EC/10302070000/13/15/7 | Total weight | 462.4g |
| WT order number | WT/ 19459 | | |
| | Specified | Supplied | |
| Material/Growth method | GaAs , VGF | GaAs , VGF | |
| Dopant | Undoped | Undoped | |
| Orientation | (100) $\pm 0.1^\circ$ | (100) $\pm 0.09^\circ$ | |
| Diameter/dimensions (mm) | 76.2 ± 0.4 | 76.0 | |
| Flat Option (EJ/SEMI) | EJ | EJ | |
| Major Flat Length(mm) | 22 ± 2 on (0-1-1) | 21.7 on (0-1-1) | |
| Minor Flat Length(mm) | 11 ± 1 on (0-11) | 11.7 on (0-11) | |
| Surface Finish/Form | One Side Polished | One Side Polished | |
| Thickness (microns) | 625 ± 25 | 632 - 645 | |
| Bow (microns) | Not Specified | Not Specified | |
| Warp (microns) | Not Specified | Not Specified | |
| TTV (microns) | Not Specified | Not Specified | |
| | Specified | Seed End | Tail End |
| Resistivity (Ωcm) | $\geq 1\text{E}7$ | 2.17E+08 | 1.00E+08 |
| Hall mobility ($\text{cm}^2\text{V}^{-1}\text{s}^{-1}$) | ≥ 5000 | 6130 | 5220 |
| Carrier concentration (cm^{-3}) | semi insulating | 4.70E+06 | 1.20E+07 |
| Average EPD (cm^{-2}) | ≤ 5000 | 452 | 644 |
| Additional Information | | | |
| We hereby certify that the above material has been fully tested and is within quoted specification | | | |
| Signed by: | Production | <i>B.J. Walsh</i> | |
| | Quality Assurance | <i>AM Macbra</i> | |
| | Date | 10/3/15 | |
| PC F 0003 Issue 2 | | | |
| Independently Approved by BSi to ISO 9001 | | | |
| Manufactured under a Quality Assurance System | | Certificate Number: FM26963 | |

34 Maryland Road, Tongwell, Milton Keynes, Bucks MK15 8HJ, England, U.K
 Tel: +44 (0)1908 210444 Fax: +44 (0)1908 210443
 www.wafertech.co.uk

7 APPENDIX B

Growth reports

The different results presented in this thesis are summarized from the following grown samples.

Homogenous deposition approach:

A1388, A1389, A1390, A1398, A1430, A1431, A1433, A1512, A1513, A1514, A1526

In-gradient:

A1900, A1901, A1911, A2150, A2150, A2151, A2153, A2154, A2156, A2157, A2158, A2159, A2160, A2161

QD size modification/ Emission energy tuning

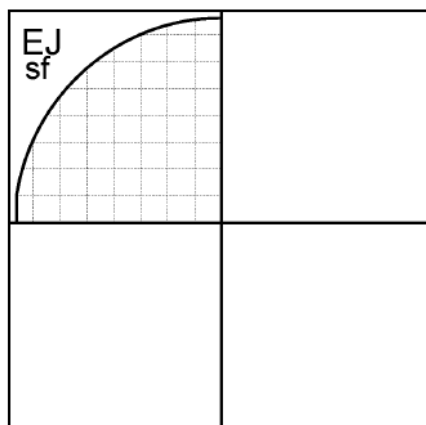
A2073, A2074, A2076, A2078, A2087, A2088, A2089, A2096, A2099, A2129, A2130, A2146

DBR Structure

A1813

Quantum Dot Molecules:

A0915, A0916, A0917, A1129, A1130, A1135, A1136, A1139, A1140, A1349, A2048.



Sample: **A0915**

Material: GaAs

Orientation: (100)

Wafer: Wv24427/un/24

Rotation: 10

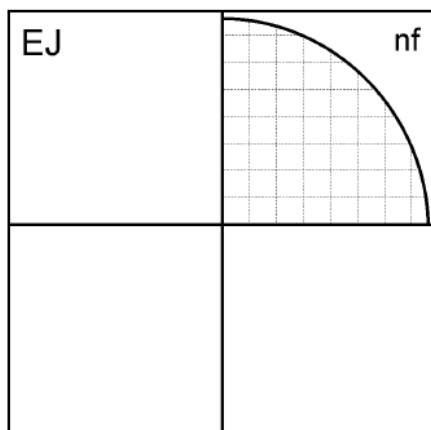
Pressure (mBar):

Date: 08.11.2018

File: a0915.asl

| | | 300K | 77K | 4.2K | 1K |
|-------|------------------------------|------|-----|------|----|
| dark | μ [cm ² / Vs] | | | | |
| | n [cm ⁻²] | | | | |
| illum | μ [cm ² / Vs] | | | | |
| | n [cm ⁻²] | | | | |

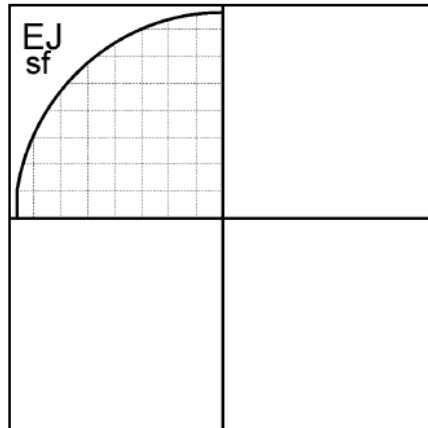
| Layer | Loop | T [°C] | Dur. [s] | Thickn. [nm] | growth rate |
|------------------------------------------|-----------|--------|----------|--------------|--------------------------------|
| GaAs | | 615.0 | 500.0 | 100 | AlAs 0.1 nm/s |
| AlAs | Start 30x | 615.0 | 20.0 | 2 | GaAs 0.2 nm/s |
| GaAs | End | 615.0 | 10.0 | 2 | |
| GaAs | | 615.0 | 1500.0 | 300 | |
| GaAs :Si | | NaN.0 | 500.0 | 100 | |
| GaAs | | 490.0 | 50.0 | 10 | |
| Al _{0.33} Ga _{0.67} As | | 490.0 | 66.7 | 20 | |
| GaAs | | 490.0 | 15.0 | 3 | |
| InAs | Do 10x | 490.0 | 4.0 | 0 | |
| InAs | | 490.0 | 4.0 | 0 | |
| GaAs | | 490.0 | 12.5 | 2.5 | Comment |
| GaAs | | 615.0 | 35.0 | 7 | InAs QDM e-storage |
| GaAs | | 490.0 | 15.0 | 3 | sample: |
| InAs | Do 10x | 490.0 | 4.0 | 0 | Bottom InAs:- 10 cycles |
| InAs | | 490.0 | 2.0 | 0 | 4.0 sec |
| GaAs | | 490.0 | 11.5 | 2.3 | Top InAs:-10 cycles |
| GaAs | | 615.0 | 475.0 | 95 | 2.0 sec |
| GaAs | | NaN.0 | 480.0 | 96 | p_As:1.5 E-5 |
| GaAs | | 490.0 | 120.0 | 24 | |
| GaAs | | 490.0 | 15.0 | 3 | |
| InAs | 10 | 490.0 | 4.0 | 0 | |
| InAs | | 490.0 | 4.0 | 0 | |
| | | | | | (Grown by A. Verma, T. Langer) |



Sample: **A0916**
 Material: GaAs
 Orientation: (100)
 Wafer: Wv24427/Un/25
 Rotation: 10
 Pressure (mBar):
 Date: 09.11.2018
 File: a0916.asl

| | | 300K | 77K | 4.2K | 1K |
|-------|------------------------------|------|-----|------|----|
| dark | μ [cm ² / Vs] | | | | |
| | n [cm ⁻²] | | | | |
| illum | μ [cm ² / Vs] | | | | |
| | n [cm ⁻²] | | | | |

| Layer | Loop | T [°C] | Dur. [s] | Thickn. [nm] | growth rate AlAs 0.1 nm/s GaAs 0.2 nm/s |
|------------------------------------------|-----------|--------|----------|--------------|---------------------------------------------------------------------------------------------------------------------------------------------------------------------------|
| GaAs | | 615.0 | 500.0 | 100 | |
| AlAs | Start 30x | 615.0 | 20.0 | 2 | |
| GaAs | End | 615.0 | 10.0 | 2 | |
| GaAs | | 615.0 | 1500.0 | 300 | |
| GaAs :Si | | NaN.0 | 500.0 | 100 | |
| GaAs | | 490.0 | 50.0 | 10 | |
| Al _{0.33} Ga _{0.67} As | | 490.0 | 66.7 | 20 | |
| GaAs | | 490.0 | 15.0 | 3 | |
| InAs | Do 10x | 490.0 | 4.0 | 0 | |
| InAs | | 490.0 | 4.0 | 0 | |
| GaAs | | 490.0 | 12.5 | 2.5 | |
| GaAs | | 615.0 | 35.0 | 7 | Comment InAs QDM e-storage sample: Bottom InAs:- 10 cycles 4.0 sec Top InAs:-11 cycles 2.0 sec p_As:1.5 E-5 (Grown by A. Verma, T. Langer) |
| GaAs | | 490.0 | 15.0 | 3 | |
| InAs | Do 11x | 490.0 | 4.0 | 0 | |
| InAs | | 490.0 | 2.0 | 0 | |
| GaAs | | 490.0 | 11.5 | 2.3 | |
| GaAs | | 615.0 | 475.0 | 95 | |
| GaAs | | NaN.0 | 480.0 | 96 | |
| GaAs | | 490.0 | 120.0 | 24 | |
| GaAs | | 490.0 | 15.0 | 3 | |
| InAs | 10 | 490.0 | 4.0 | 0 | |
| InAs | | 490.0 | 4.0 | 0 | |
| | | | | | |
| | | | | | |



Sample: **A0917**
 Material: GaAs
 Orientation: (100)
 Wafer: WV24427/Un/25
 Rotation: 10
 Pressure (mBar):
 Date: 13.11.2018
 File: a0917.asl

| | | 300K | 77K | 4.2K | 1K |
|-------|------------------------------|------|-----|------|----|
| dark | μ [cm ² / Vs] | | | | |
| | n [cm ⁻²] | | | | |
| illum | μ [cm ² / Vs] | | | | |
| | n [cm ⁻²] | | | | |

| Layer | Loop | T [°C] | Dur. [s] | Thickn. [nm] | growth rate |
|------------------------------------------|-----------|--------|----------|--------------|--------------------------------|
| GaAs | | 615.0 | 500.0 | 100 | AlAs 0.1 nm/s |
| AlAs | Start 30x | 615.0 | 20.0 | 2 | GaAs 0.2 nm/s |
| GaAs | End | 615.0 | 10.0 | 2 | |
| GaAs | | 615.0 | 1500.0 | 300 | |
| GaAs :Si | | NaN.0 | 500.0 | 100 | |
| GaAs | | 490.0 | 50.0 | 10 | |
| Al _{0.33} Ga _{0.67} As | | 490.0 | 66.7 | 20 | |
| GaAs | | 490.0 | 15.0 | 3 | |
| InAs | Do 10x | 490.0 | 4.0 | 0 | |
| InAs | | 490.0 | 4.0 | 0 | |
| GaAs | | 490.0 | 12.5 | 2.5 | Comment |
| GaAs | | 615.0 | 35.0 | 7 | InAs QDM e-storage |
| GaAs | | 490.0 | 15.0 | 3 | sample: |
| InAs | Do 10x | 490.0 | 4.0 | 0 | Bottom InAs:- 10 cycles |
| InAs | | 490.0 | 4.0 | 0 | 4.0 sec |
| GaAs | | 490.0 | 11.5 | 2.3 | Top InAs:-10 cycles |
| GaAs | | 615.0 | 1090.0 | 218 | 4.0 sec |
| | | | | | p_As:1.5 E-5 |
| | | | | | |
| | | | | | |
| | | | | | |
| | | | | | |
| | | | | | |
| | | | | | (Grown by A. Verma, T. Langer) |

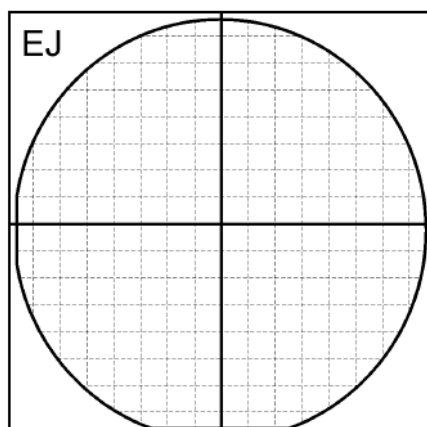


UNIVERSITÄT PADERBORN

 UNIVERSITÄT PADERBORN
Die Universität der Informationswissenschaften



UNIVERSITÄT PADERBORN
UNIVERSITY OF APPLIED SCIENCES



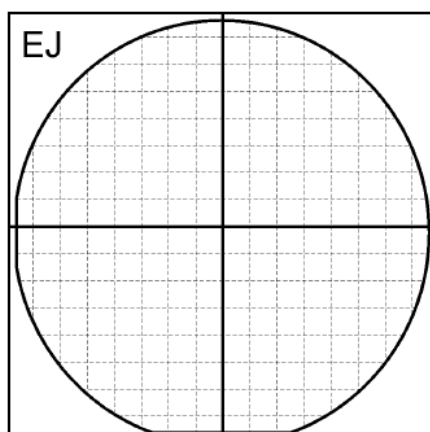
Sample: **A1136**
 Material: GaAs
 Orientation: (100)
 Wafer: WV24688/Un/29
 Rotation: 10
 Pressure (mBar):
 Date: 18.07.2019
 File: a1136.asl

| | | 300K | 77K | 4.2K | 1K |
|-------|-------------------------------------|------|-----|------|----|
| dark | μ [cm^2 / Vs] | | | | |
| | n [cm^{-2}] | | | | |
| illum | μ [cm^2 / Vs] | | | | |
| | n [cm^{-2}] | | | | |

| Layer | Loop | T [$^{\circ}\text{C}$] | Dur. [s] | Thickn. [nm] | growth rate |
|------------------------------------------|-----------|----------------------------|----------|--------------|-------------------------|
| GaAs | | 664.0 | 499.8 | 100 | GaAs 0.2 nm/s |
| AlAs | Start 30x | 664.0 | 20.0 | 2 | AlAs 0.1 nm/s |
| GaAs | End | 664.0 | 10.0 | 2 | |
| GaAs | | 664.0 | 1499.4 | 300 | |
| GaAs :Si | | NaN.0 | 499.8 | 100 | |
| GaAs | | 510.0 | 50.0 | 10 | |
| Ga _{0.67} Al _{0.33} As | | 510.0 | 66.7 | 20 | |
| GaAs | | 510.0 | 15.0 | 3 | |
| InAs | Do 13x | 510.0 | 4.0 | 0 | |
| InAs | | 510.0 | 3.1 | 0 | |
| GaAs | | 510.0 | 14.0 | 2.8 | |
| GaAs | | 664.0 | 35.0 | 7 | Comment |
| GaAs | | 510.0 | 15.0 | 3 | InAs flushed |
| InAs | Do 13x | 510.0 | 4.0 | 0 | QDM e-storage |
| InAs | | 510.0 | 2.1 | 0 | sample: |
| GaAs | | 510.0 | 14.0 | 2.8 | Homogenous Deposition |
| GaAs | | 664.0 | 474.8 | 95 | InAs flushing: |
| GaAs | | 664.0 | 479.8 | 96 | 2.8 nm |
| GaAs | | 664.0 | 120.0 | 24 | Bottom InAs:- 13 cycles |
| | | | | | 3.1 sec |
| | | | | | GaAs spacer: |
| | | | | | 10 nm |
| | | | | | Top InAs:-13 cycles |
| | | | | | 2.1 sec |
| | | | | | p_As:1.5 E-5 |
| | | | | | (Grown by A. Verma) |




UNIVERSITÄT PADERBORN
 Die Universität der Informationsgesellschaft



Sample: **A1140**

Material: GaAs

Orientation: 100

Wafer: WV24688/Un/31

Rotation: 10

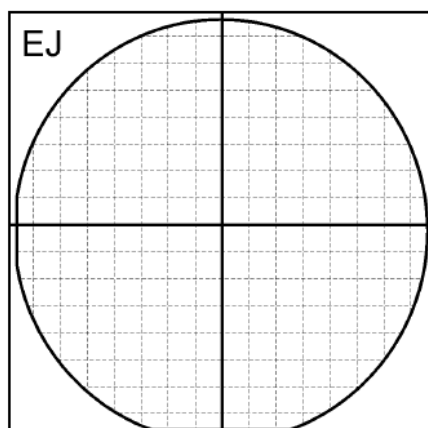
Pressure (mBar):

Date: 19.07.2019

File: a1140.asl

| | | 300K | 77K | 4.2K | 1K |
|-------|------------------------------|------|-----|------|----|
| dark | μ [cm ² / Vs] | | | | |
| | n [cm ⁻²] | | | | |
| illum | μ [cm ² / Vs] | | | | |
| | n [cm ⁻²] | | | | |

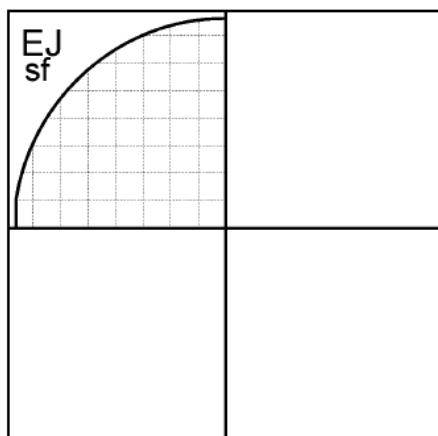
| Layer | Loop | T [°C] | Dur. [s] | Thickn. [nm] | growth rate |
|--------------------------------------------|-----------|--------|----------|--------------|-------------------------|
| GaAs | | 666.0 | 499.8 | 100 | GaAs 0.2 nm/s |
| AlAs | Start 30x | 666.0 | 20.0 | 2 | AlAs 0.1 nm/s |
| GaAs | End | 666.0 | 10.0 | 2 | |
| GaAs | | 666.0 | 1499.4 | 300 | |
| GaAs :Si | | NaN.0 | 499.8 | 100 | |
| GaAs | | 510.0 | 50.0 | 10 | |
| Ga _{0.667} Al _{0.333} As | | 510.0 | 66.7 | 20 | |
| GaAs | | 510.0 | 15.0 | 3 | |
| InAs | Do 13x | 510.0 | 4.0 | 0 | |
| InAs | | 510.0 | 3.2 | 0 | |
| GaAs | | 510.0 | 14.2 | 2850 | |
| GaAs | | 666.0 | 35.0 | 7 | Comment |
| GaAs | | 510.0 | 15.0 | 3 | InAs flushed |
| InAs | Do 13x | 510.0 | 4.0 | 0 | QDM h-storage |
| InAs | | 510.0 | 2.2 | 0 | sample: |
| GaAs | | 510.0 | 14.2 | 2850 | Homogenous Deposition |
| GaAs | | 666.0 | 474.8 | 95 | InAs flushing: |
| GaAs | | 666.0 | 479.8 | 96 | 2.9 nm |
| GaAs | | 666.0 | 120.0 | 24 | Bottom InAs:- 13 cycles |
| | | | | | 3.2 sec |
| | | | | | GaAs spacer: |
| | | | | | 10 nm |
| | | | | | Top InAs:-13 cycles |
| | | | | | 2.2 sec |
| | | | | | p_As:1.5 E-5 |
| | | | | | (Grown by A. Verma) |



Sample: **A1349**
 Material: GaAs
 Orientation: (100)
 Wafer: WV24842/Un/105
 Rotation: 10
 Pressure (mBar):
 Date: 05.02.2020
 File: a1349.asl

| | | 300K | 77K | 4.2K | 1K |
|-------|------------------------------|------|-----|------|----|
| dark | μ [cm ² / Vs] | | | | |
| | n [cm ⁻²] | | | | |
| illum | μ [cm ² / Vs] | | | | |
| | n [cm ⁻²] | | | | |

| Layer | Loop | T [°C] | Dur. [s] | Thickn. [nm] | growth rate GaAs 0.2 nm/s AlAs 0.1 nm/s |
|----------------------------------------------|-----------|--------|----------|--------------|----------------------------------------------------------------------------------------------------------------------------------------------------------------------------------------------------------------------------------------------------|
| GaAs | | 638.0 | 499.8 | 100 | |
| AlAs | Start 30x | 638.0 | 20.0 | 2 | |
| GaAs | End | 638.0 | 10.0 | 2 | |
| GaAs | | 638.0 | 1499.4 | 300 | |
| GaAs :Si | | NaN.0 | 499.8 | 100 | |
| GaAs | | 500.0 | 50.0 | 10 | |
| GaAs | | 500.0 | 434.8 | 87 | |
| GaAs | | 500.0 | 15.0 | 3 | |
| InAs | Do 18x | 500.0 | 4.0 | 0 | |
| InAs | | 500.0 | 3.9 | 0 | Comment InAs flushed QDM h-storage sample: Homogenous Deposition InAs flushing: 2.8 nm Bottom InAs:- 18 cycles 3.9 sec GaAs spacer: 8 nm Top InAs:-17 cycles 5.9 sec p_As:1.5 E-5 (Grown by A. Verma) |
| GaAs | | 500.0 | 14.0 | 2.8 | |
| GaAs | | 638.0 | 25.0 | 5 | |
| GaAs | | 500.0 | 15.0 | 3 | |
| InAs | Do 17x | 500.0 | 4.0 | 0 | |
| InAs | | 500.0 | 5.9 | 0 | |
| GaAs | | 500.0 | 14.0 | 2.8 | |
| GaAs | | 638.0 | 25.0 | 5 | |
| Ga _{0.66.7} Al _{0.33.3} As | | 638.0 | 66.7 | 20 | |
| GaAs | | 638.0 | 924.6 | 185 | |
| | | | | | |
| | | | | | |
| | | | | | |
| | | | | | |
| | | | | | |



Sample: **A1388**

Material: GaAs

Orientation: (100)

Wafer: WV24842/Un/123

Rotation: 10

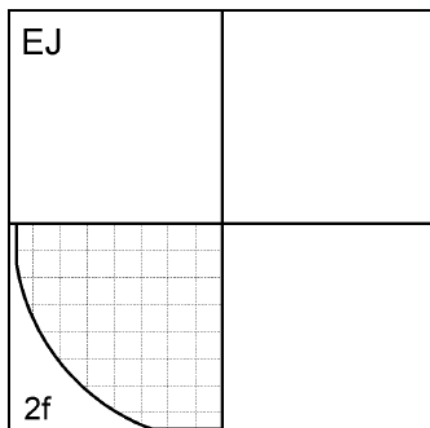
Pressure (mBar):

Date: 26.02.2020

File: a1388.asl

| | | 300K | 77K | 4.2K | 1K |
|-------|------------------------------|------|-----|------|----|
| dark | μ [cm ² / Vs] | | | | |
| | n [cm ⁻²] | | | | |
| illum | μ [cm ² / Vs] | | | | |
| | n [cm ⁻²] | | | | |

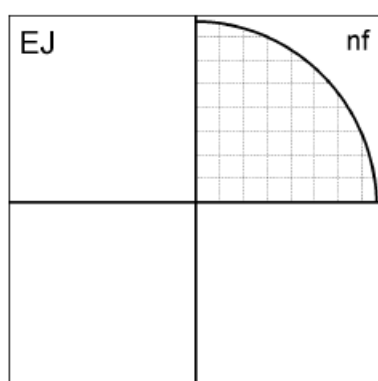
| Layer | Loop | T [°C] | Dur. [s] | Thickn. [nm] | growth rate |
|-------|------|--------|----------|--------------|-----------------------------------------------------------------------------------------------------------------------------------------------------------|
| GaAs | | 473.0 | 500.1 | 100 | GaAs 0.2 nm/s |
| GaAs | | 473.0 | 15.0 | 3 | |
| InAs | 18 | 473.0 | 4.0 | 0 | |
| InAs | | 473.0 | 3.5 | 0 | |
| | | | | | Comment Homogenous Deposition Approach QDs Surface QDs only BandiT: 480C InAs: 18x 3.5sec p_As4: 1.5 E-5 (Grown by A. Verma) |
| | | | | | |
| | | | | | |
| | | | | | |
| | | | | | |
| | | | | | |
| | | | | | |
| | | | | | |
| | | | | | |
| | | | | | |
| | | | | | |
| | | | | | |
| | | | | | |
| | | | | | |
| | | | | | |
| | | | | | |



Sample: **A1389**
 Material: GaAs
 Orientation: (100)
 Wafer: WV24842/Un/123
 Rotation: 10
 Pressure (mBar):
 Date: 26.02.2020
 File: a1389.asl

| | | 300K | 77K | 4.2K | 1K |
|-------|------------------------------|------|-----|------|----|
| dark | μ [cm ² / Vs] | | | | |
| | n [cm ⁻²] | | | | |
| illum | μ [cm ² / Vs] | | | | |
| | n [cm ⁻²] | | | | |

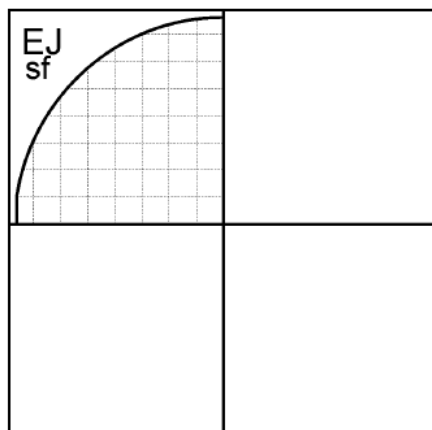
| Layer | Loop | T [°C] | Dur. [s] | Thickn. [nm] | growth rate GaAs 0.2 nm/s |
|-------|------|--------|----------|--------------|-----------------------------------------------------------------------------------------------------------------------------------------------------------|
| GaAs | | 474.0 | 500.1 | 100 | |
| GaAs | | 474.0 | 15.0 | 3 | |
| InAs | 18 | 474.0 | 4.0 | 0 | |
| InAs | | 474.0 | 3.5 | 0 | |
| | | | | | Comment Homogenous Deposition Approach QDs Surface QDs only BandiT: 480C InAs: 18x 3.5sec p_As4: 1.5 E-5 (Grown by A. Verma) |
| | | | | | |
| | | | | | |
| | | | | | |
| | | | | | |
| | | | | | |
| | | | | | |
| | | | | | |
| | | | | | |
| | | | | | |
| | | | | | |
| | | | | | |
| | | | | | |
| | | | | | |
| | | | | | |
| | | | | | |



Sample: **A1390**
 Material: GaAs
 Orientation: (100)
 Wafer: WV24842/Un/123
 Rotation: 10
 Pressure (mBar):
 Date: 26.02.2020
 File: a1390.asl

| | | 300K | 77K | 4.2K | 1K |
|-------|------------------------------|------|-----|------|----|
| dark | μ [cm ² / Vs] | | | | |
| | n [cm ⁻²] | | | | |
| illum | μ [cm ² / Vs] | | | | |
| | n [cm ⁻²] | | | | |

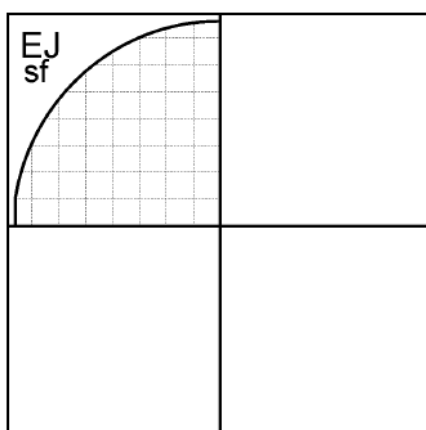
| Layer | Loop | T [°C] | Dur. [s] | Thickn. [nm] | growth rate |
|-------|------|--------|----------|--------------|----------------------------------------------------------------------------------------------------------------------------------------------------------|
| GaAs | | 475.0 | 500.1 | 100 | GaAs 0.2 nm/s |
| GaAs | | 475.0 | 15.0 | 3 | |
| InAs | 18 | 475.0 | 4.0 | 0 | |
| InAs | | 475.0 | 3.5 | 0 | |
| | | | | | Comment Homogenous Deposition Approach QDs Surface QDs only BandIT: 480C InAs:18x 3.5sec p_As4: 1.5 E-5 (Grown by A. Verma) |
| | | | | | |
| | | | | | |
| | | | | | |
| | | | | | |
| | | | | | |
| | | | | | |
| | | | | | |
| | | | | | |
| | | | | | |
| | | | | | |
| | | | | | |
| | | | | | |
| | | | | | |
| | | | | | |
| | | | | | |



Sample: **A1398a**
 Material: GaAs
 Orientation: (100)
 Wafer: WV24842/Un/125
 Rotation: 10
 Pressure (mBar):
 Date: 28.02.2020
 File: a1398a.asl

| | | 300K | 77K | 4.2K | 1K |
|-------|------------------------------|------|-----|------|----|
| dark | μ [cm ² / Vs] | | | | |
| | n [cm ⁻²] | | | | |
| illum | μ [cm ² / Vs] | | | | |
| | n [cm ⁻²] | | | | |

| Layer | Loop | T [°C] | Dur. [s] | Thickn. [nm] | growth rate GaAs 0.2 nm/s |
|----------|------|--------|----------|--------------|--------------------------------------------------------------------------------------------------------------------------|
| GaAs | | 611.0 | 250.0 | 50 | |
| GaAs :Si | | 611.0 | 1500.0 | 300 | |
| | | | | | Comment InAs Homogenous QDs sample Part a T_bandit: 610C p_As: 2.2 E-5 (Grown by A. Verma) |
| | | | | | |
| | | | | | |
| | | | | | |
| | | | | | |
| | | | | | |
| | | | | | |
| | | | | | |
| | | | | | |
| | | | | | |
| | | | | | |
| | | | | | |
| | | | | | |
| | | | | | |
| | | | | | |
| | | | | | |



Sample: **A1398b**

Material: GaAs

Orientation: (100)

Wafer: WV24842/Un/125

Rotation: 10

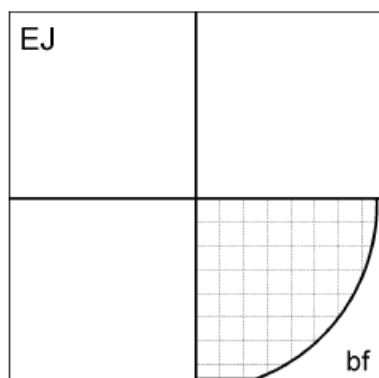
Pressure (mBar):

Date: 28.02.2020

File: a1398b.asl

| | | 300K | 77K | 4.2K | 1K |
|-------|-------------------------------------|------|-----|------|----|
| dark | μ [cm^2 / Vs] | | | | |
| | n [cm^{-2}] | | | | |
| illum | μ [cm^2 / Vs] | | | | |
| | n [cm^{-2}] | | | | |

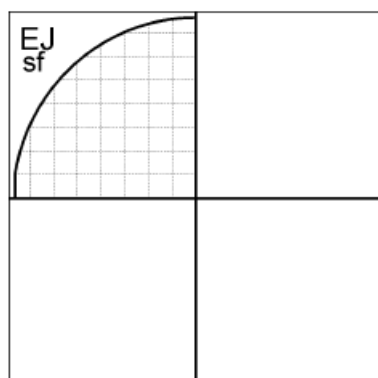
| Layer | Loop | T [$^{\circ}\text{C}$] | Dur. [s] | Thickn. [nm] | growth rate |
|------------------------------------------|--------|----------------------------|----------|--------------|-------------------------------------------------------------------------------------------------------------------------------------------------------|
| GaAs | | 473.0 | 35.0 | 7 | GaAs 0.2 nm/s |
| GaAs | | 473.0 | 200.0 | 40 | AlAs 0.1 nm/s |
| GaAs | | 473.0 | 15.0 | 3 | |
| InAs | Do 18x | 473.0 | 4.0 | 0 | |
| InAs | | 473.0 | 3.3 | 0 | |
| GaAs | | NaN.0 | 14.0 | 2800 | |
| GaAs | | 611.0 | 450.0 | 90 | |
| Ga _{66.7} Al _{33.3} As | | 611.0 | 133.3 | 40 | |
| GaAs | | 611.0 | 50.0 | 10 | |
| GaAs | | 473.0 | 25.0 | 5 | |
| InAs | 18 | 473.0 | 4.0 | 0 | Comment InAs Homogenous QDs sample Part:b T_BandIT: 473C InAs: 18 cycles 3.3 sec p_As: 1.5 E-5 (Grown by) |
| InAs | | 473.0 | 3.3 | 0 | |
| | | | | | |
| | | | | | |
| | | | | | |
| | | | | | |
| | | | | | |
| | | | | | |
| | | | | | |
| | | | | | |
| | | | | | |



Sample: **A1430**
 Material: GaAs
 Orientation: (100)
 Wafer: WV24842/Un/132
 Rotation: 10
 Pressure (mBar):
 Date: 13.03.2020
 File: a1430.asi

| | | 300K | 77K | 4.2K | 1K |
|-------|-----------------------------------|------|-----|------|----|
| dark | μ [cm^2/Vs] | | | | |
| | n [cm^{-2}] | | | | |
| illum | μ [cm^2/Vs] | | | | |
| | n [cm^{-2}] | | | | |

| Layer | Loop | T [$^{\circ}\text{C}$] | Dur. [s] | Thickn. [nm] | growth rate |
|-------|------|--------------------------|----------|--------------|----------------------------------------------------------------------------------------------------------------------------------------------------------|
| GaAs | | 474.0 | 500.1 | 100 | GaAs 0.2 nm/s |
| GaAs | | 474.0 | 15.0 | 3 | |
| InAs | 18 | 474.0 | 4.0 | 0 | |
| InAs | | 474.0 | 4.0 | 0 | |
| | | | | | Comment Homogenous Deposition Approach QDs Surface QDs only BandT: 480C InAs:18x 4.0 sec p_As4: 1.5 E-5 (Grown by A. Verma) |
| | | | | | |
| | | | | | |
| | | | | | |
| | | | | | |
| | | | | | |
| | | | | | |
| | | | | | |
| | | | | | |
| | | | | | |
| | | | | | |
| | | | | | |
| | | | | | |
| | | | | | |
| | | | | | |
| | | | | | |

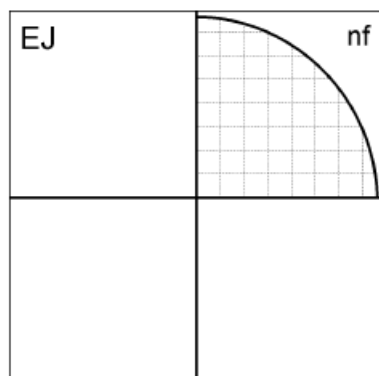


Sample: **A1431**
 Material: GaAs
 Orientation: (100)
 Wafer: WV24842/Un/132
 Rotation: 10
 Pressure (mBar):
 Date: 13.03.2020
 File: a1431.asl

| | | 300K | 77K | 4.2K | 1K |
|-------|-------------------------------------|------|-----|------|----|
| dark | μ [cm^2 / Vs] | | | | |
| | n [cm^{-2}] | | | | |
| illum | μ [cm^2 / Vs] | | | | |
| | n [cm^{-2}] | | | | |

| Layer | Loop | T [$^{\circ}\text{C}$] | Dur. [s] | Thickn. [nm] | growth rate GaAs 0.2 nm/s |
|---------------------|------|--------------------------|----------|--------------|--------------------------------------------------------------------------------------------------------------------------------|
| GaAs | | 472.0 | 500.1 | 100 | |
| GaAs | | 472.0 | 15.0 | 3 | |
| InAs | 18 | 472.0 | 4.0 | 0 | |
| InAs | | 472.0 | 4.0 | 0 | |
| | | | | | Comment Homogenous Deposition Approach QDs Surface QDs only BandIT: 480C InAs:18x 4.0 sec p_As4: 1.5 E-5 |
| | | | | | |
| | | | | | |
| | | | | | |
| | | | | | |
| | | | | | |
| | | | | | |
| | | | | | |
| | | | | | |
| | | | | | |
| | | | | | |
| | | | | | |
| | | | | | |
| | | | | | |
| | | | | | |
| | | | | | |
| (Grown by A. Verma) | | | | | |

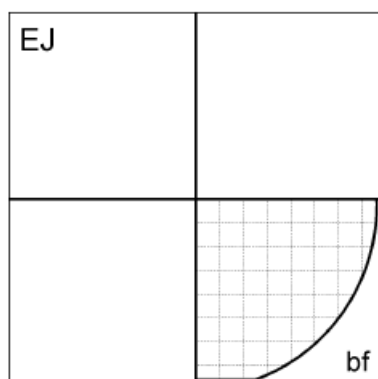
Growth reports



Sample: **A1433**
 Material: GaAs
 Orientation: (100)
 Wafer: WV24842/Un/132
 Rotation: 10
 Pressure (mBar):
 Date: 13.03.2020
 File: a1433.asl

| | | 300K | 77K | 4.2K | 1K |
|-------|-------------------------------------|------|-----|------|----|
| dark | μ [cm^2 / Vs] | | | | |
| | n [cm^{-2}] | | | | |
| illum | μ [cm^2 / Vs] | | | | |
| | n [cm^{-2}] | | | | |

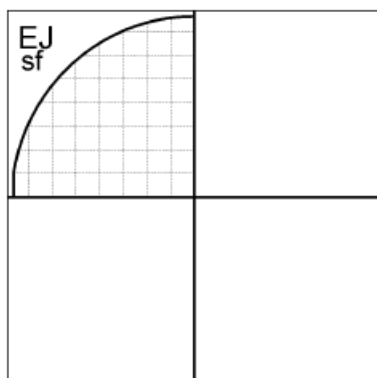
| Layer | Loop | T [$^{\circ}\text{C}$] | Dur. [s] | Thickn. [nm] | growth rate |
|-------|------|--------------------------|----------|--------------|-----------------------------------------------------------------------------------------------------------------------------------------------------------|
| GaAs | | 472.0 | 500.1 | 100 | GaAs 0.2 nm/s |
| GaAs | | 472.0 | 15.0 | 3 | |
| InAs | 18 | 472.0 | 4.0 | 0 | |
| InAs | | 472.0 | 4.0 | 0 | |
| | | | | | Comment Homogenous Deposition Approach QDs Surface QDs only BandIT: 480C InAs:18x 4.0 sec p_As4: 1.5 E-5 (Grown by A. Verma) |
| | | | | | |
| | | | | | |
| | | | | | |
| | | | | | |
| | | | | | |
| | | | | | |
| | | | | | |
| | | | | | |
| | | | | | |
| | | | | | |
| | | | | | |
| | | | | | |
| | | | | | |
| | | | | | |
| | | | | | |



Sample: **A1512**
 Material: GaAs
 Orientation: (100)
 Wafer: WV24842/Un/148
 Rotation: 10
 Pressure (mBar):
 Date: 07.06.2020
 File: a1512.asl

| | | 300K | 77K | 4.2K | 1K |
|-------|-------------------------------------|------|-----|------|----|
| dark | μ [cm^2 / Vs] | | | | |
| | n [cm^{-2}] | | | | |
| illum | μ [cm^2 / Vs] | | | | |
| | n [cm^{-2}] | | | | |

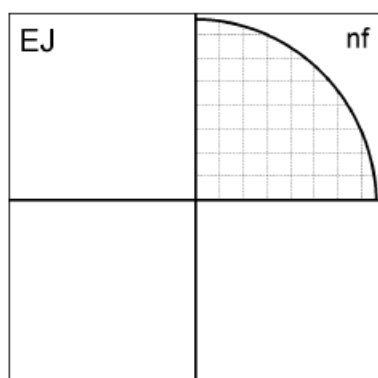
| Layer | Loop | T [$^{\circ}\text{C}$] | Dur. [s] | Thickn. [nm] | growth rate |
|-------|------|--------------------------|----------|--------------|-------------------------------------------------------------------------------------------------------------------------------------------------------|
| GaAs | | 474.0 | 500.1 | 100 | GaAs 0.2 nm/s |
| GaAs | | 474.0 | 15.0 | 3 | |
| InAs | 18 | 474.0 | 4.0 | 0 | |
| InAs | | 474.0 | 4.3 | 0 | |
| | | | | | Comment Homogenous Deposition Approach Q Surface QDs only BandIT: 480C InAs: 18x 4.3 sec p_As4: 1.5 E-5 (Grown by A. Verma) |
| | | | | | |
| | | | | | |
| | | | | | |
| | | | | | |
| | | | | | |
| | | | | | |
| | | | | | |
| | | | | | |
| | | | | | |
| | | | | | |
| | | | | | |
| | | | | | |
| | | | | | |
| | | | | | |
| | | | | | |



Sample: **A1513**
 Material: GaAs
 Orientation: (100)
 Wafer: WV24842/Un/148
 Rotation: 10
 Pressure (mBar):
 Date: 07.06.2020
 File: a1513.asl

| | | 300K | 77K | 4.2K | 1K |
|-------|------------------------------|------|-----|------|----|
| dark | μ [cm ² / Vs] | | | | |
| | n [cm ⁻²] | | | | |
| illum | μ [cm ² / Vs] | | | | |
| | n [cm ⁻²] | | | | |

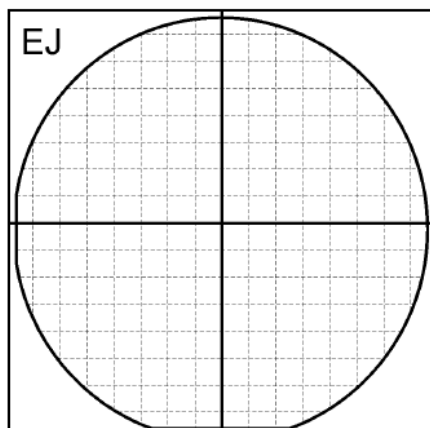
| Layer | Loop | T [°C] | Dur. [s] | Thickn. [nm] | growth rate |
|-------|------|--------|----------|--------------|---------------------------------------------------------------------------------------------------------------------------------|
| GaAs | | 472.0 | 500.1 | 100 | GaAs 0.2 nm/s |
| GaAs | | 472.0 | 15.0 | 3 | |
| InAs | 18 | 472.0 | 4.0 | 0 | |
| InAs | | 472.0 | 4.3 | 0 | |
| | | | | | Comment Homogenous Deposition Approach QDs Surface QDs only BandIT: 480C InAs: 18x 4.3 sec p_As4: 1.5 E-5 |
| | | | | | |
| | | | | | |
| | | | | | |
| | | | | | |
| | | | | | |
| | | | | | |
| | | | | | |
| | | | | | |
| | | | | | |
| | | | | | |
| | | | | | |
| | | | | | |
| | | | | | |
| | | | | | |
| | | | | | |
| | | | | | (Grown by A. Verma) |



Sample: **A1514**
 Material: GaAs
 Orientation: (100)
 Wafer: WV24842/Un/148
 Rotation: 10
 Pressure (mBar):
 Date: 07.06.2020
 File: a1514.asl

| | | 300K | 77K | 4.2K | 1K |
|-------|------------------------------|------|-----|------|----|
| dark | μ [cm ² / Vs] | | | | |
| | n [cm ⁻²] | | | | |
| illum | μ [cm ² / Vs] | | | | |
| | n [cm ⁻²] | | | | |

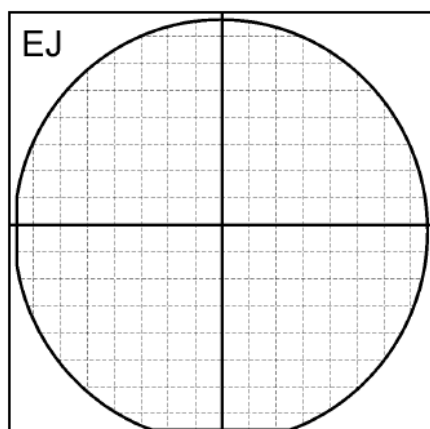
| Layer | Loop | T [°C] | Dur. [s] | Thickn. [nm] | growth rate |
|-------|------|--------|----------|--------------|------------------------------------------------------------------------------------------------------------------------------------------------------------|
| GaAs | | 473.0 | 500.1 | 100 | GaAs 0.2 nm/s |
| GaAs | | 473.0 | 15.0 | 3 | |
| InAs | 18 | 473.0 | 4.0 | 0 | |
| InAs | | 473.0 | 4.3 | 0 | |
| | | | | | Comment Homogenous Deposition Approach QDs Surface QDs only BandIT: 480C InAs: 18x 4.3 sec p_As4: 1.5 E-5 (Grown by A. Verma) |
| | | | | | |
| | | | | | |
| | | | | | |
| | | | | | |
| | | | | | |
| | | | | | |
| | | | | | |
| | | | | | |
| | | | | | |
| | | | | | |
| | | | | | |
| | | | | | |
| | | | | | |
| | | | | | |
| | | | | | |



Sample: **A1526a**
 Material: GaAs
 Orientation: (100)
 Wafer: WV24976/Un/3
 Rotation: 10
 Pressure (mBar):
 Date: 14.06.2020
 File: a1526a.asl

| | | 300K | 77K | 4.2K | 1K |
|-------|------------------------------|------|-----|------|----|
| dark | μ [cm ² / Vs] | | | | |
| | n [cm ⁻²] | | | | |
| illum | μ [cm ² / Vs] | | | | |
| | n [cm ⁻²] | | | | |

| Layer | Loop | T [°C] | Dur. [s] | Thickn. [nm] | growth rate GaAs 0.2 nm/s |
|----------|------|--------|----------|--------------|--------------------------------------------------------------------------------------------------------------------------|
| GaAs | | 646.0 | 250.0 | 50 | |
| GaAs :Si | | 646.0 | 1500.0 | 300 | |
| | | | | | |
| | | | | | Comment InAs Homogenous QDs sample Part a T_bandit: 610C p_As: 2.2 E-5 (Grown by A. Verma) |
| | | | | | |
| | | | | | |
| | | | | | |
| | | | | | |
| | | | | | |
| | | | | | |
| | | | | | |
| | | | | | |
| | | | | | |
| | | | | | |
| | | | | | |
| | | | | | |
| | | | | | |
| | | | | | |
| | | | | | |

Sample: **A1526b**

Material: GaAs

Orientation: (100)

Wafer: WV24976/Un/3

Rotation: 10

Pressure (mBar):

Date: 14.06.2020

File: a1526b.asl

| | | 300K | 77K | 4.2K | 1K |
|-------|------------------------------|------|-----|------|----|
| dark | μ [cm ² / Vs] | | | | |
| | n [cm ⁻²] | | | | |
| illum | μ [cm ² / Vs] | | | | |
| | n [cm ⁻²] | | | | |

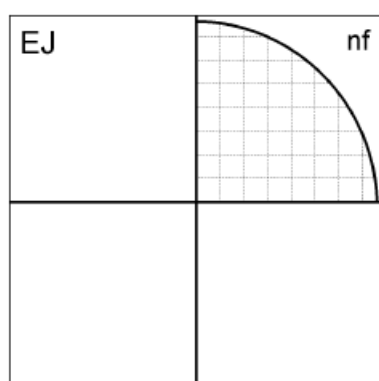
| Layer | Loop | T [°C] | Dur. [s] | Thickn. [nm] | growth rate |
|------------------------------------------|--------|--------|----------|--------------|---------------------------------------------------------------------------------------------------------------------------------------------------------------|
| GaAs | | 504.0 | 35.0 | 7 | GaAs 0.2 nm/s |
| GaAs | | 504.0 | 200.0 | 40 | AlAs 0.1 nm/s |
| GaAs | | 504.0 | 15.0 | 3 | |
| InAs | Do 18x | 504.0 | 4.0 | 0 | |
| InAs | | 504.0 | 3.4 | 0 | |
| GaAs | | NaN.0 | 14.0 | 2.8 | |
| GaAs | | 646.0 | 450.0 | 90 | |
| Ga _{66.7} Al _{33.3} As | | 646.0 | 133.3 | 40 | |
| GaAs | | 646.0 | 50.0 | 10 | |
| GaAs | | 504.0 | 25.0 | 5 | |
| InAs | 18 | 504.0 | 4.0 | 0 | Comment InAs Homogenous QDs sample Part:b T_BandIT: 504C InAs: 18 cycles 3.4 sec p_As: 1.5 E-5 (Grown by A. Verma) |
| InAs | | 504.0 | 3.4 | 0 | |
| | | | | | |
| | | | | | |
| | | | | | |
| | | | | | |
| | | | | | |
| | | | | | |
| | | | | | |
| | | | | | |



UNIVERSITÄT PADERBORN
 Die Universität der Informationsgesellschaft

 Chair of Information Systems
 Chair of Information Systems

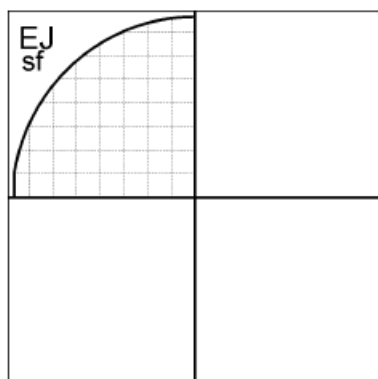
 Chair of Information Systems
 Chair of Information Systems



Sample: **A1900**
 Material: GaAs
 Orientation: (100)
 Wafer: WV24976/Un/66
 Rotation: 10
 Pressure (mBar):
 Date: 19.03.2021
 File: a1900.asl

| | | 300K | 77K | 4.2K | 1K |
|-------|------------------------------|------|-----|------|----|
| dark | μ [cm ² / Vs] | | | | |
| | n [cm ⁻²] | | | | |
| illum | μ [cm ² / Vs] | | | | |
| | n [cm ⁻²] | | | | |

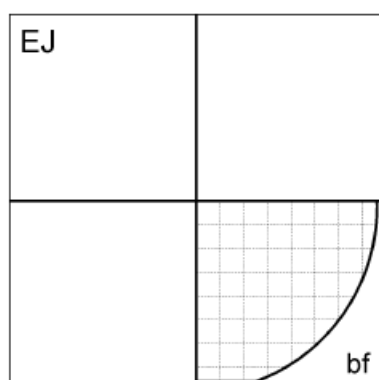
| Layer | Loop | T [°C] | Dur. [s] | Thickn. [nm] | growth rate |
|-----------|--------|--------|----------|--------------|----------------------------------------------------------------------------------------------------------------------------------------------|
| GaAs | | 614.0 | 250.0 | 50 | GaAs 0.2 nm/s |
| GaAs:Si | | 614.0 | 1500.0 | 300 | AlAs 0.1 nm/s |
| GaAs | | 499.0 | 185.0 | 37 | |
| GaAs | | 499.0 | 15.0 | 3 | |
| InAs | Do 15x | 499.0 | 4.0 | 0 | |
| InAs | | 499.0 | 3.0 | 0 | |
| GaAs | | 474.0 | 50.0 | 10000 | |
| GaAs | | 614.0 | 450.0 | 90 | |
| GaAs:AlAs | | 614.0 | 133.3 | 40 | |
| GaAs | | 499.0 | 25.0 | 5 | |
| GaAs | | 499.0 | 15.0 | 3 | |
| InAs | 15 | 499.0 | 4.0 | 0 | Comment In-gradient QDs: (Un-flushed) InAs QDs at Bandit-505C, InAs:15x 3sec 10nm GaAs cap. (Grown by A. Verma) |
| InAs | | 499.0 | 3.0 | 0 | |
| | | | | | |
| | | | | | |
| | | | | | |
| | | | | | |
| | | | | | |
| | | | | | |
| | | | | | |
| | | | | | |



Sample: **A1901**
 Material: GaAs
 Orientation: (100)
 Wafer: WV24976/Un/66
 Rotation: 10
 Pressure (mBar):
 Date: 19.03.2021
 File: a1901.asl

| | | 300K | 77K | 4.2K | 1K |
|-------|-------------------------------------|------|-----|------|----|
| dark | μ [cm^2 / Vs] | | | | |
| | n [cm^{-2}] | | | | |
| illum | μ [cm^2 / Vs] | | | | |
| | n [cm^{-2}] | | | | |

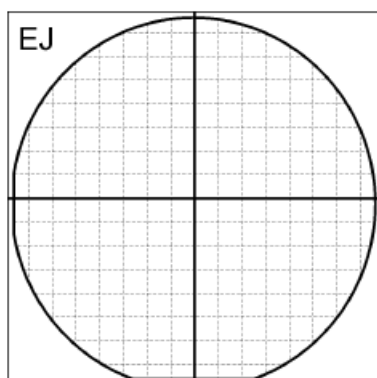
| Layer | Loop | T [$^{\circ}\text{C}$] | Dur. [s] | Thickn. [nm] | growth rate |
|----------------------------|--------|--------------------------|----------|--------------|----------------------------------------------|
| GaAs | | 614.0 | 250.0 | 50 | GaAs 0.2 nm/s |
| GaAs :Si | | 614.0 | 1500.0 | 300 | AlAs 0.1 nm/s |
| GaAs | | 499.0 | 185.0 | 37 | |
| GaAs | | 499.0 | 15.0 | 3 | |
| InAs | Do 15x | 499.0 | 4.0 | 0 | |
| InAs | | 499.0 | 3.0 | 0 | |
| GaAs | | 474.0 | 13.5 | 2700 | |
| GaAs | | 614.0 | 450.0 | 90 | |
| GaAs:Al _{0.33} As | | 614.0 | 133.3 | 40 | |
| GaAs | | 499.0 | 25.0 | 5 | |
| GaAs | | 499.0 | 15.0 | 3 | |
| InAs | 15 | 499.0 | 4.0 | 0 | Comment |
| InAs | | 499.0 | 3.0 | 0 | In-gradient QDs: (flushed) |
| | | | | | full-gradient |
| | | | | | InAs QDs at Bandit-505C, InAs:15x 3sec |
| | | | | | InAs Flushing 2.7nm : |
| | | | | | |
| | | | | | |
| | | | | | |
| | | | | | |
| | | | | | |
| | | | | | |
| | | | | | |
| | | | | | |
| | | | | | (Grown by A. Verma) |



Sample: **A1911**
 Material: GaAs
 Orientation: (100)
 Wafer: WV24976/Un/68
 Rotation: 10
 Pressure (mBar):
 Date: 16.04.2021
 File: a1911.asl

| | | 300K | 77K | 4.2K | 1K |
|-------|------------------------------|------|-----|------|----|
| dark | μ [cm ² / Vs] | | | | |
| | n [cm ⁻²] | | | | |
| illum | μ [cm ² / Vs] | | | | |
| | n [cm ⁻²] | | | | |

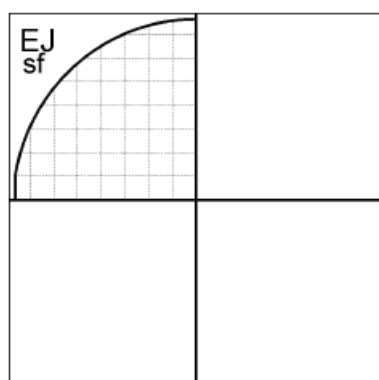
| Layer | Loop | T [°C] | Dur. [s] | Thickn. [nm] | growth rate |
|------------------------------------------|--------|--------|----------|--------------|------------------------------------------------------------------------------------------------------------------------------------------------------------------------------|
| GaAs | | 617.0 | 250.0 | 50 | GaAs 0.2 nm/s |
| GaAs :Si | | 617.0 | 1500.0 | 300 | AlAs 0.1 nm/s |
| GaAs | | 500.0 | 185.0 | 37 | |
| GaAs | | 500.0 | 15.0 | 3 | |
| InAs | Do 17x | 500.0 | 4.0 | 0 | |
| InAs | | 500.0 | 4.0 | 0 | |
| GaAs | | 475.0 | 14.0 | 2800 | |
| GaAs | | 617.0 | 450.0 | 90 | |
| Ga _{0.67} Al _{0.33} As | | 617.0 | 133.3 | 40 | |
| GaAs | | 500.0 | 25.0 | 5 | |
| GaAs | | 500.0 | 15.0 | 3 | |
| InAs | 17 | 500.0 | 4.0 | 0 | Comment In-gradient QDs: (flushed) InAs QDs at Bandit-505C, InAs:17x 4sec InAs Flushing 2.8nm : (Grown by A. Verma) |
| InAs | | 500.0 | 4.0 | 0 | |
| | | | | | |
| | | | | | |
| | | | | | |
| | | | | | |
| | | | | | |
| | | | | | |
| | | | | | |
| | | | | | |



Sample: **A2048**
 Material: GaAs
 Orientation: (100)
 Wafer: WV25035/Un/35
 Rotation: 10
 Pressure (mBar):
 Date: 18.06.2021
 File: a2048.asl

| | | 300K | 77K | 4.2K | 1K |
|-------|-----------------------------------|------|-----|------|----|
| dark | μ [cm^2/Vs] | | | | |
| | n [cm^{-2}] | | | | |
| illum | μ [cm^2/Vs] | | | | |
| | n [cm^{-2}] | | | | |

| Layer | Loop | T [°C] | Dur. [s] | Thickn. [nm] | growth rate |
|---------|-----------|--------|----------|--------------|--------------------------------------------------------------------------------------------------------------------------------------------------------|
| GaAs | | 646.0 | 500.0 | 100 | GaAs 0.2 nm/s |
| AlAs | Start 30x | 646.0 | 20.0 | 2 | AlAs 0.1 nm/s |
| GaAs | End | 646.0 | 10.0 | 2 | |
| GaAs | | 646.0 | 359.1 | 67 | |
| AlAs | Start 18x | 646.0 | 834.3 | 81 | |
| GaAs | End | 646.0 | 359.1 | 67 | |
| AlAs | | 646.0 | 834.3 | 81 | |
| GaAs | | 646.0 | 335.8 | 62.7 | |
| GaAs:Si | | 646.0 | 267.8 | 50 | |
| GaAs | | NaN.0 | 537.3 | 100 | |
| GaAs | | 536.0 | 351.3 | 65.6 | Comment QDM h-storage sample In-gradient QDs BandiT: 480C InAs:18x 4.0 sec p_As4: 1.5 E-5 Bottom DBR-19 pairs (Grown by A. Verma) |
| GaAs | | 536.0 | 16.1 | 3 | |
| InAs | Do 8x | 536.0 | 4.0 | 0 | |
| InAs | | 536.0 | 5.5 | 0 | |
| InAs | Do 8x | 536.0 | 4.0 | 0 | |
| InAs | | 536.0 | 5.5 | 0 | |
| GaAs | | 511.0 | 14.0 | 2.8 | |
| GaAs | | 646.0 | 20.0 | 4 | |
| InAs | Do 8x | 536.0 | 4.0 | 0 | |
| InAs | | 536.0 | 5.5 | 0 | |
| InAs | Do 8x | 536.0 | 4.0 | 0 | |
| InAs | | 536.0 | 5.5 | 0 | |
| GaAs | | 511.0 | 13.5 | 2.7 | |
| GaAs | | 646.0 | 29.5 | 5 | |

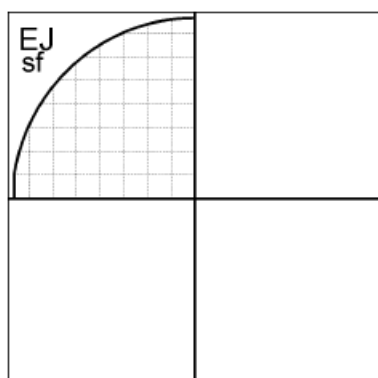


Sample: **A2074**
 Material: GaAs
 Orientation: (100)
 Wafer: WV25035/Un/41
 Rotation: 10
 Pressure (mBar):
 Date: 04.07.2021
 File: a2074.asl

| | | 300K | 77K | 4.2K | 1K |
|-------|-----------------------------------|------|-----|------|----|
| dark | μ [cm^2/Vs] | | | | |
| | n [cm^{-2}] | | | | |
| illum | μ [cm^2/Vs] | | | | |
| | n [cm^{-2}] | | | | |

| Layer | Loop | T [$^{\circ}\text{C}$] | Dur. [s] | Thickn. [nm] | growth rate |
|------------------------------------------|------|--------------------------|----------|--------------|----------------------------|
| GaAs | | 615.0 | 250.0 | 50 | GaAs 0.2 nm/s |
| GaAs :Si | | 615.0 | 1500.0 | 300 | AlAs 0.1 nm/s |
| GaAs | | 475.0 | 185.0 | 37 | InAs 0.002 nm/s |
| GaAs | | 475.0 | 15.0 | 3 | |
| InAs | | 475.0 | 124.0 | 0.3 | |
| GaAs | | 450.0 | 100.0 | 20 | |
| GaAs | | 615.0 | 450.0 | 90 | |
| Ga _{0.95} Al _{0.05} As | | 615.0 | 133.3 | 40 | |
| GaAs | | 475.0 | 25.0 | 5 | |
| GaAs | | 475.0 | 15.0 | 3 | |
| InAs | | 475.0 | 124.0 | 0.3 | |
| | | | | | Comment |
| | | | | | LGR QDs |
| | | | | | InAs QDs |
| | | | | | In:720C; |
| | | | | | BandIT: 480C |
| | | | | | InAs:36x 4.0 Break:4/0sec; |
| | | | | | 20nm GaAs capping; |
| | | | | | surface QDs |
| | | | | | (Grown by A. Verma) |

Growth reports



Sample: **A2076**
 Material: GaAs
 Orientation: (100)
 Wafer: WV25035/Un/42
 Rotation: 10
 Pressure (mBar):
 Date: 05.07.2021
 File: a2076.asi

| | | 300K | 77K | 4.2K | 1K |
|-------|------------------------------|------|-----|------|----|
| dark | μ [cm ² / Vs] | | | | |
| | n [cm ⁻²] | | | | |
| illum | μ [cm ² / Vs] | | | | |
| | n [cm ⁻²] | | | | |

| Layer | Loop | T [°C] | Dur. [s] | Thickn. [nm] | growth rate |
|-----------------------------|--------|--------|----------|--------------|----------------------------|
| GaAs | | 615.0 | 250.0 | 50 | GaAs 0.2 nm/s |
| GaAs :Si | | 615.0 | 1500.0 | 300 | AlAs 0.1 nm/s |
| GaAs | | 487.0 | 185.0 | 37 | |
| GaAs | | 487.0 | 15.0 | 3 | |
| InAs | Do 30x | 487.0 | 4.0 | 0 | |
| InAs | | 487.0 | 4.0 | 0 | |
| GaAs | | 442.0 | 100.0 | 20 | |
| GaAs | | 615.0 | 450.0 | 90 | |
| GaAs/Al _{0.33} SAs | | 615.0 | 133.3 | 40 | |
| GaAs | | 487.0 | 25.0 | 5 | |
| GaAs | | 487.0 | 15.0 | 3 | |
| InAs | 30 | 487.0 | 4.0 | 0 | Comment |
| InAs | | 487.0 | 4.0 | 0 | LGR QDs |
| | | | | | InAs QDs |
| | | | | | In:720C; |
| | | | | | BandIT: 470C |
| | | | | | InAs:30x 4.0 Break:4/4sec; |
| | | | | | 20nm GaAs capping; |
| | | | | | surface QDs |
| | | | | | (Grown by A. Verma) |

| | |
|------------------|---------------|
| Sample: | A2078 |
| Material: | GaAs |
| Orientation: | (100) |
| Wafer: | WV25035/Un/42 |
| Rotation: | 10 |
| Pressure (mBar): | |
| Date: | 05.07.2021 |
| File: | a2078.asi |

UNIVERSITÄT PADERBORN
die Universität der Informationsgesellschaft

| | |
|------------------|---------------|
| Sample: | A2087 |
| Material: | GaAs |
| Orientation: | (100) |
| Wafer: | WV25035/Un/43 |
| Rotation: | 10 |
| Pressure (mBar): | |
| Date: | 08.07.2021 |
| File: | a2087.asl |

UNIVERSITÄT PADERBORN
Die Universität der Informationsgesellschaft

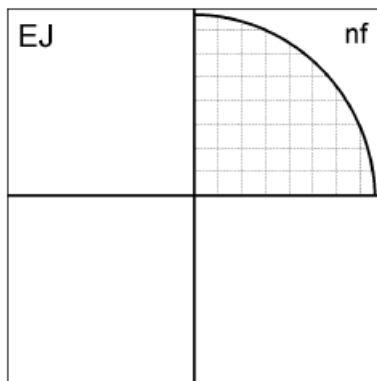
File: a2089.asl

Kein Waferbild vorhanden

[illegible]

| | |
|------------------|---------------|
| Sample: | A2096 |
| Material: | GaAs |
| Orientation: | (100) |
| Wafer: | WV25035/Un/45 |
| Rotation: | 10 |
| Pressure (mBar): | |
| Date: | 10.07.2021 |
| File: | a2096.asi |

(Grown by A. Verma)



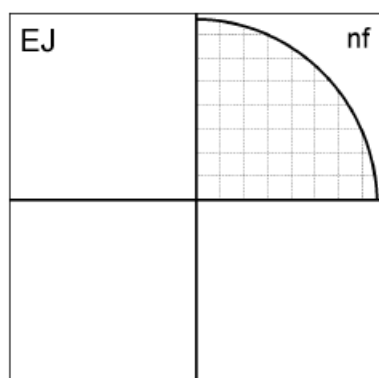
Sample: **A2129**
 Material: GaAs
 Orientation: (100)
 Wafer: WV25035/Un/47
 Rotation: 10
 Pressure (mBar):
 Date: 19.07.2021
 File: a2129.asi

| | | 300K | 77K | 4.2K | 1K |
|-------|------------------------------|------|-----|------|----|
| dark | μ [cm ² / Vs] | | | | |
| | n [cm ⁻²] | | | | |
| illum | μ [cm ² / Vs] | | | | |
| | n [cm ⁻²] | | | | |

| Layer | Loop | T [°C] | Dur. [s] | Thickn. [nm] | growth rate |
|------------------------------|--------|--------|----------|--------------|--------------------------------------------------------------------------------------------------------------------------------------|
| GaAs | | 615.0 | 250.0 | 50 | GaAs 0.2 nm/s |
| GaAs :Si | | 615.0 | 1500.0 | 300 | AlAs 0.1 nm/s |
| GaAs | | 501.0 | 185.0 | 37 | |
| GaAs | | 501.0 | 15.0 | 3 | |
| InAs | Do 37x | 501.0 | 4.0 | 0 | |
| InAs | | 501.0 | 4.0 | 0 | |
| GaAs | | 476.0 | 100.0 | 20 | |
| GaAs | | 615.0 | 450.0 | 90 | |
| GaAs / Al _{0.33} As | | 615.0 | 133.3 | 40 | |
| GaAs | | 501.0 | 25.0 | 5 | |
| GaAs | | 501.0 | 15.0 | 3 | |
| InAs | 38 | 501.0 | 4.0 | 0 | Comment LGR QDs InAs QDs In:720C; BandIT: 505C InAs:37x 4.0sec Break:4/8sec; 20nm GaAs capping; surface QDs |
| InAs | | 501.0 | 4.0 | 0 | |
| | | | | | |
| | | | | | |
| | | | | | |
| | | | | | |
| | | | | | |
| | | | | | |
| | | | | | |
| | | | | | |
| | | | | | (Grown by A. Verma) |

The diagram shows a square divided into four equal quadrants by a horizontal and a vertical line. The top-left quadrant is labeled 'EJ'. The bottom-left quadrant contains a quarter-circle arc with radius '2f' and is shaded with a grid pattern.

| | | 300K | 77K | 4.2K | 1K |
|------------------------------------------|------------------------------|--------|----------|--------------|----------------------------|
| dark | μ [cm ² / Vs] | | | | |
| | n [cm ⁻²] | | | | |
| illum | μ [cm ² / Vs] | | | | |
| | n [cm ⁻²] | | | | |
| Layer | Loop | T [°C] | Dur. [s] | Thickn. [nm] | growth rate |
| GaAs | | 615.0 | 250.0 | 50 | GaAs 0.2 nm/s |
| GaAs :Si | | 615.0 | 1500.0 | 300 | AlAs 0.1 nm/s |
| GaAs | | 500.0 | 185.0 | 37 | |
| GaAs | | 500.0 | 15.0 | 3 | |
| InAs | Do 36x | 500.0 | 4.0 | 0 | |
| InAs | | 500.0 | 4.0 | 0 | |
| GaAs | | 475.0 | 100.0 | 20 | |
| GaAs | | 615.0 | 450.0 | 90 | |
| Ga _{0.97} Al _{0.03} As | | 615.0 | 133.3 | 40 | |
| GaAs | | 500.0 | 25.0 | 5 | |
| GaAs | | 500.0 | 15.0 | 3 | |
| InAs | 36 | 500.0 | 4.0 | 0 | Comment |
| InAs | | 500.0 | 4.0 | 0 | LGR QDs |
| | | | | | InAs QDs |
| | | | | | In:720C: |
| | | | | | BandiT: 505C |
| | | | | | InAs:36 4sec Break:4/4sec; |
| | | | | | 20nm GaAs capping; |
| | | | | | surface QDs |
| | | | | | |
| | | | | | |
| | | | | | |
| | | | | | |
| | | | | | |
| | | | | | |
| | | | | | (Grown by A. Verma) |

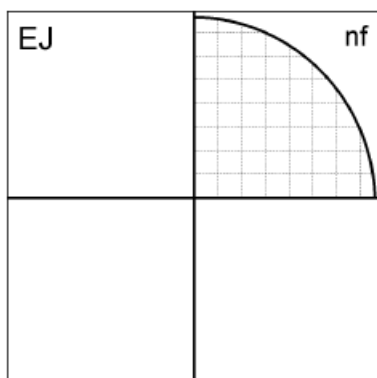


Sample: **A2146**
 Material: GaAs
 Orientation: (100)
 Wafer: WV25035/Un/50
 Rotation: 10
 Pressure (mBar):
 Date: 22.07.2021
 File: a2146.asi

| | | 300K | 77K | 4.2K | 1K |
|-------|------------------------------|------|-----|------|----|
| dark | μ [cm ² / Vs] | | | | |
| | n [cm ⁻²] | | | | |
| illum | μ [cm ² / Vs] | | | | |
| | n [cm ⁻²] | | | | |

| Layer | Loop | T [°C] | Dur. [s] | Thickn. [nm] | growth rate |
|------------------------------------------|------|--------|----------|--------------|--------------------------------|
| GaAs | | 615.0 | 250.0 | 50 | GaAs 0.2 nm/s |
| GaAs :Si | | 615.0 | 1500.0 | 300 | AlAs 0.1 nm/s |
| GaAs | | 500.0 | 185.0 | 37 | |
| GaAs | | 500.0 | 15.0 | 3 | |
| InAs | | 500.0 | 1080.0 | 0.3 | |
| GaAs | | 475.0 | 100.0 | 20 | |
| GaAs | | 615.0 | 450.0 | 90 | |
| Ga _{0.92} Al _{0.08} As | | 615.0 | 133.3 | 40 | |
| GaAs | | 500.0 | 25.0 | 5 | |
| GaAs | | 500.0 | 15.0 | 3 | |
| InAs | | 500.0 | 900.0 | 0.3 | |
| | | | | | Comment |
| | | | | | LGR QDs |
| | | | | | InAs QDs |
| | | | | | In: 659.7C; |
| | | | | | BandIT: 505C |
| | | | | | InAs: 1080 sec Break: 4/4 sec; |
| | | | | | 20nm GaAs capping; |
| | | | | | surface QDs |
| | | | | | (Grown by A. Verma) |

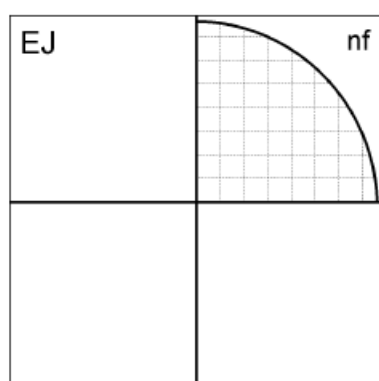
Growth reports



Sample: **A2150**
 Material: GaAs
 Orientation: (100)
 Wafer: WV25035/Un/51
 Rotation: 10
 Pressure (mBar):
 Date: 23.07.2021
 File: a2150.asi

| | | 300K | 77K | 4.2K | 1K |
|-------|------------------------------|------|-----|------|----|
| dark | μ [cm ² / Vs] | | | | |
| | n [cm ⁻²] | | | | |
| illum | μ [cm ² / Vs] | | | | |
| | n [cm ⁻²] | | | | |

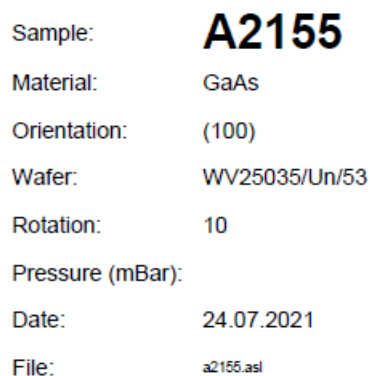
| Layer | Loop | T [°C] | Dur. [s] | Thickn. [nm] | growth rate |
|------------------------------------------|-------|--------|----------|--------------|---------------------------------------------------------------------------------------------------------------------------------------------------------------|
| GaAs | | 615.0 | 250.0 | 50 | GaAs 0.2 nm/s |
| GaAs :Si | | 615.0 | 1500.0 | 300 | AlAs 0.1 nm/s |
| GaAs | | 499.0 | 185.0 | 37 | |
| GaAs | | 499.0 | 15.0 | 3 | |
| InAs | Do 8x | 499.0 | 4.0 | 0 | |
| InAs | | 499.0 | 6.0 | 0 | |
| InAs | Do 8x | 499.0 | 4.0 | 0 | |
| InAs | | 499.0 | 6.0 | 0 | |
| GaAs | | 474.0 | 14.0 | 2800 | |
| GaAs | | 615.0 | 450.0 | 90 | |
| Ga _{0.17} Al _{0.33} As | | 615.0 | 133.3 | 40 | Comment In-gradient QDs half-gradient BandIT: 505C InAs deposition (8x 6.0sec) with rotation (8x 6.0sec) without rotation p_As4: 1.5 E-5 |
| GaAs | | 499.0 | 25.0 | 5 | |
| GaAs | | 499.0 | 15.0 | 3 | |
| InAs | Do 8x | 499.0 | 4.0 | 0 | |
| InAs | | 499.0 | 6.0 | 0 | |
| InAs | 8 | 499.0 | 4.0 | 0 | |
| InAs | | 499.0 | 6.0 | 0 | |
| | | | | | |
| | | | | | |
| | | | | | |
| | | | | | |
| | | | | | (Grown by A. Verma) |



Sample: **A2154**
 Material: GaAs
 Orientation: (100)
 Wafer: WV25035/Un/53
 Rotation: 10
 Pressure (mBar):
 Date: 24.07.2021
 File: a2154.asl

| | | 300K | 77K | 4.2K | 1K |
|-------|------------------------------|------|-----|------|----|
| dark | μ [cm ² / Vs] | | | | |
| | n [cm ⁻²] | | | | |
| illum | μ [cm ² / Vs] | | | | |
| | n [cm ⁻²] | | | | |

| Layer | Loop | T [°C] | Dur. [s] | Thickn. [nm] | growth rate |
|-----------------------------|--------|--------|----------|--------------|-------------------------------|
| GaAs | | 615.0 | 250.0 | 50 | GaAs 0.2 nm/s |
| GaAs :Si | | 615.0 | 1500.0 | 300 | AlAs 0.1 nm/s |
| GaAs | | 499.0 | 185.0 | 37 | |
| GaAs | | 499.0 | 15.0 | 3 | |
| InAs | Do 18x | 499.0 | 4.0 | 0 | |
| InAs | | 499.0 | 4.0 | 0 | |
| GaAs | | 474.0 | 14.0 | 2800 | |
| GaAs | | 615.0 | 450.0 | 90 | |
| GaAs/Al _{0.35} SAs | | 615.0 | 133.3 | 40 | |
| GaAs | | 499.0 | 25.0 | 5 | |
| GaAs | | 499.0 | 15.0 | 3 | Comment |
| InAs | 18 | 499.0 | 4.0 | 0 | In-gradient QDs |
| InAs | | 499.0 | 4.0 | 0 | full-gradient |
| | | | | | BandiT: 505C |
| | | | | | InAs deposition |
| | | | | | (18x 4.0sec) without rotation |
| | | | | | p _{As4} : 1.5 E-5 |
| | | | | | |
| | | | | | |
| | | | | | |
| | | | | | |
| | | | | | |
| | | | | | |
| | | | | | |
| | | | | | (Grown by A. Verma) |

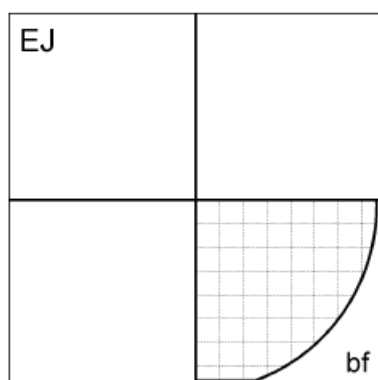
 UNIVERSITÄT PADERBORN
Die Universität der Informationsgesellschaft

| | |
|------------------|---------------|
| Sample: | A2156 |
| Material: | GaAs |
| Orientation: | (100) |
| Wafer: | WV25035/Un/53 |
| Rotation: | 10 |
| Pressure (mBar): | |
| Date: | 24.07.2021 |
| File: | a2156.asi |

 UNIVERSITÄT PADERBORN
 die Universität der Informationsgesellschaft

| | |
|------------------|---------------|
| Sample: | A2157 |
| Material: | GaAs |
| Orientation: | (100) |
| Wafer: | WV25035/Un/53 |
| Rotation: | 10 |
| Pressure (mBar): | |
| Date: | 24.07.2021 |
| File: | a2157.asi |

(Grown by A. Verma)

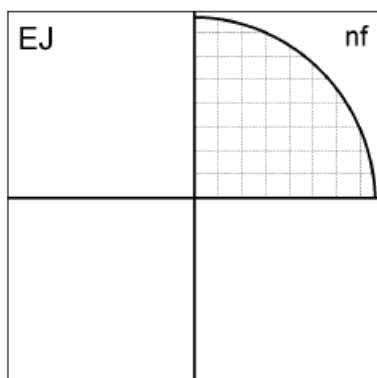


Sample: **A2158**
 Material: GaAs
 Orientation: (100)
 Wafer: WV25035/Un/54
 Rotation: 10
 Pressure (mBar):
 Date: 25.07.2021
 File: a2158.asi

| | | 300K | 77K | 4.2K | 1K |
|-------|-----------------------------------|------|-----|------|----|
| dark | μ [cm^2/Vs] | | | | |
| | n [cm^{-2}] | | | | |
| illum | μ [cm^2/Vs] | | | | |
| | n [cm^{-2}] | | | | |

| Layer | Loop | T [$^{\circ}\text{C}$] | Dur. [s] | Thickn. [nm] | growth rate |
|------------------------------------------|--------|--------------------------|----------|--------------|-------------------------------------------------------------------------------------------------------------------------------------------------------------------|
| GaAs | | 615.0 | 250.0 | 50 | GaAs 0.2 nm/s |
| GaAs :Si | | 615.0 | 1500.0 | 300 | AlAs 0.1 nm/s |
| GaAs | | 499.0 | 185.0 | 37 | |
| GaAs | | 499.0 | 15.0 | 3 | |
| InAs | Do 6x | 499.0 | 4.0 | 0 | |
| InAs | | 499.0 | 6.0 | 0 | |
| InAs | Do 10x | 499.0 | 4.0 | 0 | |
| InAs | | 499.0 | 6.0 | 0 | |
| GaAs | | 474.0 | 14.0 | 2800 | |
| GaAs | | 615.0 | 450.0 | 90 | |
| Ga _{0.67} Al _{0.33} As | | 615.0 | 133.3 | 40 | Comment In-gradient QDs shallow-gradient BandIT: 505C InAs deposition (6x 6.0sec) with rotation (10x 6.0sec) without rotation p_As4: 1.5 E-5 |
| GaAs | | 499.0 | 25.0 | 5 | |
| GaAs | | 499.0 | 15.0 | 3 | |
| InAs | Do 6x | 499.0 | 4.0 | 0 | |
| InAs | | 499.0 | 6.0 | 0 | |
| InAs | 10 | 499.0 | 4.0 | 0 | |
| InAs | | 499.0 | 6.0 | 0 | |
| | | | | | |
| | | | | | |
| | | | | | |
| | | | | | |
| | | | | | (Grown by A. Verma) |

Growth reports



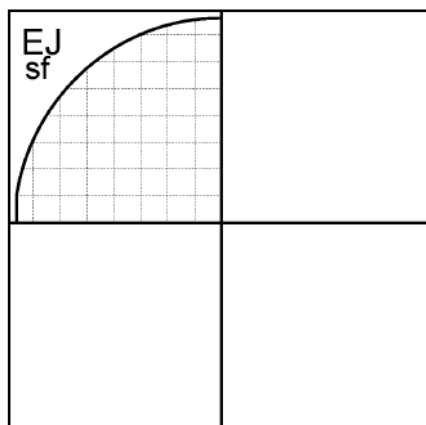
Sample: **A2159**
 Material: GaAs
 Orientation: (100)
 Wafer: WV25035/Un/54
 Rotation: 10
 Pressure (mBar):
 Date: 25.07.2021
 File: a2159.asi

| | | 300K | 77K | 4.2K | 1K |
|-------|------------------------------|------|-----|------|----|
| dark | μ [cm ² / Vs] | | | | |
| | n [cm ⁻²] | | | | |
| illum | μ [cm ² / Vs] | | | | |
| | n [cm ⁻²] | | | | |

| Layer | Loop | T [°C] | Dur. [s] | Thickn. [nm] | growth rate |
|--------------------------------------------|--------|--------|----------|--------------|-------------------------------|
| GaAs | | 615.0 | 250.0 | 50 | GaAs 0.2 nm/s |
| GaAs :Si | | 615.0 | 1500.0 | 300 | AlAs 0.1 nm/s |
| GaAs | | 499.0 | 185.0 | 37 | |
| GaAs | | 499.0 | 15.0 | 3 | |
| InAs | Do 6x | 499.0 | 4.0 | 0 | |
| InAs | | 499.0 | 6.0 | 0 | |
| InAs | Do 10x | 499.0 | 4.0 | 0 | |
| InAs | | 499.0 | 6.0 | 0 | |
| GaAs | | 474.0 | 14.0 | 2800 | |
| GaAs | | 615.0 | 450.0 | 90 | |
| Ga _{0.967} Al _{0.033} As | | 615.0 | 133.3 | 40 | Comment |
| GaAs | | 499.0 | 25.0 | 5 | In-gradient QDs |
| GaAs | | 499.0 | 15.0 | 3 | shallow-gradient |
| InAs | Do 6x | 499.0 | 4.0 | 0 | BandIT: 505C |
| InAs | | 499.0 | 6.0 | 0 | InAs deposition |
| InAs | 10 | 499.0 | 4.0 | 0 | (6x 6.0sec) with rotation |
| InAs | | 499.0 | 6.0 | 0 | (10x 6.0sec) without rotation |
| | | | | | p_As4: 1.5 E-5 |
| | | | | | In-grad(6x 6.0sec) |
| | | | | | Homo(10x 6.0sec) |
| | | | | | |
| | | | | | |
| | | | | | |
| | | | | | |
| | | | | | (Grown by A. Verma) |

| | |
|------------------|---------------|
| Sample: | A2161 |
| Material: | GaAs |
| Orientation: | (100) |
| Wafer: | WV25035/Un/54 |
| Rotation: | 10 |
| Pressure (mBar): | |
| Date: | 25.07.2021 |
| File: | a2161.asi |

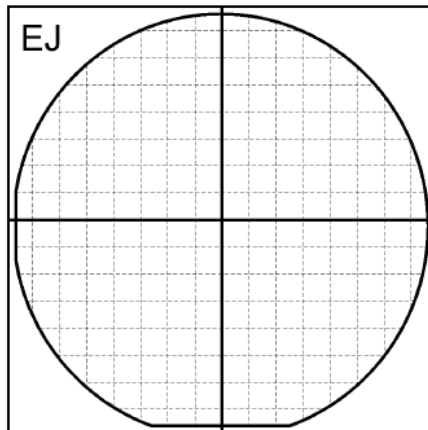
UNIVERSITÄT PADERBORN
University of Applied Sciences



Sample: **A0915**
 Material: GaAs
 Orientation: (100)
 Wafer: Wv24427/un/24
 Rotation: 10
 Pressure (mBar):
 Date: 08.11.2018
 File: a0915.asl

| | | 300K | 77K | 4.2K | 1K |
|-------|------------------------------|------|-----|------|----|
| dark | μ [cm ² / Vs] | | | | |
| | n [cm ⁻²] | | | | |
| illum | μ [cm ² / Vs] | | | | |
| | n [cm ⁻²] | | | | |

| Layer | Loop | T [°C] | Dur. [s] | Thickn. [nm] | growth rate |
|------------------------------------------|-----------|--------|----------|--------------|-------------------------------------------------------------------------------------------------------------------------------------------------------------------------------|
| GaAs | | 615.0 | 500.0 | 100 | AlAs 0.1 nm/s |
| AlAs | Start 30x | 615.0 | 20.0 | 2 | GaAs 0.2 nm/s |
| GaAs | End | 615.0 | 10.0 | 2 | |
| GaAs | | 615.0 | 1500.0 | 300 | |
| GaAs :Si | | NaN.0 | 500.0 | 100 | |
| GaAs | | 490.0 | 50.0 | 10 | |
| Al _{0.33} Ga _{0.67} As | | 490.0 | 66.7 | 20 | |
| GaAs | | 490.0 | 15.0 | 3 | |
| InAs | Do 10x | 490.0 | 4.0 | 0 | |
| InAs | | 490.0 | 4.0 | 0 | |
| GaAs | | 490.0 | 12.5 | 2.5 | Comment InAs QDM e-storage sample: Bottom InAs:- 10 cycles 4.0 sec Top InAs:-10 cycles 2.0 sec p_As:1.5 E-5 (Grown by A. Verma, T. Langer) |
| GaAs | | 615.0 | 35.0 | 7 | |
| GaAs | | 490.0 | 15.0 | 3 | |
| InAs | Do 10x | 490.0 | 4.0 | 0 | |
| InAs | | 490.0 | 2.0 | 0 | |
| GaAs | | 490.0 | 11.5 | 2.3 | |
| GaAs | | 615.0 | 475.0 | 95 | |
| GaAs | | NaN.0 | 480.0 | 96 | |
| GaAs | | 490.0 | 120.0 | 24 | |
| GaAs | | 490.0 | 15.0 | 3 | |
| InAs | 10 | 490.0 | 4.0 | 0 | |
| InAs | | 490.0 | 4.0 | 0 | |
| | | | | | |
| | | | | | |



Sample: **A1139**
 Material: GaAs
 Orientation: (100)
 Wafer: WV24688/Un/30
 Rotation: 10
 Pressure (mBar):
 Date: 19.07.2019
 File: a1139.asl

| | | 300K | 77K | 4.2K | 1K |
|-------|-------------------------------------|------|-----|------|----|
| dark | μ [cm^2 / Vs] | | | | |
| | n [cm^{-2}] | | | | |
| illum | μ [cm^2 / Vs] | | | | |
| | n [cm^{-2}] | | | | |

| Layer | Loop | T [°C] | Dur. [s] | Thickn. [nm] | growth rate |
|----------------------------------------|-----------|--------|----------|--------------|-------------------------|
| GaAs | | 664.0 | 499.8 | 100 | GaAs 0.2 nm/s |
| AlAs | Start 30x | 664.0 | 20.0 | 2 | AlAs 0.1 nm/s |
| GaAs | End | 664.0 | 10.0 | 2 | |
| GaAs | | 664.0 | 1499.4 | 300 | |
| GaAs :Si | | NaN.0 | 499.8 | 100 | |
| GaAs | | 510.0 | 50.0 | 10 | |
| GaAs | | 510.0 | 100.0 | 20 | |
| GaAs | | 510.0 | 15.0 | 3 | |
| InAs | Do 13x | 510.0 | 4.0 | 0 | |
| InAs | | 510.0 | 3.1 | 0 | |
| GaAs | | 510.0 | 14.2 | 2850 | |
| GaAs | | 664.0 | 35.0 | 7 | Comment |
| GaAs | | 510.0 | 15.0 | 3 | InAs flushed |
| InAs | Do 13x | 510.0 | 4.0 | 0 | QDM h-storage |
| InAs | | 510.0 | 2.1 | 0 | sample: |
| GaAs | | 510.0 | 14.2 | 2850 | Homogenous Deposition |
| GaAs | | 664.0 | 25.0 | 5 | InAs flushing: |
| Ga _{0.7} Al _{0.3} As | | 664.0 | 66.7 | 20 | 2.85 nm |
| GaAs | | 664.0 | 924.6 | 185 | Bottom InAs:- 13 cycles |
| | | | | | 3.1 sec |
| | | | | | GaAs spacer: |
| | | | | | 10 nm |
| | | | | | Top InAs:-13 cycles |
| | | | | | 2.1 sec |
| | | | | | p_As:1.5 E-5 |
| | | | | | (Grown by A. Verma) |

Publication

Publication

Submissions to international conferences

- A. K. VERMA, F. BOPP, J.J. FINLEY, B. JONAS, A. ZRENNER, AND D. REUTER: ‘Low Areal Densities of InAs Quantum Dots on GaAs(100) Prepared by Molecular Beam Epitaxy’. *ICMBE online conference 2021*.

Curriculum Vitae

Personal

Name Akshay Kumar Verma

Place of birth Unnao, India

Education

2018-2021 PhD student, Paderborn University, Germany

Thesis title: '*Molecular Beam Epitaxy of InAs Quantum Dot and Quantum Dot Molecule Heterostructures*,' in the group of Optoelectronic Materials and Devices

2015-2017 Master of Science in Physics, Indian Institute of Technology, Indore, India

Thesis title: '*Single crystal synthesis of V-doped NbSe₂ Superconductor and its Properties Measurements*'

2012-2015 Bachelor of Science, Lucknow University, Lucknow, India

2010-2012 Higher Secondary School, Ben-Hur Inter College, Unnao, India

2009-2010 High-School, Ben-Hur Inter College, Unnao, India

Acknowledgments

First I would like to thank my thesis supervisor **Prof. Dr. Dirk Reuter** for giving me the opportunity to work on this intriguing topic and guiding me throughout during this work. His consistent support and encouragement, with all of his time and expertise helped me during all of this time.

I also thank **Prof. Dr. Cedrik Meier** for his work as co-supervisor.

I am thankful to **Prof. Dr. Stefan Schumacher** to chair the doctoral committee and also like to thank **Dr. Thomas Riedl** for being part of committee.

I especially like to thank **Prof. Dr. J. J. Finley** and his group, my collaboration institute at the Technical University, Munich. Special thanks to **Mr. Frederik Bopp** for performing optical and electrical measurements of my samples. It was really great to have a through discussion that helped to understand and interpret the results.

I would like to thank **Prof. Dr. Artur Zrenner** for allowing for PL measurements and **Mr. Björn Jonas** for performing wafer mapping PL experiments and guiding to interpret the data.

I would like to thank **Prof. Dr Donat J.** As for for scientific support and a very friendly talk and courteous encouragements.

I especially like to thank **Mr. Timo Langer** for the helping me during the initial learning with MBE and passing on their valuable QDs work experience and insightful discussions. I would like to thank **Dr. Alexander Trapp** for introduction of the MBE and other knowledgeable discussions.

I would like to thank **Dr. Victoryia Zolatanosha** for performing FTIR and SEM measurements for my samples. I am thankful for her assistance during the time. Also such a great colleague to work with.

I would like to thank **Dr. Tobias Henksmeier**, for his assistance with MBE and other stuffs.

I would like to thank whole working group present and past, **Dr. Yunyan Zhang, Dennis Deutsch, Norman Aular, Falco Meier,**

Mario Littmann, Nithin Khatri, , Dr. Michael Deppe, Nithin Gowda, Christian Kiessler, Martian Eppinger for keeping such a great atmosphere.

I would like to thank **Anja Blank** for her administrative support.

I would especially like to thank Mr. **Bastian Aisenbrey** for his technical support and imparting technical knowledge of MBE. It was really great of his assistance during all time.

Furthermore, I am very thankful to the BMBF via the Q.Link.X project for the financial support.

At last, I would like to thank all of my family and friends for being there.